Modern Environmental Science and Engineering

Volume 5, Number 9, September 2019

Academic Star

Subscription Information:

Price: US$500/year (print)
Those who want to subscribe to our journal can contact: finance@academicstar.us.

Peer Review Policy:

Modern Environmental Science and Engineering (ISSN 2333-2581) is a refereed journal. All research articles in this journal undergo rigorous peer review, based on initial editor screening and anonymous refereeing by at least two anonymous referees. The review process usually takes 2-4 weeks. Papers are accepted for publication subject to no substantive, stylistic editing. The editor reserves the right to make any necessary changes in the papers, or request the author to do so, or reject the paper submitted.

Database Index:

Modern Environmental Science and Engineering (ISSN 2333-2581) is indexed by SSRN, CrossRef and Ulrich now.

Contact Information:

Manuscripts can be submitted to: mese@academicstar.us, environment@academicstar.us. Constructions for Authors and Submission Online System are available at our website: http://www.academicstar.us/onlineupload.asp?shaction=show.

Address: 257 Grand Street #1147, Brooklyn, NY 11211, USA
Tel: 347-566-2247, 347-566-2153, **Fax:** 646-619-4168
E-mail: mese@academicstar.us, environment@academicstar.us

Modern Environmental Science and Engineering

Volume 5, Number 9, September 2019

Contents

Technical Papers

775 **A Thread Parallel Sparse Matrix Chemistry Algorithm for the Community Multiscale Air Quality Model**

George Delic

792 **Nuclear Licensees Activities in Japan for Mindfulness of Nuclear Safety**

Akihide Kugo

803 **Vertical Fences in Housing Units: The Use of Prefabricated Panels**

Leandro Reis Andrade, and Gisleine Coelho de Campos

811 **Evaluation of Remedial Works for a Spillway on Landslide-dammed Lakes by an Earthquake: A Case Study in the Jiufengershan Landslide**

I-Hui Chen, Kuo-Ching Chang, Yu-Chin Chen, and Miau-Bin Su

821 **Modern School Architecture: Analysis of the Educational Research Center Applied in Maceió, Alagoas, Brazil**

Camila Matos de Oliveira Silva, Dilson Batista Ferreira, Jéssica Caroline Rodrigues de Lima, Leila Vieira Torres, and Morgana Maria Pitta Duarte Cavalcante

827 **Design and Manufacturing of a System That Generates Renewable Energy from A Permanent Magnet Generator**

Tripodi R., Cowes D., Montenegro S., Ganiele M., Alcantar S., Lucio G., Arcone D., Daverio N., Pereira C., Moreno M., and Ponzoni L.

837 **Temporary Effect of Mining on Breathing and on the Physicochemical Conditions of Soil**

Giovanny Ramírez Moreno, Harley Quinto, Lady Vargas Porras, and J. Orlando Rangel Ch.

849 **Real-Time Optimal Energy Management for Hybrid and Plug-In Hybrid Electric Vehicles**

Jian Dong, Zuomin Dong, and Curran Crawford

854 **Cluster Analysis of the Soil Physical Attributes under Soil Preparation Systems**

Sálvio Napoleão Soares Arcoverde, Cristiano Marcio Alves de Souza, Weslley Rodrigues Santos, and Egas José Armando

860 **Ecological Interactions in Epiphytic Orchids in the Archaeological Zone "El Tajín", Papantla, Veracruz**

Guadalupe Deniss Ortiz de Angel, José Luis Alanís Méndez, José G. García Franco, and Juan Manuel Pech Canché

867 **Using the BIM 5D Tool for Public Works in Brazil**

Leandro Dias Viana, and Eduardo Marques Arantes

872 **Modeling the Water Balance in the Micro Basin of the Region of Tabuleiro Costeiro, Brazil**

Marcos Vinícius de Souza Chaves, Mariana Dias Meneses, Bruno Javier Carozo Arze, and André Quintão de Almeida

Modern Environmental Science and Engineering (ISSN 2333-2581)
September 2019, Volume 5, No. 9, pp. 775-791
Doi: 10.15341/mese(2333-2581)/09.05.2019/001
Academic Star Publishing Company, 2019
www.academicstar.us

A Thread Parallel Sparse Matrix Chemistry Algorithm for the Community Multiscale Air Quality Model*

George Delic
HiPERiSM Consulting, LLC, USA

Abstract: This reports on integration of a new Chemistry Transport Model (CTM) sparse matrix algorithm (FSPARSE) as a replacement of the legacy JSPARSE algorithm in the U.S. EPA Community Multiscale Air Quality (CMAQ) model. This has been implemented in both Rosenbrock and Gear methods for aqueous chemistry in a hybrid MPI and OpenMP implementation. Both methods are well suited for an OpenMP thread-parallel version. For a 24 hour scenario, execution performance results for both MPI and OpenMP thread parallel scaling are presented with the CMAQ5.3b release on a heterogeneous cluster of 10 nodes with a total of 128 cores. The FSPARSE version of CMAQ typically provides significant speedup over the standard EPA release with similar precision in predicted species concentration values.

Key words: air quality models, sparse matrix methods, MPI, OpenMP, rosenbrock solver, gear solver

1. Introduction

This study reports on major performance enhancements for the Community Multi-scale Air Quality Model (CMAQ) that add new levels of parallelism and replaces the legacy algorithm for a sparse matrix linear equation solver. CMAQ is a major air quality model (AQM) developed by the U.S. EPA [1] and is supported through the Community Modeling and Analysis System (CMAS) [2], as a part of the University of North Carolina, Institute for the Environment, Chapel Hill, North Carolina, USA [3]. CMAQ has a world-wide user base with over 3000 downloads as reported by CMAS. The release used in this analysis is 5.3b and is available for download at Github [4]. The remainder of this section reviews some preparatory background to set the context of this work.

1.1 Air Quality Modeling: Use and Regulation

The role of air quality modeling is to study and predict the chemical interaction, atmospheric transport, and deposition of Criteria Pollutants (and other species) in out-door air on metropolitan, regional, and continental temporal scales. The AQM initiative in the USA dates from the 1970's and is a response to the Clean Air Act [5]. Title 1 of the Clean Air Act (CAA) directs the U.S. EPA to establish National Ambient Air Quality Standards (NAAQS) for common pollutants posing health risks. Federal regulation requires States to demonstrate attainment of the NAAQS and together with the U.S. EPA, they enact regulations to control industrial and commercial pollutant emission sources, while only the U.S. EPA regulates mobile emissions sources. In 1990 the CAA was amended to add Air Toxics and Acid Rain provisions and so-called non-attainment areas were classified.

The criteria pollutants identified in the CAA [5] include:

- Ground level ozone (O_3 - contributor to smog)
- Particulate Matter (PM) in the 2.5 to 10 micron range ($PM_{2.5}$ and PM_{10}) that poses atmospheric haze and respiratory risk

* In memoriam Jeffy O. Young, National Exposure Research Laboratory, Computational Exposure Division, U.S. EPA.

Corresponding author: George Delic, Ph.D.; research areas/interests: air quality and global climate models and performance. E-mail: hiperismllc@gmail.com.

- Lead (Pb)
- Nitrogen dioxide (NO_2)
- Sulfur dioxide (SO_2)
- Carbon monoxide (CO).

CMAQ is used on continental and regional scales in the USA to predict concentrations and transport of criteria pollutants and also as a real-time forecasting model. At the State level, its use is often driven by a State Implementation Plan (SIP), as developed by a given State. A SIP defines regulations and their scope within that State and also spells out consequences for NAAQS when implemented. A SIP may only be approved by the appropriate U.S. EPA Regional Office for that State and typically uses environmental models to demonstrate NAAQS attainment. The CMAQ model, when used in the AQM, is first validated by application to historical episodes and only then is it applied to future scenarios to demonstrate compliance with the NAAQS. Thus, with the aid of an AQM, an approved SIP must demonstrate either NAAQS attainment by the predetermined date, or NAAQS non-attainment. In the case of NAAQS attainment, a 10 year Maintenance Plan is imposed. Whereas in the case of non-attainment, a Federal Implementation Plan (FIP) is developed at the local U.S. EPA Regional Office and Federal sanctions may be applied on the State in question.

Over the decades the science in the CMAQ model has increased in complexity and continues to do so. As a result, both the magnitude of the wall clock time and volume of output data has escalated over time with each new release. Therefore there is always a latent need to improve CMAQ efficiency in performing simulations on modern computer architectures. Advances in processor and memory architecture, as well as software paradigms, are regularly explored with a view to their utility for improved efficiency and scalable performance.

1.2 Parallelism in the Computing Market Place

The High Performance Computing (HPC) marketplace is now dominated by parallel architectures of several different types and requires a careful analysis of the hardware model before a port of legacy applications is attempted to any new architecture. Table 1 summarizes some traditional HPC hardware models and their acronyms, such as processing element (PE). From the end-user (or application) viewpoint this means choosing a parallel program paradigm amongst the dominant multi-platform ones currently available by categories such as those summarized in Table 2. Typical modern commodity architectures include clusters of computer nodes containing one or more central processing units (CPU), with each CPU populated by multiple cores, or PEs, each of which may operate independently in a SIMD environment (Table 1). In recent years, nodes have acquired add-on co-processor devices that host their own local memory and are populated with many (hundred's of) cores. The former will be referred to as multi-core and the latter as many-core devices. Both types of hardware environments delegate subtasks to thread processes that execute on individual cores.

Table 1 High performance computing (HPC) hardware models.

Mnemonic	Functionality	Features
SIMD	Single Instruction Stream Multiple Data Stream	All PEs execute exactly the same instruction at the same time
	SMP = Shared Memory Parallel	Memory is global to all PEs
MIMD	Multiple Instruction Stream Multiple Data Stream	All PEs execute different instructions at the same time
	DMP = Distributed Memory Parallel	Memory is local to each PE
	SMP = Shared Memory Parallel	Part of memory is global to all PEs and part is local to each PE

Table 2 High performance computing (HPC) parallel program paradigms.

Paradigm	Model	Features
MPI (Message Passing Interface)	Functional parallel (or task parallel)	Distinct tasks perform operations simultaneously (on different data)
OpenMP (compiler directives)	Master-worker	Master task spawns subtasks (workers) to other processes to distribute subtasks
MIC® (Many Intergrated Core device)	Massive parallelism	Cohorts of thread teams

1.3 Parallel Programming Styles in CMAQ

The standard distribution of CMAQ [2,4] implements a MIMD/DMP hardware model (Table 1) and uses MPI (Table 2) to implement this by distributing partitions of the grid domain to different MPI processes. It also relies on instruction level parallelism [6] by invoking vector instructions (where they are not otherwise inhibited) for the innermost loops. However, the standard distribution of CMAQ does not implement a SIMD/SMP (Tables 1 and 2) hardware model. Therefore, one major performance enhancement reported here is the inclusion of a thread parallel program paradigm into the standard U.S. EPA release of CMAQ for one of the most time consuming modules of the CMAQ code. To achieve more efficient parallel performance, the legacy sparse matrix algorithm in the standard release of CMAQ is replaced with a modern version.

The new version of CMAQ described here has three levels of parallelism:

1) The outer MPI level is the one previously delivered in the standard U.S. EPA distribution.
2) Each MPI process activates its own team of threads in a thread parallel layer.
3) Instruction-level parallelism at the vector loop level is preserved for each thread.

This new hybrid version of CMAQ is suitable for either multi-core commodity processors or for many-core general purpose add-on accelerators. The suitability of the latter was explored previously [12] for the case of the Intel Many Integrated Core® (MIC) architecture but is not discussed here for CMAQ.

1.4 Algorithms in CMAQ

A brief summary of the algorithm design in CMAQ is given here as a background to the descriptions of the new algorithmic changes that follow. A comprehensive survey of the science and algorithms developed and applied in CMAQ is to be found in a detailed report prepared by the U.S. EPA [8].

1.4.1 Science Processes in CMAQ

A one-atmosphere model was developed and this describes the dynamics by a set of governing equations on a regular grid of cells populating a global array dimensioned by column, row, and level (or layer), for the terrestrial atmosphere. This atmospheric model uses a transport mechanism that consists primarily of numerical algorithms for advection, with vertical and horizontal diffusion, using meteorological input data from another model. In this dynamical model, multiple science modules describe various physical processes such as advection, diffusion, photolysis, aqueous chemistry and cloud dynamics, gas-phase chemistry, etc. An operator splitting methodology allows a fractional time step implementation of the science processes that are integrated over time. The numerical integration of the advection time step imposes input synchronization at a time step interval Δt_{sync}. This time stepping method relies on the approximation that the computational grid remains constant for the duration of the interval of the synchronization time step. All chemical species concentrations are stored in a global array (indexed as described above) and this is accessible to all science processes that may affect them. Chemical transformations occur in gas, liquid, or solid phases and each is modeled separately. The gas phase is dominant and these transformations are described in the CMAQ Chemical Transport Model (CCTM). Operator splitting allows the gas-phase chemistry to be

decoupled from other physical processes. The CCTM module computes the gas phase chemistry in a numerical model of reaction kinetics for production and loss of chemical species. This is accomplished through solution of equations that arise from the mathematical representation of the gas phase chemistry where reaction rates determine production (or loss) of chemical species in the gas phase. The number of reactions that transform reactants into products varies from approximately 90 to several hundred, and the number of species may have a similar range. The selection of the chemical species and the group of governing chemical reactions, known as a chemical mechanism, are predetermined and are interchangeable in the CMAQ model as the knowledge base improves.

1.4.2 Gas Phase Chemistry Solver

Operator splitting in the CMAQ dynamical model allows gas-phase chemistry to be de-coupled from physical processes. As a consequence continuity equations for each gas-phase mechanism species are formulated and solved independently in each cell of the regular grid over column, row and level dimensions. The CCTM module computes the gas phase chemistry in a numerical model for reaction kinetics where reaction rates determine production, or loss, of chemical species in the gas phase. A simple first order ordinary differential equation (ODE) relates the rate of change of species concentration to production and loss terms on the right hand side, with one such equation for each species. Concentrations of species at a later time are obtained from an integration scheme for the first order ODE [9]. However, in the case of CMAQ, the ODE forms a coupled system of order N, the number of reacting species, with some set of initial values of each. The system is non-linear because the production and loss terms on the right hand side may include second and third order reactions for some species. Furthermore, because of widely varying time scales of the reactions, the system of ODE's is stiff (see [9] for a definition). The ratio of largest to smallest eigenvalues of the Jacobian matrix is typically of the order of 10^{10} (or larger) in atmospheric chemistry problems and this represents an extreme case. The system of ODE's of rank N needs to be solved many times for each cell in the grid domain of the advection time step scheme for the dynamical processes. Not surprisingly the execution time of the gas chemistry solver is a substantial fraction of the total wall clock time of a simulation and depends on the ODE solution method.

1.4.3 The Gear Algorithm as Applied in CMAQ

While the following description is predominantly focused on the Gear algorithm, results for the case of the Rosenbrock algorithm [10] are also included here. The Rosenbrock algorithm in CMAQ has been previously investigated by Delic [11] and uses the same sparse Gaussian elimination method discussed here for the Gear algorithm. The same FSPARSE algorithm was also applied to the Global Modelling Initiative (GMI) under contract to NASA and is reported in [12]. These are two of the three numerical integration schemes used in the CCTM module of CMAQ. The method proposed by Gear [13], was adapted by Jacobson and Turco [14]. This is explained by Jacobson [15] for AQM, and was later modified by the U.S. EPA for application to CMAQ. Even with the efficiencies developed in [14,15] the execution time is typically 60% of the total wall clock time of a simulation. Since the Gear solver is well documented [16] it will be summarized briefly here only to the extent needed to understand the application in CMAQ.

The Gear method is a numerical ODE integration formula that is a multi-step and multi-order predictor-corrector algorithm, where the corrector part implements a Newton iteration requiring computation of a Jacobian matrix. After convergence is achieved a local truncation error is computed in an L_2 norm over species and this is used to determine both the chemistry time step size and the order of the method.

On entry the dynamical time step, Δt_{sync}, is subdivided into chemistry time steps and, with an initial estimate, the Gear algorithm begins with an order one predictor formula. The predictor-corrector

method proceeds until a prescribed error tolerance in the local error is either achieved or not. If achieved, then the predicted concentration is accepted and the next chemistry time step, and the order of the integration formula, are estimated. Since the Gear method is a multi-order one, the next time step is estimated for the current order, one lower order and one higher order, based on the respective local errors. If either the convergence or error test fails, the integration is restarted at the beginning of the failed time step after a new computation of the Jacobian matrix, reduction of the time step size, and/or lowering of the order of the integration formula. These procedures are automated in the Gear algorithm subject to several heuristic choices to control computational demand including:

- Update of the Jacobian matrix only after completion of a prescribed number of successful chemistry time steps, if the order changes, or if the convergence (or error test) fails.
- Halting Newton iterations if convergence progress is insufficient
- Limiting changes to the chemistry time step and the order of the method to once every $p+1$ steps for a p-th order method for stability reasons.

The Rosenbrock algorithm differs from the Gear case in that it is not a multi-order, multi-step method. One predictor iteration is followed by three corrector iterations before computing the final solution to determine a new time step increment. At the time, modifications introduced in Refs. [14, 15] took advantage of vector processing on the pipelined vector architectures of Cray computers [17]. However, on Cray computers, the cost was prohibitive if the Gear method is applied to each cell of a multidimensional grid. Therefore one modification introduced in [14] was to apply the Gear algorithm to a block of grid cells simultaneously. This modification allowed vector instructions to be applied for an innermost loop over the block dimension length, NUMCELLS, equal to the size of the block (BLKSIZE). This method has the disadvantage that it requires a memory copy of concentrations from an array dimensioned by column, row, and level, into a one-dimensional array dimensioned by a cell index. Nevertheless, this blocking method worked well on Cray architectures with 128 word vector registers using a choice of BLKSIZE = 500 grid cells. However, such a choice has a memory copy penalty on current commodity CPUs where a choice of BLKSIZE larger than approximately 64 leads to increased computational time. Another disadvantage of choosing larger values of BLKSIZE is that the time step size is the same for all cells in a block, and cells with faster rates of species concentration change may not converge as well as those cells with slower concentration rate changes (i.e., cells differ in "stiffness"). To ameliorate the negative consequences of disparate cell stiffness, the algorithm (JSPARSE herafter) in Refs. [14, 15] offers an option to order all cells in the grid into blocks of cells having similar stiffness, with each block having a length of NUMCELLS.

Two additional improvements implemented in Refs. [14, 15] are applied in the JSPARSE procedure to exploit the sparse structure of the Jacobian in the direct Gaussian linear solver:

1) Terms are ordered in the Jacobian matrix to reduce fill-in when applying decomposition and forward/back substitution.
2) algebraic manipulations involving zero numerical values are eliminated in explicit "hardwired" coding using multiple levels of indirect subscript references.

Both these improvements are implemented in symbolic manipulations that need be performed only once using the known (unchanging) sparse structure of the Jacobian matrix in the JSPARSE procedure. However, the use of complex loop ranges based on indirect array references that are evaluated only at runtime, prohibits parallelization of outer loop nests. When originally developed on Cray computers the use of indirect addressing was not a major performance

inhibitor because that architecture allowed hardware gather-scatter operations. However, today's commodity architectures do not support hardware gather-scatter instructions and indirect addressing carries a penalty because it cannot be parallelized easily. It also leads to excessive translation look-aside buffer (TLB) cache look-up that inevitably stalls a commodity CPU. For some details of analysis for this performance bottleneck see Young and Delic [18]. The exception is the Intel MIC® architecture [7] which does support gather/scatter operations in hardware.

In the U.S. EPA implementation of the Gear algorithm additional changes include:

- code changes to integrate into the CCTM structure,
- prohibition of negative concentration values that are possible when rapid species depletion occurs,
- choice of a relative error (RTOL) of 10^{-3} and absolute error (ATOL) 10^{-9} ppm.

It should be noted that CMAQ, unlike the GMI [12] implementation does not apply mass conservation for species.

However, error tolerance values may be changed (as input parameters in CMAQ), and they are based on heuristic proposals by Byrne and Hindmarsh [19]. It is important to note that these tolerances are applied to the L_2 norm of species errors for all cells in a block of cells. Therefore, not all individual species in a block of cells may satisfy them. Application of a mini-max norm such as L_∞ would be considerably more stringent, but is also more expensive in computation time. Also, more accurate results would be obtained with a block size (BLKSIZE) of one, i.e., a single cell. However, this choice also increases computation time substantially.

2. New Sparse Matrix Algorithm in CMAQ

For the reasons outlined in the previous Sections, a new sparse solver was developed to replace the legacy method of Refs. [14,15] and this section gives some detail on two of the major performance enhancements for CMAQ with the Gear solver. The same description applies to the Rosenbrock algorithm since it shares the same computational modules with the Gear case. The first change replaces the sparse matrix solver used for chemical species concentrations in the standard U.S. EPA distribution. The second modification integrates the new solver into the transit over grid cells so that separate blocks of cells are distributed to different threads. Applying both modifications together improves CMAQ efficiency. This was previously observed to be the case in application to CMAQ with the Rosenbrock solver [11].

2.1 Gaussian Elimination in the Gear Solver

The Gear chemistry solver in CMAQ applies direct Gaussian elimination [20] of a sparse matrix system Ax = b many millions of times per simulation. The dimension of matrix A is determined by the number, N, of reacting chemical species (N = 149 in this study). While the species matrix has some N^2 = 22,201 elements, the number of non-zero entries, NZ, is 1338 (day) and 1290 (night) for chemistry mechanisms, respectively. The matrix solution has three stages:

(i) decomposition A=LU,

(ii) forward solve for Lz=b,

(iii) backward solve for Ux=z,

where L and U, are lower and upper triangular matrices such that A=LU. For CMAQ, matrix A has large condition numbers and is diagonally dominant by many orders of magnitude, and therefore pivoting is not applied in step (i). Scaling is applied to A to permit exception handling at runtime. This allows underflows and avoids the execution halting as a result of overflows when no scaling is used. The above solution is applied to each block of grid cells passed to the chemistry solver. The choice of block size is a user selectable parameter (BLKSIZE) but the actual value has consequences for cache behavior on commodity CPUs at runtime [11]. For all test cases reported here the choice was limited to a default of BLKSIZE = 50.

2.2 New Sparse Matrix Solver

This section summarizes the algorithmic choices that transform JSPARSE into a new procedure (FSPARSE hereafter) for the Gear algorithm. The same method applies to the Rosenbrock chemistry algorithm that was previously described in [11]. First of all, a few words about sparse matrix storage schemes are in order. All sparse matrix algorithms reference only non-zero elements and store the value in an array, but they differ in the storage method for the row and column location in the full matrix. Each scheme requires indirect subscript references at some level, but the implementation has consequences for parallel algorithm opportunities. The Triplet storage scheme (used in JSPARSE) scans rows and columns of the matrix and stores column and row index values in two integer arrays. Alternatively, for NZ non-zero elements in the matrix, the Compressed Column (CC) scheme scans down successive columns and uses an integer array i of length NZ together with another pointer array p of length N+1 so that row indices of entries in column j are stored in integer arrays i(p(j)) through i(p(j+1) -1). The CC scheme is described in chapter 2 of Davis [21] for the C language case. In another method, Compressed Row (CR) storage scans across successive rows and uses a similar pointer scheme described for CC (above). The starting point in FSPARSE is the CSparse C language library developed by Davis [21] which uses the CC storage form and has been implemented with substantial modification in the FSPARSE version of CMAQ. The CSparse library is quite general and extensive, but only the sparse Gaussian procedures have been adopted for this CMAQ application. CSparse allows a generalized factorization of the type PAQ = LU, where P is obtained from partial pivoting and Q is chosen to reduce fill-in in LU. In CMAQ the permutation matrix Q, is in effect, the result of the re-ordering step taken over from the JSPARSE procedure [14]. However, P = I (the identity matrix) is the choice in the CMAQ model because the matrix A is diagonally dominant and no pivoting is applied.

The CSparse procedures listed in Table 3 have been extracted and translated into FORTRAN for integration into the FSPARSE version of the Gear algorithm. However, local modifications have been made. For example, cs_lsolve and cs_usolve, will not allow parallel/vector instructions on inner loops because the CC form uses indirect addressing of array indexes on the left hand side of the assignment ("="). This is demonstrated by the compiler message in the extract from FSPARSE shown in Fig. 1.

However, if the indirect reference is on the right hand side then parallel/vector instructions are enabled. The transformation is achieved by using a Compressed Row (CR) storage scheme as is demonstrated in Fig. 2. The suggestion for the CR form enabling a parallel/vector algorithm is from Björck [22]. Because of this benefit of the CR form, FSPARSE has an option to convert L and U to the Compressed Row (CR) storage scheme after the sparse CC decomposition step for A = LU. This enables vector SSE instructions to schedule the inner loops of forward and backward solve steps (see Section 2.1) while also allowing parallel potential in the outer loop. Such parallel loop nests may easily be parallelized in a many core version, or whenever nested parallel threads are enabled in the OpenMP model.

In the code for the solver part of FSPARSE that corresponds to Fig. 2, the forward solve is performed for all cells in a block of cells as shown in the example of Fig. 3.

Table 3 C language procedures from CSparse translated to FORTRAN in FSPARSE.

CSparse procedure	Description
cs_compress	Map Triplet to CC storage
cs_lu	Driver for LU decomposition
cs_spsolve	Sparse solve for L, and U
cs_reach	Reach function
cs_dfs	Depth first search
cs_lsolve[a]	Solve Lz = b
cs_usolve[a]	Solve Ux = z
cs_norm	Compute 1-norm of A
[a] Converted to parallel and vector form using Compressed Row (CR) format for L and U	

```
!   inner loop _will_ not vectorize in CC format – compiler message:
!   row_f, Loop not vectorized: data dependency
!              Loop unrolled 4 times
!
        col_f: do s_j = 0, N - 1                                    ! col index
               s_x(s_j) = s_x(s_j) / s_Lx( s_Lp(s_j,sn),sn )
               row_f: do s_k = s_Lp(s_j,sn)+1 , s_Lp(s_j+1,sn)-1
                  s_x(s_Li(s_k,sn))=s_x(s_Li(s_k,sn)) - s_Lx( s_k,sn)*s_x(s_j)
               end do row_f
        end do col_f
```

Fig. 1 Example of FORTRAN version of compressed column (CC) format for a solve loop that inhibits vector instructions on the inner loop.

```
!   inner loop _will_ vectorize in CR format – complier message:
!   col_fr: Generated 2 alternate versions of the loop
!              Generated vector sse code for the loop
!              Generated a prefetch instruction for the loop
!
        row_fr: do s_i = 1, N - 1                                   ! row index
               s_s = s_x(s_i)
               col_fr: do s_j = L_w(s_i,sn) , L_w(s_i+1,sn)-2
                  s_s = s_s - L_Cx( s_j,sn ) * s_x( L_Cj(s_j,sn) )
               end do col_fr
               s_x(s_i) = s_s
        end do row_fr
```

Fig. 2 Example of FORTRAN version of compressed row (CR) format for a solve loop that does allow vector instructions for the inner solve loop.

```
row_fr1: do s_i = 1, NS - 1                                 ! row
      DO NCELL = 1, NUMCELLS                                ! vector loop # 31
         rivot(NCELL) = K1( NCELL ,s_i)
      ENDDO
      col_fr1: do s_j = L_w(s_i,sn) , L_w(s_i+1,sn)-2       ! col
            DO NCELL = 1, NUMCELLS                          ! vector loop # 32
               rivot(NCELL) = rivot(NCELL) - Lr_Cx( NCELL,s_j ) *
&                                        K1( NCELL, L_Cj(s_j,sn) )
            ENDDO
      end do col_fr1

      DO NCELL = 1, NUMCELLS                                ! vector loop # 33
         K1( NCELL,s_i) = rivot(NCELL)
      ENDDO
  end do row_fr1
```

Fig. 3 Example of FORTRAN version of Compressed Row (CR) format for a solve loop that expands the example of Fig. 2 to vector loops over blocks of cells of length NUMCELLS.

In Fig. 3 the outer row loop (row_fr1) is not parallelizable because of the recurrence on array K1. The column loop (col_fr1) is parallelizable because the CR format places the indirect reference on the second index of the K1 array. All loops contain a vector loop on the cell index NCELL for the current block and NUMCELLS is the blocksize. At the cost of a memory copy, a temporary array (rivot) is introduced so that a vector-inhibiting recurrence is avoided on the innermost loop (# 32).

2.3 Driver Procedure

The CCTM driver procedure is CHEM in CMAQ and has major loops over the blocks of cells in a grid dimensioned by column, row, and level. The MPI implementation partitions the entire grid on the column and row dimensions into sub-domains where the number of cells in each sub-domain depends on the number of MPI processes (NP). Each sub-domain has blocks of cells that are processed in the solve steps as described in Sections 2.1 and 2.2. The number of blocks is calculated from the BLKSIZE parameter choice in a grid initialization procedure GRID_CONF. However, the number of blocks diminishes as NP increases. For each MPI process the chemistry solver time step for each block is independent of all others, and different blocks are distributed amongst available threads in a thread parallel team using an appropriate scheduling algorithm. This strategy is attractive because it creates coarse parallel granularity for thread teams as a result of the substantial scope of the contained arithmetic operations. Thus the Gear algorithm is applied independently by each thread in the team to its own chosen block of cells.

Table 4 shows the subroutines modified in the FSPARSE version of CMAQ. This indicates those subroutines inlined into the new version of CHEM that has two large thread parallel regions: one for reordering (as in the original JSPARSE version), and a second for the chemistry solution with time step integration. Both parallel regions contain loops over the total number of grid blocks for each MPI process, but the first takes only a small fraction of the time spent in CHEM.

The new version of CHEM was created by successive code structure modifications of the standard U.S. EPA Gear solver without changing the science of the model in any way. Specific restructuring steps applied to the standard CMAQ gas chemistry solver included:

- New modules for procedures (see Table 3)
- Arrangement of inner loops so that they enable vector instructions.
- Declaration of thread parallel regions by insertion of OpenMP directives and classification of local (thread private) and global (shared) variables.
- Simplification/streamlining of redundant code.

The modified FSPARSE version of CMAQ applies a thread parallel strategy that has three prongs:

1) Partitioning storage into global shared variables and those private to threads.
2) Distribution of NUMCELLS sized chunks of the grid domain to separate threads in a parallel thread team.
3) Ensuring each thread has inner loops that vectorize where ever possible.

The two parallel regions in the FSPARSE CHEM version invoke OpenMP thread parallel teams that execute either on a host processor or on many integrated core® (MIC) processors through the offload option in the Intel compiler. This thread-vector parallel strategy can only succeed if there is sufficient coarse grain parallel work for each thread. This is achieved with the modifications described above by creating a large parallel region for the block loop and it is this loop that has a diminishing range as the number of MPI processes increases.

Table 4 The U.S. EPA procedures of the Gear solver modified in the FSPARSE algorithm.

CMAQ procedure	Description of computational function in separate modules
GRID_CONF	Define grid and set BLKSIZE
GRVARS	Declare allocatable arrays
GRINIT	Initialize and allocate arrays
JSPARSE	Define chemistry structure and symbolic Gaussian elimination
CHEM	Loop over grid blocks and call Gear solver
CALCKS	Prepare reaction rate coefficients
PHOT	Prepare photolytic rate coefficients
SMVGEAR[a]	Implementation of Gear ODE algorithm
SUBFUN	Rate of change of species concentrations
PDERIV	Jacobian matrix
DECOMP	LU decomposition
BACKSUB	Forward and backward solve

[a] Inlined into FSPARSE CHEM procedure with calls to the others in this table

3. Test Bed Environment

3.1 Hardware

The hardware systems chosen were the platforms at HiPERiSM Consulting, LLC, shown in Table 5. Nodes 20 and 21 host two Intel E5v3 CPUs with 16 cores and each node has four Intel Phi® co-processor (MIC) processors [7] with, respectively, 60 and 59 cores each. These are the base nodes of a heterogeneous cluster that includes an HP blade server hosting nodes 27 to 34 with dual 4-core Intel E5640 CPUs. The total core count of this cluster is 128 with ~2 Tflops (peak) floating point performance in single precision. The MPI executions are launched across multiple combinations of these nodes using an Infiniband (IB) fabric with a theoretical bandwidth limit of 40G bits/sec. This cluster allows for comparison of the FSARSE hybrid (MPI + OpenMP) parallel versions of CMAQ with the original EPA JSPARSE version.

3.2 Compilers

This report implemented the Intel Parallel Studio® [7] (release 17.6), for CMAQ on 64-bit Linux operating systems. The HiPERiSM Consulting, LLC, version of CMAQ, with multi-threaded parallelism, was compiled and executed for this heterogeneous cluster. Other compilers have been used in the past, but results reported here will be confined to the Intel case.

Table 5 Test bed platforms and their attributes.

Platform	Node20-21 (each node)	Node27-34 (each node)
Processor	Intel™ E5-2698v3	Intel™ E5640
Peak Gflops (SP)	~589	~170
Power consumption	135 Watts	80 Watts
Cores per processor	16	4
Processor count	2	2
Total core count	32	8
Clock	2.3 GHz	2.67 GHz
Band-width	68 GB/sec	25.6 GB/sec
Bus speed	2133 MHz	2933 MHz
L1 cache	32 KB	32 KB
L2 cache	256 KB	256 KB
L3 cache	40 MB	12 MB

3.3 Episode Studied

The 5.3b release of CMAQ was used in all results reported here with the source code and model episode data available at the download site [4]. This 24 hour episode was for July 1st, 2011, using the cb6r3_ae6_aq mechanism with 149 active species and 329 reactions. For day/night chemistry this results in 1338/1290 non-zero entries in the Jacobian matrix. The episode was run for a full 24 hour scenario on a 80 *x* 100 California domain at 12 Km grid spacing and 35 vertical layers for a total of 280,000 grid cells. This case represent a modest grid size but is substantial enough with the number of species and reactions included.

Partitioning of the grid amongst the available number of MPI processes (after division into blocks of 50 cells) gives 280,000/50 = 5600 blocks for NP = 1, and 5600/NP thereafter, when NP > 1. For example, with 8 MPI processes there are approximately 700 blocks per MPI process. As a result the workload per thread is also diminished. Thus both increasing MPI process and OpenMP thread count have consequences for performance scaling because the number of blocks is further subdivided.

4. Performance

4.1 Speedup and Scaling

In this section two performance metrics are defined to assess thread parallel performance in the FSPARSE modified code for CMAQ:

a) *Speedup* is the gain in runtime over the standard U.S. EPA runtime,
b) *Scaling* is the gain in runtime with thread (or MPI process) counts larger than 1, relative to the result for a single thread (or MPI process).

For the CCTM each grid of cells is partitioned into blocks of size BLKSIZE and these blocks are distributed to threads in an OpenMP thread team in FSPARSE. In the previous study for the Rosenbrock algorithm [11] values of 16, 32, 48, and 64 were

investigated for impact on wall clock times due to cache effects. However, variations in wall clock time for BLKSIZE changes in this range were small and shrank as the number of threads increased. Nevertheless, wall clock time did rise for BLKSIZE greater than 64 therefore in this study of the CMAQ, the EPA default value of BLKSIZE = 50 was used.

4.2 MPI Scaling

CMAQ in the U.S. EPA JSPARSE version was scaled on the homogeneous cluster (node20 and 21) in the MPI range 1 to 64 processes for both Gear and Rosenbrock algorithms. Wall clock time (in minutes) is shown in Fig. 4 where a sharp decline in improvement is visible, especially above 8 MPI processes. The MPI parallel efficiency in Fig. 5 is calculated from speedup divided by the process count. This average reflects values of ~70% and ~55% with 32 and 64 MPI processors respectively. The latter efficiency value suggests that, on average, the CPU is idle half of the wall clock time. This is caused by the increasing dominance of MPI communication time over arithmetic compute time, specifically an MPI barrier call at the synchronization time step.

4.3 Results for one MPI Process

This section presents results for serial execution with one MPI process (NP = 1) on node20 and compares

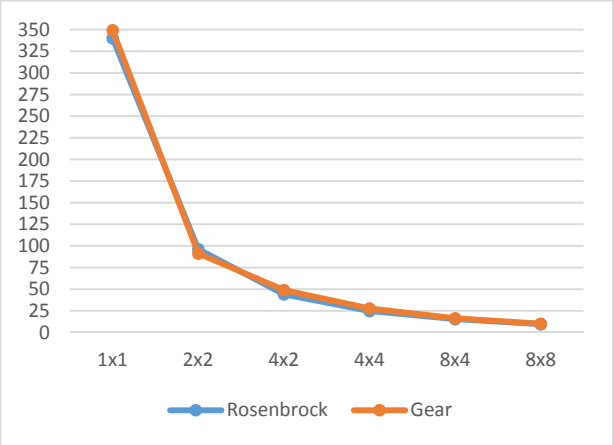

Fig. 4 Wall clock time (minutes) versus MPI process count (assigned row x column) for the EPA JSPARSE version of CMAQ for Rosenbrock and Gear algorithms.

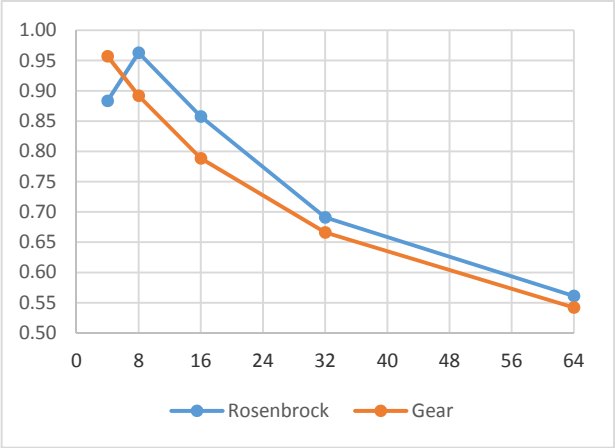

Fig. 5 Corresponding to the times of Fig. 4 this shows MPI parallel efficiency versus MPI process count for the EPA JSPARSE version of CMAQ for Rosenbrock and Gear algorithms.

JSPARSE and FSPARSE versions of CMAQ. For this discussion Table 6 defines the major CMAQ science processes and their acronyms.

To compare JSPARSE and FSPARSE version, Figs. 6 and 7, respectively, show the fraction of wall clock time as a function of science process, for Gear and Rosenbrock algorithms. The CHEM and AERO processes dominate with diminishing contributions to wall clock time for others. For the Gear case with JSPARSE (Fig. 6) the fraction of the total runtime used by CHEM dominates at ~50%. The next largest fraction, at ~26%, is AERO, and all other science processes have considerably smaller fractions. For the Rosenbrock case with JSPASE (Fig. 7) AERO is the dominant process, but CHEM is close to ~33%. Therefore any improvement in the CHEM subroutine will significantly impact the total wall clock time. Such an improvement is visible in the FSPARSE case for both Gear (Fig. 6) and Rosenbrock (Fig. 7) algorithms when comparing the effects of increasing thread count in the range 8, 12, 16 (omp8 to omp16). In the last case the FSPARSE CHEM fraction is half of the EPA JSPARSE value. This shows that the fraction of time consumed in CHEM diminishes, and as it does so the fractions of other science processes correspondingly increase.

Table 6 CMAQ science processes and the module name.

Process and function	module name
CCTM Chemical transport model	CHEM
Aerosol species processing	AERO
Asymmetric convective model (ACM) for vertical diffusion	VDIFF
Photolysis processes	PHOT
Advection in the horizontal plane	HADV
Advection in the vertical (Z) direction	ZADV
ACM and resolved cloud processes	CLDPROC
Horizontal diffusion	HDIFF
Couple concentration values for transport	COUPLE
Decouple concentration values for transport	DECOUPLE

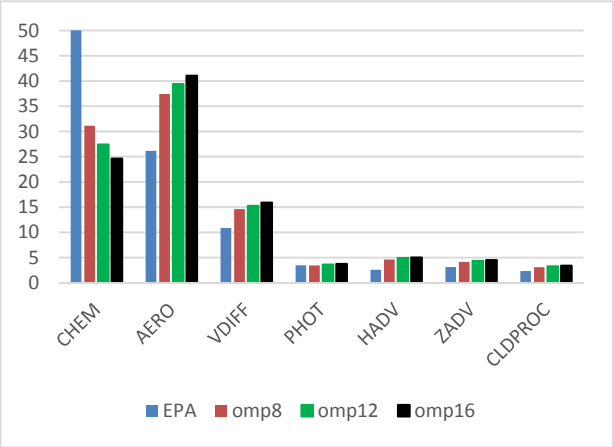

Fig. 6 Fraction of wall clock time (percent) by science process in CMAQ for the FSPARSE Gear algorithm compared to JSPARSE (EPA) for NP = 1 MPI process and OpenMP thread counts of 8, 12, and 16 (omp8, omp12 and omp16).

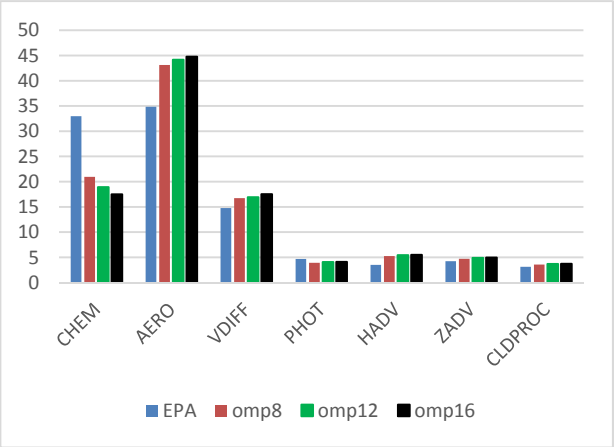

Fig. 7 Fraction of wall clock time (percent) by science process in CMAQ for the FSPARSE Rosenbrock algorithm compared to JSPARSE (EPA) for NP=1 MPI process and OpenMP thread counts of 8, 12, and 16 (omp8, omp12 and omp16).

In more detail, Fig. 8 shows the speedup of FSPARSE over JSPARSE for thread counts of 8, 12, and 16, in 288 individual calls to CHEM for the full 24 hour simulation with the best results for 12 or 16 threads (with speedup ~3). Because of the core count limitations on the blade server (node27 to 34), a default of 8 threads is chosen for execution on the heterogeneous cluster.

Table 7 lists the total time (in minutes) expended individually for each of the physical processes in CMAQ for the 24 hour episode described in Section 3.3. The results for node20 with NP = 1 are separated for Gear and Rosenbrock CCTM algorithms in CHEM. The original (JSPARSE) results are compared with the FSPARSE version for 8 threads, and the Total entry shows the speed up in parentheses: 1.32 (Gear) and 1.14 (Rosenbrock), respectively.

4.4 MPI Speedup and Scaling (Heterogeneous Cluster)

To compare the effects of increasing MPI process count for JSPARSE and FSPARE versions of CMAQ, Table 8 shows the fraction of wall clock times in MPI communication, serial computation, and OpenMP regions (in the case of FSPARSE). What was only serial computation in JSPARSE, is split into serial and OpenMP fractions in FSPARSE. Two important

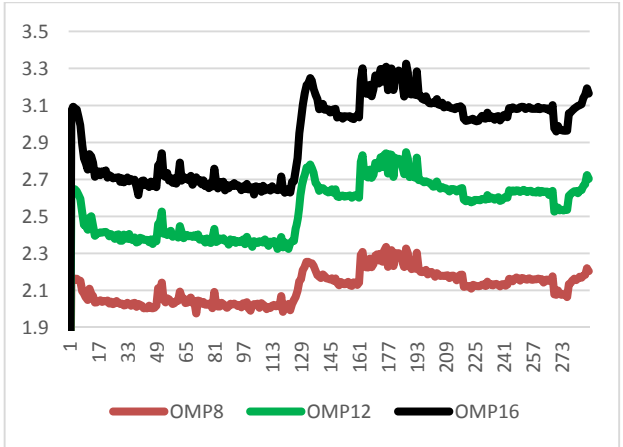

Fig. 8 Parallel thread speedup over the standard U.S. EPA model in 288 calls to CHEM with the Gear algorithm for 8, 12 and 16 threads (OMP8 to OMP16), for NP = 1 MPI process.

Table 7 CMAQ wall clock times (minutes) by science process for a 24 hour simulation with NP = 1 for the Gear and Rosenbrock algorithms in the CTM.

Science process	JSPARSE		FSPARSE (8 threads)	
	Gear	Rosenbrock	Gear	Rosenbrock
Total	496.2	390.2	374.9 (x1.32)	328.3 (x1.14)
CHEM	248.2	128.7	116.7	68.8
AERO	129.8	135.9	140.3	141.5
VDIFF	54.0	57.7	54.7	55.0
PHOT	17.3	18.3	17.4	17.2
HADV	12.9	13.7	12.9	12.9
ZADV	15.6	16.5	15.5	15.4
CLDPROC	11.6	12.2	11.7	11.7
HDIFF	2.20	2.36	2.18	2.18
COUPLE	1.97	2.10	1.80	1.80
DECOUPLE	2.57	2.73	1.82	1.82

Table 8 For the heterogeneous cluster this shows CMAQ fraction of wall clock time (percent) in MPI, serial, or OpenMP time, in a one-day simulation, for the Gear algorithm in the CTM for the number of MPI processes (NP) shown in the first column.

NP	JSPARSE		FSPARSE (8 threads)		
	MPI	Scalar	MPI	Scalar	OpenMP
4	13.5	86.5	10.9	61.0	28.1
8	15.1	84.9	11.0	62.1	26.9
16	27.2	72.8	15.5	51.3	33.2

observations are that MPI process time increases with increasing NP, but less so for the FSPARSE case. Also, as expected, note the diminished scalar time in the FSPARSE case.

Fig. 9 shows the speedup of the FPSARSE version (with 8 threads) over the EPA JSPARSE original for Gear and Rosenbrock algorithms. These executions were on the heterogeneous cluster, with one MPI process on node20, and others on individual blade nodes for NP = 4, 8, 16. Speed up in the Rosenbrock case is less than that of the Gear algorithm because there is less arithmetic computation per thread (i.e., reduced computational intensity per thread). A notable feature of Fig. 9 is the diminution in speedup for NP = 16 cases. This is the consequence of two observations. First is the diminished workload per thread because of the reduced block count with increasing NP (as noted above in Section 3.3). Second is that 4 MPI processes are on each of the two fastest nodes. Overall the speedup ranges from 1.16 to 1.46 (Gear) and 1.01 to 1.25 (Rosenbrock).

4.5 MPI Speedup and Scaling (Homogeneous Cluster)

For execution on the homogeneous cluster (node20 and 21), Figs. 10 and 11 compare performance results for Rosenbrock and Gear algorithms with 8, 12, and 16 threads, on each node, and NP = 1, 4, and 8. Speedup with FSPARSE is relative to the EPA JSPARSE version executed on the same homogeneous cluster configuration. Here, for Rosenbrock, the speedup

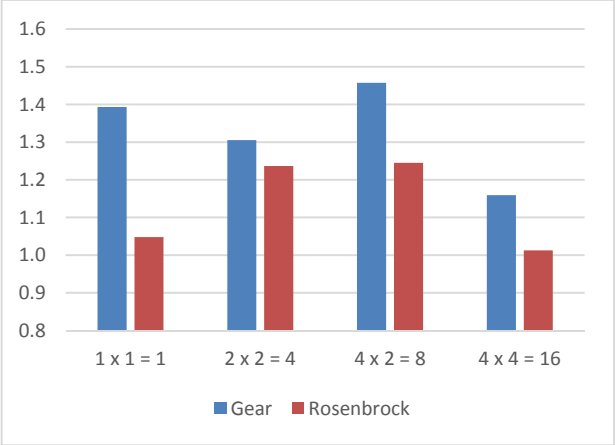

Fig. 9 Parallel thread speedup over the standard U.S. EPA model for the Gear and Rosenbrock algorithms with 8 threads, for NP = 1 to 16 MPI processes (assigned row x column) on the heterogeneous cluster.

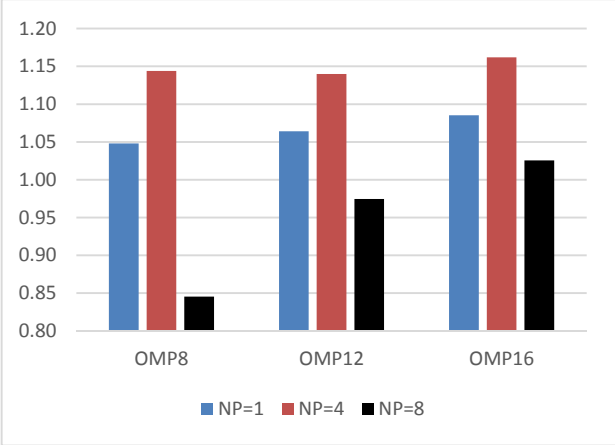

Fig. 10 Parallel thread speedup over the standard U.S. EPA model for the Rosenbrock algorithm with 8,12, and 16 threads, for NP = 1 to 16 MPI processes (assigned row *x* column) on the homogeneous cluster.

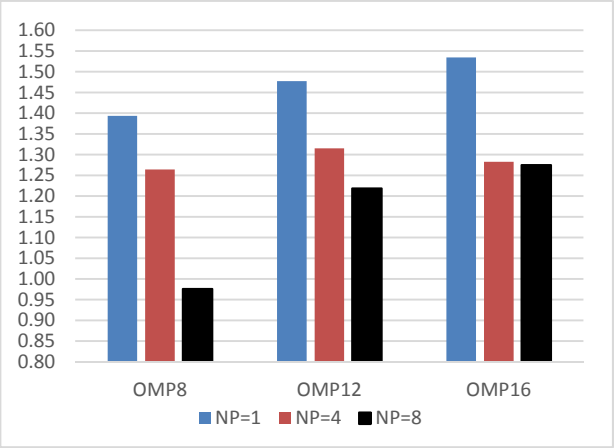

Fig. 11 Parallel thread speedup over the standard U.S. EPA model for the Gear algorithm with 8,12, and 16 threads, for NP = 1 to 16 MPI processes (assigned row *x* column) on the homogeneous cluster.

ranges from 0.85 to 1.14 (8 threads), 0.97 to 1.14 (12 threads), and 1.03 to 1.16 (16 threads). Whereas for Gear, the speedup ranges from 0.98 to 1.39 (8 threads), 1.22 to 1.48 (12 threads), and 1.27 to 1.53 (16 threads).

Speedup for the Rosenbrock algorithm is overall less than that for Gear due to less arithmetic work per thread compared to Gear. It is interesting to observe the increasing speedup for 16 threads when NP = 8, even though cores are oversubscribed. The core count is limited to 32 per node and this means that the FSPARSE case may be limited by thread population counts per node. Never the less, cores can be oversubscribed by hosting more than one thread on each. Such oversubscription occurs with16 OpenMP threads per MPI process for NP = 8 (with 4 on each node) resulting in a total 64 threads per node sharing 32 cores. For example, with 16 threads and NP = 8, speedup is in the range 1.03 (Rosenbrock) and 1.27 (Gear). Part of the explanation for this phenomenon (in the Gear case) when cores are oversubscribed, is due to the fact that calls to CHEM from different grid cell blocks are asynchronous and contention for core resources on the CPU is ameliorated.

Table 9 repeats the measurements of Table 8, but now for the homogeneous cluster case of node20 and 21 again with 8 threads. Whereas the fraction of wall clock time in MPI communication rises in the

Table 9 For the homogeneous cluster this shows CMAQ fraction of wall clock time (percent) in MPI, serial, or OpenMP time in a 24 hour simulation for the Gear algorithm in the CTM for the number of MPI processes (NP) shown in the first column.

NP	JSPARSE		FSPARSE (8 threads)		
	MPI	Scalar	MPI	Scalar	OpenMP
4	11.4	88.5	11.5	57.3	31.1
8	13.2	86.7	9.7	46.5	43.6
16	17.8	82.1	11.7	45.9	42.2

JSPARSE case, it is significantly reduced in the FSPARSE algorithm. Also the increased fraction in the OpenMP parallel region is obvious.

5. Numerical Analysis

5.1 Chemistry Convergence Criteria

To understand numerical precision this section discusses some numerical metrics that affect concentration value predictions in CMAQ. In the CCTM convergence is controlled in both Gear and Rosenbrock methods by accuracy parameters ATOL and RTOL. In the standard U.S. EPA version of CMAQ the default values chosen are RTOL = 1.E-03 and ATOL = 1.E-09 for the Gear algorithm, whereas Rosenbrock uses ATOL = 1.E-07. The choice ATOL = 1.E-09 for Gear is based on the heuristic observations in Ref. [19].

5.2 Norms in the Concentration Solution

There are two classes of error in this application of the Gear solver. The first is the global and local error metrics used in controlling the progress of the Gear, or Rosenbrock, algorithm chemistry time stepping algorithm controlled by the parameters RTOL and ATOL. The other class of error is demonstrated in metrics that show precision after the decomposition and solve steps of the sparse linear system Ax = y. Such metrics are monitored in FSPARSE with an option to calculate several types of norms including |A|, |x|, and |Ax-y|. In the CC formulation the norms are chosen as the infinity norms, norm(Ax – y, inf), norm(x, inf), and norm(y, inf), where the length of the vector (Ax-y, x, or

y) is the number of chemical species. The "inf" norm selects the maximum value of each vector. While details are not shown here these norm results suggest that the residual remains very small in the FSPARSE algorithm for the chemistry solver.

Previous study has shown that correlation between the value of ATOL and the norm of the residual for solution of the sparse linear system is negligible. This leaves open the choice that optimizes both runtime and accuracy for species concentrations.

5.3 Species Concentration Predictions

A direct comparison of accuracy for species concentration values predicted by the FSPARSE version against the U.S. EPA standard release of CMAQ is shown in Figs. 12 (a) to (d) for four selected species concentrations: O_3, CO, SO_2, and NO_2, respectively. These are absolute errors for all 8,000 concentration values of each selected species in layer 1 at the end of a one-day simulation. The solid line is the species concentration value predicted by JSPARSE for a single MPI process (NP = 1) ranked in increasing magnitude from left to right. Corresponding to each value, the difference (scattered points) is the absolute error value of the concentration between FSPARSE and the JSPARSE result. The first feature to note in the results is that O_3 and CO concentration values are of similar magnitude and differ in less than an order of magnitude over the full range. Whereas, SO_2 varies by over four orders of magnitude, and NO_2 by two orders of magnitude. Therefore a uniform precision in significant figures of accuracy would have to be more

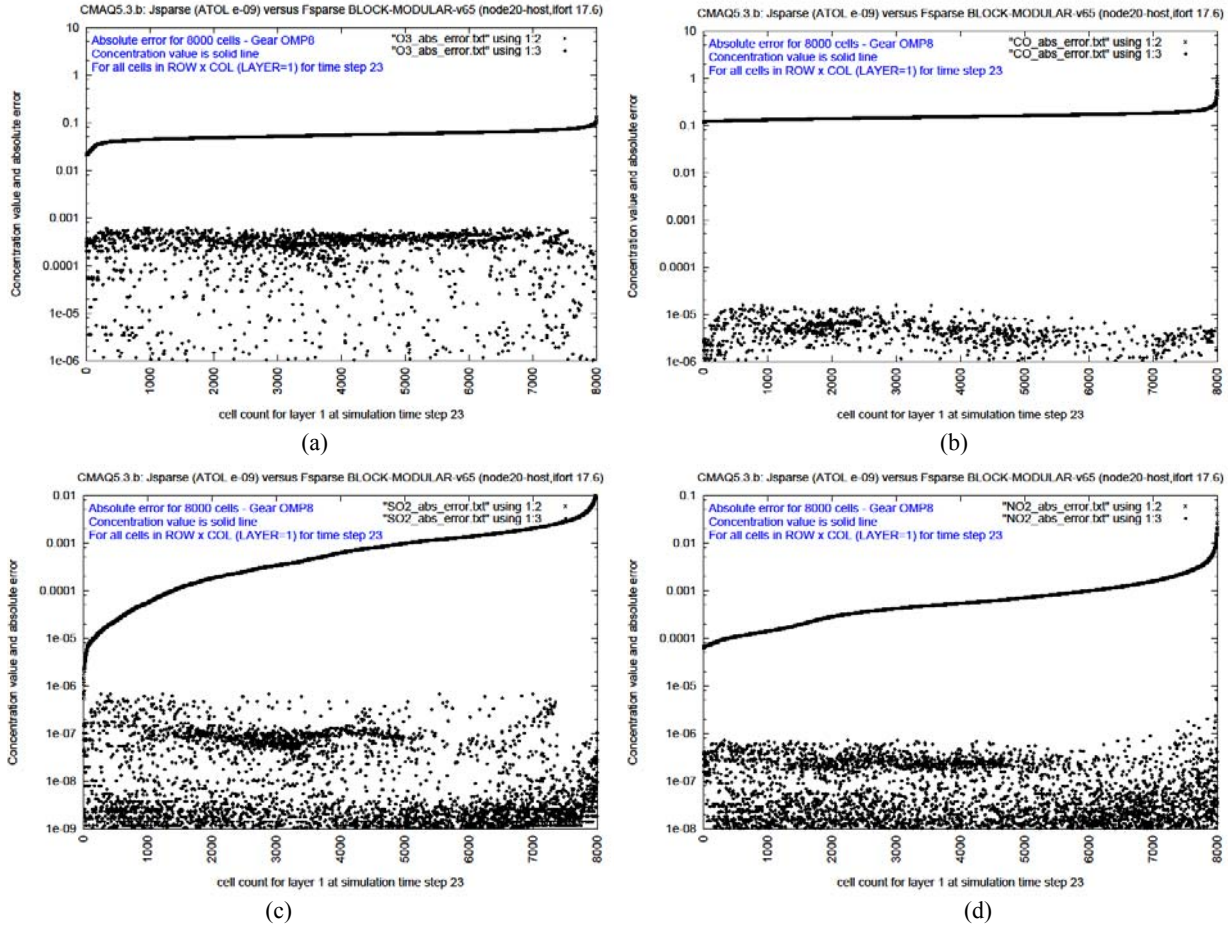

Fig. 12 For the FSPARSE GEAR solver of CMAQ (with 8 OpenMP threads) this shows the species concentration absolute error (scattered points) and concentration value (solid line) for 8000 values in layer 1 of the domain for species O_3 (a), CO (b), SO_2 (c), and NO_2 (d). The ranking is in increasing concentration value from left to right.

than 4, and this is hardly possible if a relative tolerance RTOL = 1.E-03 is applied for the L_2 norm over species concentration in the Gear convergence criterion. The second feature to note is that the absolute error threshold ranges from 1.E-02 (O_3) to 1.E-05 (CO) below the corresponding concentration value. Therefore the anticipated accuracy in the Gear solver in CMAQ differs for different species. However, in view of the precision issues noted above, these results are deemed as acceptable pending test with constrained values of RTOL and ATOL. However, such tests are limited by the use of single precision values passed to the CCTM by other CMAQ processes.

6. Lessons Learned

6.1 Benefits of the FSPARSE Method

Comparing performance for CMAQ 5.3b in the new OpenMP parallel version with the U.S. EPA release with either Gear or Rosenbrock chemistry solver showed:

- A speedup in the range 0.9 to 1.5 depending on the parallel thread and MPI process counts.
- Comparable numerical precision in species concentration values.

6.2 Comparing Species Concentrations

A comparison of species concentration values predicted by JSPARSE and FSPARSE versions of CMAQ showed acceptable agreement for species such as O_3, NO_2, NO_3, SO_2, and others not shown. Remaining differences in species concentration values could be due to cumulative error propagation in the U.S. EPA method.

7. Conclusions

This study reported on major performance enhancements for the Community Multi-scale Air Quality Model (CMAQ) chemistry-transport model (CCTM) that add new levels of parallelism and replace the legacy algorithm in the Gear and Rosenbrock methods. The CCTM is computationally intensive when the Gear (or Rosenbrock) algorithm is used to solve a stiff system of ordinary differential equations (ODE), with sparse Jacobians, and accounts for over 50% (or 33%) of the wall clock time of a simulation. To improve performance two important changes were made, the first of which replaced the sparse matrix solver. The second modification integrated the new solver into the transit over the grid domain so that separate blocks of cells are distributed to different threads in a team. The resulting sparse solver (FSPARSE) replaced the legacy JSPARSE sparse method. The FSPARSE solver is portable across hardware and compilers that support vector and thread parallelism and it adds both to the existing distributed memory (message passing) level in the standard EPA CMAQ release. Observed numerical differences between the two methods are related to the numerical precision achieved in each, and were observed to be due (in part) to the way arithmetic precision is treated in the U.S. EPA method. On Intel platforms a 24-hour simulation on a continental U.S.A. grid of 280,000 cells, showed that with 8 to 16 threads the FSPARSE version of CMAQ typically provides significant speedup over the standard EPA release without loss of precision in predicted concentration values.

References

[1] U.S. EPA, Office of Research and Development, National Exposure Research Laboratory (NERL), Computational Exposure Division, available online at: https://www.epa.gov/aboutepa/about-national-exposure-research-laboratory-nerl-computational-exposure-division-ced.

[2] Community Modeling and Analysis System, available online at: http://www.cmascenter.org/cmaq/.

[3] University of North Carolina, Institute for the Environment, available online at: https://ie.unc.edu/.

[4] CMAQ, available online at: https://www.epa.gov/cmaq, https://github.com/USEPA/CMAQ.

[5] U.S. EPA Clean Air Act, available online at: https://www.epa.gov/laws-regulations/summary-clean-air-act.

[6] John L. Hennessy and David A. Patterson, *Computer Architecture: A Quantitative Approach* (4th ed.), Morgan Kaufmann Publishers, Elsevier, Amsterdam, 2007.

[7] Intel Corporation, available online at: http://www.intel.com.

[8] D. W. Byun and J. K. S. Ching, Science algorithms of the EPA Models-3 community multiscale air quality (CMAQ) Modeling System, United States Environmental Protection Agency, Office of Research and Development, Washington, DC, EPA/600/R-99/030, March 1999, available online at: https://www.cmascenter.org/cmaq/science_documentation.

[9] Leon Lapidus and John H. Seinfeld, *Numerical Solution of Ordinary Differential Equations*, Academic Press, New York, 1971.

[10] W. H. Press, S. A. Teukolsky, W. T. Vetterling and B. P. Flannery, *Numerical Recipes in FORTRAN* (2nd ed.), Cambridge University Press, New York, 1992.

[11] G. Delic, *12th Annual CMAS Conference*, Chapel Hill, NC, October 28-30, 2013, available online at: https://www.cmascenter.org/conference/2013/agenda.cfm.

[12] T. Clune, M. R. Damon and G. Delic, *14th Annual CMAS Conference*, Chapel Hill, NC, 2015, available online at: https://www.cmascenter.org/conference/2015/agenda.cfm.

[13] C. William Gear, The automatic integration of ordinary differential equations, *Comm. ACM* 14 (1971) 176-179.

[14] M. Jacobson and R.P. Turco, SMVGEAR: A sparse-matrix, vectorized Gear code for atmospheric models, *Atmos. Environ.* 28 (1994) 273-284.

[15] M. Z. Jacobson, *Fundamentals of Atmospheric Modeling* (2nd ed.), Cambridge University Press, New York, 2005.

[16] C. William Gear, *Numerical Initial Value Problems in Ordinary Differential Equations*, Prentice-Hall, Englewood Cliffs, New Jersey, 1971.

[17] Cray computer, available online at: http://www.cray.com/, http://en.wikipedia.org/wiki/Vector_processor.

[18] Jeffrey O. Young and G. Delic, *7th Annual CMAS Conference*, Chapel Hill, NC, October 6-8, 2008, available online at: https://www.cmascenter.org/conference/2008/agenda.cfm.

[19] G. D. Byrne and A. C. Hindmarsh, Stiff ODE solvers: A review of current and coming attractions, *J. Comput. Phys.* 70 (1987) 1-62.

[20] I. S. Duff, A. M. Erisman, and J. K. Reid, *Direct Methods for Sparse Matrices* (2nd ed.), Oxford University Press, 2017.

[21] T. A. Davis, *Direct Methods for Sparse Linear Systems*, SIAM, Philadelphia, 2006.

[22] Åke Björck, *Numerical Methods for Least Squares Problems*, SIAM, Philadelphia, 1996.

Modern Environmental Science and Engineering (ISSN 2333-2581)
September 2019, Volume 5, No. 9, pp. 792-802
Doi: 10.15341/mese(2333-2581)/09.05.2019/002
Academic Star Publishing Company, 2019
www.academicstar.us

Nuclear Licensees Activities in Japan for Mindfulness of Nuclear Safety

Akihide Kugo
Japan Nuclear Safety Research Institute, Japan

Abstract: The IAEA Report on Fukushima Daiichi Accident indicated that a basic assumption or preconception was widely shared by the nuclear industry in Japan and it led to a thought which made Japanese nuclear operators not being proactively prepared for unexpected severe accidents. To prevent the recurrence from holding such an assumption, organizational culture for nuclear safety led by top management and followed by all employees will be a key issue. Top management of Japanese nuclear operators have been making much efforts to improve their corporate culture, not only complying with the regulatory standards but also enhancing self-regulated excellence. This paper introduces their voluntary efforts in the light of human and organizational aspects and analyzes their ex-assumption and discusses measures to break negative thought chain.

Key words: leadership, culture for safety, organizational culture, human factor

1. Introduction

After the devastating Fukushima Daiichi Nuclear Power Plant accident (hereafter, the "Fukushima Accident") in 2011, new safety regulatory standard in Japan has been come in to effect July 2013. The operators strengthened equipment modification and operation management to meet this new regulatory standard, and applied for conformity examination for 27 nuclear reactors. As shown in Table 1, as of May 2019, fifteen nuclear reactors have passed the Nuclear Regulation Authority's conformity review, and nine units among them currently in operation after completion of construction work. Therefore, nuclear operators which have already succeeded in plant restarting should much more focus on management for safe operation as it is commonly shared that one of the factors behind the Fukushima Accident is that the Japanese operators fell into overconfidence and were not proactive about preparing for unexpected risks. For this reason, it has been pointed out that we must examine measures focusing on the organizational culture for nuclear safety.

This paper describes operators' voluntary activities by focusing on operators' efforts of strengthening the organizational culture and discusses on the countermeasures for thorough utilization of operating experience based on the lessons learned of Fukushima Accident.

First, challenges of nuclear operators by focusing on organizational perspectives which are derived from the lessons learned of Fukushima Accident are described in chapter 2. Second, in chapter 3, activities for strengthening safety consciousness are introduced, which are divided into four categories such as 1) enhancing safety consciousness, 2) reinforcing risk management, 3) improving communication environment, and 4) strengthening governance of operator's activities. Third, in chapter 4, consideration on the measures which would enable nuclear operators to avert falling into basic assumptions that negatively affects nuclear safety is explored in light of the necessity of more focusing on the human-organization

Corresponding author: Akihide Kugo, Ph.D.; research area/interest: risk communication, organizational culture, nuclear safety. E-mail: kugo.akihide@genanshin.jp.

Table 1 Current status of nuclear power plants in japan, review on conformity to new regulatory requirement (as of May 20, 2019).

	Number of units	Output (Mwe)	Application by operator	Official approval by NRA	Restart of commercial operation
Operationunits/Operable units	37	37483	25	15	9
Under constraction units	3	4141	2		
Total	40	41624	27		
Closed down units	23	13480			

aspects. Finally, conclusion is summarized in chapter 5.

2. Challenge for Organizational Culture

The government accident investigation report and the Diet accident investigation report, which summarized the causes and lessons of the Fukushima Accident, indicate that the nuclear operators in Japan (including Tokyo Electric Power Company; hereafter TEPCO) were laboring under the assumption that a severe accident could not happen in Japan and were unable to comprehend a hazard as a potential reality that could occur [1, 2]. Now that this assumption has been recognized, it is important that it gives rise to an organizational culture reform for operators.

This assumption resulted in Japan's nuclear power industry being vulnerable in its preparation for a situation where a reactor core is seriously damaged due to a tsunami or other natural disaster. When this situation actually arose, the emergency response demonstrated how an organization was powerless or less leadership toward unexpected situation. The government accident investigation report describes that, at the time of actual emergency response, the sense of a vertically-structured organization was not strong, which made flexible response difficult for tasks that had not been assumed previously.

TEPCO's reported its activities aim to change the organizational culture that resulted in such a situation by breaking the organization's negative "chains of thought" from the following three viewpoints [3, 4].

The first viewpoint is cutting off certain chains of thought: of underestimating the uncertainty of the risk of external events, of not trying to learn from the operating experience of other companies, and of not recognizing that safety improvement should be tackled every day. This will result in outgrowing the assumption that safety has already been established.

The second viewpoint is outgrowing the chain of thought of not incorporating the design technical capabilities into the company by considering availability as an prioritized issue for management, being devoted to equipment modifications that contribute to the current availability improvement, and excessively depending on the design technique of the manufacturer to put it into practice, as well as the chain of thought of depreciating on-site capabilities (such as the employees not having practical technical capabilities) as a result of leaving all site work to partner companies and the company's having treated emergency training as a formality.

The third is the viewpoint of outgrowing the atmosphere in which employees believe that the current level of nuclear technology is sufficient to ensure safety and are hesitant to raise issues proactively, even if they notice a risk that exists in their facilities.

In the next chapter, the current activities of nuclear operators for improving organizational culture such as 1) strengthening safety consciousness which focuses on top management's safety consciousness reform, activities of instilling safety attitudes and leadership training for emergency, 2) risk management which focuses on handling of hazards, utilization of operating experience and emergency commanding and on-site capabilities in an emergency, 3) securing communication environment, and 4) strengthening governance of operator's activities are introduced.

3. Improving Organizational Culture

3.1 Strengthening Safety Consciousness

3.1.1 Reform of Top Management's Consciousness

The most important matter in strengthening the organizational culture of safety must be reforming the top management's consciousness. JANSI educates CEOs, CNOs, or other senior executives of nuclear operators on the concept of independent oversight in order to supervise and perform surveillance of the unconscious, inherent risks that undercut safety for the purpose of risk management. JANSI also provides leadership training programs focused on human skills, including conductor's skills at the time of emergency and communication skills.

3.1.2 Permeation of Culture for Safety

The government accident investigation report says of the organizational culture of TEPCO that "the attitude of the employees of the company was not proactive enough to face the situation by themselves, and the flexible and positive thinking needed for crisis resolution was lacking". To improve this aspect of the employee passive attitude, TEPCO started establishing a behavior pattern to fix the organization's safety culture. The behavior pattern is that each day, every worker takes about 10 to 15 minutes to ask themselves if their behavior that day was adequate in comparison with the excellent attributes of safety culture. The results are then scored and entered into the computer system to calculate the total score. When the total shows unusual or abnormal trends, TEPCO holds both a regular group discussion and a special discussion to find out the cause. Naturally, the status of this activity is reported to the management meeting, which then brings it to further action, if necessary.

The purpose of these company-wide activities is for each employee to regularly take the opportunity to reflect on familiar safety-related matters and develop it into way of thinking that they try to master nuclear safety for themselves.

3.1.3 Leadership Training for Emergency

On-site Emergency Management Drill is one of the courses of leadership training that JANSI provides to operators. JANSI developed this program based on the individual experiences at the control rooms and the on-site headquarter. Some of the experiences had been openly described in accident investigation reports as semantic memories. On the other hand, other experiences had been only kept personally as episodic memories. These seldom experienced lessons should be shared among all nuclear operators and transferred to next generation. Therefore, by integrating their semantic and episodic memories into a training drill scenario, training drill program is implemented in the simulated alternative conditions of Fukushima Accident with the very difficult mission.

Participant who joined this training program would be able to have the similar experience of Fukushima Accident as an episodic memory. JANSI expects that participants will bring their individual episodic memory back to their site and they will make similar scenarios of drills for their colleagues at their site, finally leading their training experience to their unconscious skills as their procedural memories. The concept of this program is aiming at an exercise in which participants come to realize that the situation is one that they cannot bring to an end if they don't try proactively to solve a problem.

3.2 Strengthening Risk Management Process

3.2.1 Risk Identification

Risk management procedures generally begin from risk identification and risk profiling first. Corrective action program contributes to gathering potential risks and hazard analysis also contributes to precise risk profiling. The ability to efficiently carry out both corrective action program and hazard analysis are both fundamental elements in risk recognition.

The government accident investigation report says that, before the Fukushima Accident, operators were not proactive about taking measures for events that seemed to be infrequent or uncertain. It means that the

attitude of risk identification and hazard analysis revealed unfortunately insufficient for unexpected severe accident. After the accident, operators have been trying to revise such attitudes. For example, TEPCO established a full-time team to carry out hazard analysis. The mission of this team is to positively put potential hazards to an agenda of company-wide risk management meeting without hesitation, even if they occur infrequently and it is uncertain to what extent they may cause serious damage. As a company-wide risk management objective, operators in Japan are paying attention not only to events that would have an economic impact on their economic performance but also to those that pose a risk to nuclear safety and social trust.

3.2.2 Importance of Operating Experience

Also, given that the Fukushima Accident was caused by a lack of understanding of the risk of external events, it is understood that both the willingness to study continuously and the willingness to express doubt are indispensable to an organization.

To strengthen the willingness to study continuously, all TEPCO personnel who are engaged in the nuclear business participate in a training program that reviews operating experience from around the world. Participants engage in debate comparing the lessons obtained from accidents such as the accident at the Three Miles Island nuclear power station with the Fukushima Accident.

3.2.3 Emergency Commanding

Nuclear Operators in Japan (including TEPCO) had prepared manuals that define the establishment of an emergency headquarters etc. to cope with nuclear hazards. They had also prepared functional groups such as a power generation group, a restoration group, and a technical support group in the headquarters, and they have allocated roles for event response. However, looking back on the situation at the time of the Fukushima Accident, these functional groups were not able to effectively make decisions or give directions quickly and appropriately because they were confused by facing a situation where multiple nuclear reactors were damaged. In such chaotic situation there were naturally miscommunications between the on-site headquarter and the head office headquarter.

Taking this into consideration, TEPCO for example, has reduced the range of the conductor's management span by introducing an incident command system and decentralizing the plant director's role in the unit directors responsible for each unit. This is to ease the burden on the plant director, who is the highest director of the on-site headquarters. Emergency staffs are also repeatedly carrying out exercises that simulate the Fukushima Accident to confirm information sharing and instructions with the head office and the regulatory body.

3.2.4 On-site Capabilities in Emergency

It was also made clear that conventional table-top training and book knowledge alone are not sufficient for the inherent qualities and abilities needed in the event of a severe accident like this one. Emergencies necessitate the abilities to consider all possibilities based on the available information, to sort out the cases obtained from the information, and to quickly determine which matters require action and then take such action. Considering these lessons, to support the conductor's decision making, TEPCO is making efforts to develop systems engineers who comprehend the design requirement functions and can propose measures from the viewpoint of defense in depth.

Also, the nuclear operators in Japan recognize that it is difficult to receive external support in such a serious situation, especially in the early stages of accident, and that the top priority is first to master for themselves the ability to react quickly so that they can complete the countermeasures that are necessary for the time being.

3.3 Communication

3.3.1 Internal Communication

Looking back the history of Fukushima plant, pre-alarms were occasionally sounded based on the latest technology and similar operating experiences. The

question has been raised of to what extent these alarms were truly comprehended among management level, in the height evaluation of the tsunami that directly caused the Fukushima Accident and in the review of experience of the unavailability of emergency diesel generator due to leakage from sea water pipe line, for examples.

More than a few people must have felt that it was risky to have an emergency DG or switchboard installed in the turbine building on floors below sea level. It is recognized that there is a need to enhance communication abilities so that the risks that workers perceive can be shared in the organization. Accordingly, it has been decided in TEPCO to appoint a new, full-time executive manager called the Corporate Functional Area Manager (CFAM) and the Site Functional Area Manager (SFAM) to play the role of the facilitator who reports such concerns to upper-level personnel.

3.3.2 External Communication

There are variety of stake holders including regulatory body and local governments around nuclear plants. When the Fukushima Accident happened, huge communication gaps between the operator and stakeholders were recognized. It seems to take long time to close these gaps by gaining mutual trust. To strive for this difficult challenge, TEPCO assigned the special staff to sincerely deal with local government and residence people.

3.4 Corporate Governance

3.4.1 Oversight

To strengthen defense in depth philosophy comprehensively, it is important to secure diversity in risk awareness. So that they can obtain advice from objective, external viewpoints and from different perspectives, some Japanese operators have established an oversight committee that reports to and advises a certain management level.

For example, TEPCO is undertaking organizational management reform as described above, and other operators are also working on organizational culture improvement activities to outgrow the assumption that was a background factor of the Fukushima Accident, albeit in different forms and depths as suits each operator. For TEPCO, the independent oversight department is separate from the company's execution line, and it checks these line activities whenever necessary as is called nuclear oversight.

TEPCO has also established a nuclear safety advisory committee of very experienced external experts who had been involved in nuclear business for long times. In this external committee, management member is advised objectively based on the external different viewpoints and experiences toward nuclear safety at the site activities, which is called external oversight. Further, to perform surveillance of whether these companywide activities toward nuclear safety reform are being carried out smoothly, TEPCO has established a nuclear reform surveillance commission of domestic and overseas experts as the consultative body of the board of directors. By reporting the progress of these activities every year and releasing all the results to the public, TEPCO is making efforts toward restoring society's trust.

It is expected that the activities of this committee will bring to light the basic assumption that safety is already ensured, which was indicated as a background factor of the Fukushima Accident.

3.4.2 Peer Pressure

The function of checks and balances among peers, peer pressure in other words, is also an important keyword. It is expected that the CEO's commitment to the results of peer review (in which the behavior of people in the field is compared with the global excellences of the industry) is shared among the CEOs of operators, and thereby serves as peer pressure. Peer pressure among top management of each operator will certainly increase the safety consciousness of people of the on-site field.

So far, the current state of operators' activities for improving organizational culture for nuclear safety has

been introduced. The discussion points to make these activities more effective will be described in the following chapter 4 from the five viewpoints of human characteristics such as selective attention, heuristic decision making, protective attitude for organization, judging other stakeholders by yourself, and influence of vertical prioritized authority, which are updated from my previous research paper [5].

First, the elements of concern of why operating experience and the latest technical knowledge cannot be utilized are described in section 4.1. Second, the countermeasure towards each element is described in section 4.2

4. Discussion

4.1 Why Operating Experience and the Latest Knowledge Cannot Be Utilized

4.1.1 Selective Attention

The IAEA Director General Report on the Fukushima Accident states "The reinforced basic assumption among the stakeholders about the robustness of the technical design of NPPs resulted in a situation where safety improvements were not introduced promptly" [6].

Certainly, the operators had pride in their technologies based on the remarkably low scram rate on an international level and other index and were overconfident in their belief that the Japanese nuclear industry had high safety awareness and that a serious accident would not occur. This had become an unconsciously shared preconception and had permeated the awareness of those involved in the nuclear business.

We cannot deny the possibility that this assumption acted as a cognitive bias, causing underestimation of the scale and the probability of hazards. If the assumption is a major factor behind the Fukushima Accident, it is necessary to review the characteristics of human beings and organizations.

One of the characteristics can be "selective attention", a universal human characteristic [7]. As a behavioral trait, once we are given a task and our attention is focused on that task, then we begin to select information necessary for efficiently achieving the task at hand. Experimental psychology has proven that "beliefs" affect this selection mechanism and that we all have a train where we adopt "tunnel vision," a state of narrow-mindedness where despite seeing things with our eyes, we do not see them with our brain. This is called "selective attention." When this characteristic is at work, we concentrate too much our awareness on the target and fall into a state where our visual field narrows, meaning that our brains may not recognize the objects in our surrounding vision. This mechanism illustrates that once this switch is flipped, it engages the information choice function of the reticular activating system, and the brain preferentially intakes information with a high degree of necessity and urgency to itself. Conversely, if information is considered as a low level of necessity or urgency, the brain eliminates it unconsciously. In a behavioral psychology experiment, when subjects were asked to observe an experimental video and given a task–such as to answer how many times a sports team in a white uniform successfully exchanged passes–the result was that subjects concentrated excessively on carrying out this task, with many failing to notice the other peripheral information entirely.

When considering nuclear safety, first of all, the following must be recognized as a human physiological characteristic: because of the underlying preconception at work (that the Japanese nuclear industry has high safety awareness and a serious accident will not occur), there is a tendency to unconsciously suppress the feeling of cognitive dissonance (registering that something is wrong from the viewpoint of nuclear safety), and selective attention causes a tendency to underestimate the hazards.

4.1.2 Heuristic Decision

Natural threats such as large-scale earthquake and tsunami often affected living life including recording devices themselves, resulting in lost records. In such a case, it is not easy to predict the future based on past aftermath and to estimate the damage. In addition, in the 50 years histry of nuclear energy in Japan, there had been no events of loss of power supply which led to loss of core cooling function. Lack of real experience made it more difficult to recognize the reality.

That said, when people are forced to make decisions with less information, people postpone their decisions or try to make an intuitive conclusion based on small clues and their own experiences. This way of thinking by using these clues is called heuristic. Considering the situation before Fukushima Accident, it is easy to imagine that the manager who was responsible for company account and technology made a heuristic judgement when he was standing on the turning point to make a large amount of financial investment for safety, based on the consideration of uncertainity about the tsunami assessment methodology and few data for natural hazard.

4.1.3 Protective Attitude for Organization

The second of the characteristics can be an instinct which is naturally possessed by a member of organizations. The people of an organization, especially those responsible for management, have a way of thinking as a member of the organization, whereby they are careful in how they treat the information that could have a major impact on their organization. When considering the measures necessary for what may be a highly unlikely, “once in a thousand years” event, for example, it is natural for a manager to make judgment based on economic rationality and to try to avoid damaging the organization which he/her works for. The author believes that the desire to minimize the impact on management may have led them to adopt a cautious decision, delaying the investment in anti-tsunami measures.

When managing such a risk, the decision-making on whether to execute the measures is not performed just by obtaining technical information on the event’s occurrence probability and impact level on equipment (core damage); rather, it must also be recognized that an important factor in decision-making is the judgment standard of organizational defense, namely, the desire to minimize the impact on management. The preconception that a serious accident would not occur in Japan was shared by the parties, and this is thought to have acted as a bias in the decision to postpone the measures for low probability events.

4.1.4 Judging Other Stakeholders by Yourself

The management of nuclear power plants involves many parties, including municipalities with nuclear power plants and supervisory authorities. These parties are called stakeholders. These stakeholders also shared the preconception that Japan’s nuclear technology is very safe and a major accident would not occur. Since adding a new risk factor would reverse this shared awareness, there can be a strong mental resistance to doing so. It is thought that the stakeholders' feelings are inferred so as to prevent a mental mismatch between the awareness shared with the stakeholders so far and the addition of a new risk factor, and the mental position to want to avoid causing unease as much as possible and to affirm the present condition may have acted.

This resulted in the preconception shared by the parties being considered absolutely true and inviolable, and the stakeholders’ feelings were inferred, causing less recognition of the urgency in the evaluation of the anti-tsunami measures.

4.1.5 Influence of Vertical Prioritized Authority

The fourth is the characteristics brought by the organizational structure. Cultural anthropologists have contended that organizations in which personal relationships are strongly influenced by a layered structure or rank with upper and lower levels, vertical societies in other words, are weak in the ability to show interest in the outside in which it is considered

important for the attributes of the individuals constituting the organization align with the same quality or the same rank, horizontal societies in other words [8].

Therefore, in vertical society organizations, the propriety of an activity is not judged by the experience of others or by the idea professed by the organization, but rather by inferences about personal relationships with one's superiors. In this way, organizations that value vertical personal relationships tend to easily share preconceptions that are convenient for the organization, and if such preconceptions are shared for a certain period, it leads to an organizational culture. If that is the case, the organization will show no interest in the activities to internalize the important operating experiences of others and prevent failures beforehand.

Based on the characteristics of this vertical organization, one lesson learned from the Fukushima Accident seems to be that there is a need for measures to strengthen the scheme to learn the operating experiences of others.

4.2 The Way to Break Basic Assumption

4.2.1 Questioning Attitude

To escape the preconception described in Section 4.1.1 and 4.1.2, which serve as the start of selective attention and heuristic decision, it is considered to be effective for us to make intentional question by oneself, which is called "critical thinking" [9].

If a shared idea takes root in an organization, a bias effect acts on the function of selective attention in the brain, giving rise to the possibility of overlooking the elements necessary for nuclear safety. This aspect of human psychology is inconvenient for nuclear safety. To combat it, it is considered effective to ask "Is this sufficiently effective in light of nuclear safety?" and to generally question oneself. Asking questions like this trigger the brain to start to look for the answer, increasing the possibility that previously overlooked risks will be reviewed.

Needless to say, it is important to recognize that questioning oneself involves awareness of and responsibility for actions as a person involved in the inherent risks of nuclear power. This "awareness and the accompanying responsibility" means to be aware of the spatial and temporal size of the impact of a nuclear accident all the time, as well as to recognize one's role in a community. The term "hostage of each other", expresses the characteristics of the nuclear industry [10]. This term implies that in ensuring nuclear safety, it is not satisfactory just to grasp nuclear safety by focusing on the average level of a community group, and that even the lowest level members of a group should play the role of concentrating firmly on maintaining nuclear safety, with a strong awareness of the magnitude of the spatial and long-time impact that is inherent to nuclear power.

4.2.2 Oversight Function

To avoid basic assumption which can be a cause of protective attitude for an organization stated in 4.1.3, a variety of trials have been performed and proposed from past experience of management [11]. For example, deference to expertise is proposed to develop a high reliable organiztion. It is said that expertise will be born among dialogs in which people question each other and provide data and opinion in it [12].

One of these manegement systems is a monitoring organization in which the organization establishes a line that is different from the execution line and that objectively investigates the activities of the execution line in pursuit of nuclear safety, which is generally called "internal oversight" or "corporate oversight and nuclear oversight." Another is a monitoring organization that consists of experts with significant experience in nuclear safety and that provides suggestions to management from the outside of the organization, which is called "external oversight" or "Nuclear Safety Review Board."

Moreover, these activities are stratified into voluntary activities carried out by the operator, regulatory activities by regulatory organizations, mutual monitoring activities carried out by an

international framework, etc. and are proposed by IAEA as a deeply structured monitoring system [13] [14].

In the U.S. nuclear industry, for example, internal monitoring system which is called “nuclear oversight” as an independent function of monitoring is provided. In addition, another internal monitoring system called “corporate oversight” which checks the attitude of on-site managers for nuclear safety from the corporate strategic viewpoints is also provided. Moreover, external monitoring system called “Nuclear Safety Review Board” which provides the thought insight with board members and/or CEO based on the rich experiences of management of nuclear business is established. All these functions are non-regulatory activities of nuclear operators.

In addition, the peer review activities carried out by organizations such as WANO (World Association of Nuclear Operators), INPO (Institute of Nuclear Power Companies), JANSI (Japan Nuclear Safety Institute) are an example of monitoring activities carried out from outside of the organization as an operators’ framework. IAEA’s OSART (Operational Safety Review Team) is a regulatory framework as an international framework.

These multilayered activities serve to provide advice on the activities of said operator to ensure nuclear safety in light of the standard activities being conducted internationally or good practices. This will provide the parties with an important viewpoint for breaking through the preconception to carry out an actual condition survey of the field by using this function from viewpoints such as whether the pursuit of nuclear safety is obstructed by the shared value in the organization, or whether a risk is recognized properly in the same manner as others.

4.2.3 Communication and Transparency

To prevent nuclear operators to adverse action for nuclear safety in too much consideration of the relationship with the stakeholders mentioned in 4.1.4, it is necessary to ensure that high transparency between the two parties must be necessary. Intensive risk communication can be one of the measures for keeping transparency. For example, it has been already introduced that publicly operate the reviewing committee in which stakeholders participate. Furthermore, it will be necessary to reform the double regulation structure between the national government and local governments, which is behind the fact that operators feel burdensome for implementing proactive measures. The dual systems for securing nuclear safety, one is implemented by the national government from the viewpoint of state of the art technology and the other is implemented by the local governments from the viewpoint of securing peace of mind of residents, both can be requisite. However, it should be necessary to analyze the reason that this dual social systems have resulted in the delay of accident management measures.

In addition, there should be paid more attention to the characteristics of “Hindsight Bias” which is likely to lead a attitude of making a scapegoat in pursuit of the cause of failure when an accident or a scandal occurs [15]. This mental pressure may cause cover-up mistake with an excuse, so called a closed-loop phenomenon. In order to avert a closed-loop society above this, an open-loop society that seeks to learn from other people's experiences would fundamentally require the trust on the stakeholders with legal systems which could help create a climate in which freely telling accounts of what happened [16].

4.2.4 Systemic Approach

When analyzing the human behavior and organizational culture aiming at avoiding the negative impact of organizational culture as stated in 4.1.5, it can be vital to focus on the interaction between management and employees, or how the authority exerts its invisible power to the individual attitude. Social cultural scientists assume that the belief that technology does not exist without human or organization has been getting familiar among nuclear industry. For example, some scientist points out that

"To depart from technology in itself without recognition of its interaction with human and organizations makes little sense and depart from "culture" in itself without understanding how technology and organizations shape beliefs, moral, value, attitudes and behaviors is also problematic" [17].

IAEA General Safety Requirement GSR Part 2 proposes a method called systemic approach to look for preconceptions in an organization which invades nuclear safety; analyze the correlations between the people, the organization, and the technology; and try to evaluate the organizational culture comprehensively [18]. The IAEA Report on the Fukushima Accident describes the effect of systemic approach: Taking into account the interaction between all the individual, technical and organizational factors reveals the complexity and non-linearity of the operations at an NPP [19]. It is necessary to better examine the ways in which the weaknesses and strengths of all these factors influence one another in order proactively to reduce or eliminate risks. The key points of this approach is called Integrative Thinking Skills or System Thinking [20, 21]. By using these way of thinking, we should keep reluctance to simplyfy the root cause.

To activate this approach, we need knowledge not only of the natural sciences but also of the social sciences, such as organizational theory and psychology. Namely, it is necessary to have profound insights about issues such as the humility to question responsibility at all times, the leadership to act in the aim of raising the organization to a higher goal, and what the organizational culture should be in order to enhance safety.

Also, in order for an organization to discover its preconceptions and see itself objectively, the scientist on organizational culture assumes that it can be important to consider dividing the organization into the following three layers: the surface level comprising the organizational structure, rules as well as other artifacts and behaviors, the middle level comprising goals the organization is to achieve, strategic means and other such administration, and a deeper level embracing unconsciously shared values and other behaviors that are taken for granted [22]. To more accurately understand the organizational culture, it will be effective to conduct the investigation using the above monitoring function based on this organizational structure theory.

The expression "You cannot see the forest for the trees" warns us about seeking to improve the part but missing the whole. It is considered essential to constantly enhance technical capabilities from the social science viewpoint of how the technology is used for people in society, without focusing only on improving the technology of natural science.

5. Conclusions

The lessons from the Fukushima Daiichi Accident served as a trigger to teach the importance of organizational culture for safety and the difficulty of creating such a culture, and to realize the role of a nuclear specialist.

As stated in Chapter 2, Nuclear Operators in Japan (including TEPCO) were laboring under the basic assumption that a serious severe accident could not happen in a nuclear power plant in Japan. This left them unable to comprehend a hazard as a potential reality that could occur. If an organization's sensitivity to nuclear safety has deteriorated and it has developed negative chains of thought, it is not easy to change the organization so that it will continuously make efforts to enhance safety. In order to do this, it is necessary to start by having the top management tackle consciousness reform with a strong sense of will, then improve the system and develop human resources.

As stated in Chapter 3, nuclear operators have commenced the activities aiming at change of organizational culture. To realize the effect of such efforts, countermeasure for creating robust organizational culture for safety stated in Chapter 4, questioning attitude for vitalizing safaty awareness,

oversight function for introducing diverse and long-term perspectives, communication and transparencey for securing trust and systemic approach for taking into consideration about interactive influences between individual and its organization, should be required, not to be influenced by negative assumptions.

In light of the pursuit of nuclear safety, the managers, engineers, and researchers involved in nuclear power business face many occasions for decision-making. The knowledge required in pursuing nuclear safety is not limited to natural science and technology and logical thinking, such as nuclear reactor physics, reactor control theory, and radiation protection. It is also necessary for them to be aware that they themselves bear responsibility for the consequences of the risks inherent to nuclear power. They must learn from the operational experience of their predecessor and others and should be proactive in adopting and incorporating the latest knowledge based on their experiences.

After all, it is human beings who make judgment in each situation, and the influence of an organization is certain to arise there. To ensure nuclear safety, it is important to have a good understanding of the characteristics of human beings and of organizations. The lessons learned from the accident at Fukushima Daiichi Nuclear Power Station remind us of the importance of an organizational culture for safety and the difficulty of creating one, and provides us with the opportunity to once again realize our roles as nuclear power experts.

References

[1] Y. Hatamura et al., Investigation Committee on the Accident at the Fukushima Nuclear Power Stations of Tokyo Electric Power Company, Final Report, 2012.

[2] K. Kurokawa et al., The National Diet of Japan, The official report of The Fukushima Nuclear Accident Independent Investigation Commission 2012.

[3] Tokyo Electric Power Company, Fukushima Daiichi Nuclear Power Plant Accident Investigation Final Report, 2012.

[4] Tokyo Electric Power Company, Nuclear Safety Reform Plan, 2013.

[5] A. Kugo, Licensees activities for nuclear safety: Organizational culture ans leadership, *Nuclear Safety and Simulation* 9 (2019) 28-36.

[6] IAEA, The Fukushima Daiichi Accident report by the Director General, 2015, pp. 67-73.

[7] N. Osaka, Brain which controls attention (Tyui-wo Kanki-suru Nou (in Japanese), Shinyosya, 2013.

[8] C. Nakane, Japanese Society, *A practical Guide to Understanding the Japanese Mindset and Culture*, Turtle Publishing, 1973.

[9] R. Paul and L. Edler, *Critical Thinking*, Prentice Hall Inc., 2001, Kuritikaru sinking, Toyokeizai Inc., 2003, pp. 61-82. (in Japanese)

[10] J. Rees, *Hostage of Each Other: The Transformation of Nuclear Safety Since Three Mile Island*, University of Chicago Press, 1996.

[11] K. E. Weick and K. M. Sutchliffe, *Managing the Unexpected* (3rd ed.), Souteigai no Manejimento, 2015, pp. 119-136. (in Japanese)

[12] S. Dekker, *Safety Differently*, Routledge, 2014, p. 261.

[13] IAEA, International Nuclear Safety Group, INSAG-27, Ensuring Robust National Nuclear Safety Systems - Institutional Strength in Depth, IAEA, 2017.

[14] IAEA, WANO, Guideline-Independent Oversight, GL2018-01, 2018

[15] M. Syed, Black Box Thinking (Shippai no Kagaku (in Japanese)) 238-261, John Murrey Publishers 2016.

[16] S. Decker, Just Cluture second edition, CRC Press, 2012

[17] C. Rollenhagen, and T. Reiman, Does the concept of safety culture help or hinder systems thinking in safety?, Accident Analysis and Prevention 68, Elsevier, (2014) 5-15.

[18] IAEA, Leadership and Management for Safety, General Safety Requirements No. GSR Part2, (2016) 16.

[19] IAEA, The Fukushima Daiichi Accident report by the Director General, Box 2.11. Systemic approach to safety [67] (2015) 69.

[20] R. Martin, How successful leaders think, *Harvard Business Review* (2007) 60-90

[21] M. A. Roberto, Know what you don't know, 2009, (Naze kikini kizukanakattanoka (in Japanese), 2010, pp. 279-280.

[22] E. H. Schein, *The Corporate Culture Survival Guide*, John Wiley & Sons, Inc., 2009, pp. 21-27.

Modern Environmental Science and Engineering (ISSN 2333-2581)
September 2019, Volume 5, No. 9, pp. 803-810
Doi: 10.15341/mese(2333-2581)/09.05.2019/003
Academic Star Publishing Company, 2019
www.academicstar.us

Vertical Fences in Housing Units: The Use of Prefabricated Panels

Leandro Reis Andrade, and Gisleine Coelho de Campos

1. Egis Engenharia e Consultoria Ltda, Brazil

2. Instituto de Pesquisas Tecnológicas do Estado de São Paulo – IPT, Brazil

Abstract: The performance of prefabricated reinforced concrete panels, used as internal and external vertical fences of isolated and twinned housing units, was evaluated in this study. The main innovative feature refers to its thickness: only eight centimeters, since panels with higher thicknesses are traditionally well accepted and used in civil construction works. The evaluations included project analysis, audits in ready and running housing, and manufacturing industry. In addition, technological control tests were carried out to characterize the materials and also to attest the quality of the construction system composed of this kind of panels. The buildings executed with this system are also destined to housing of social interest, and the cost of execution can be reduced in comparison to the conventional system using the process of industrialization of its components, in which control of losses is emphasized based on the principle of loss reduction. To collect the data, two institutions were selected: one in the state of Paraná and another in Santa Catarina. Similar methodologies are used by both companies: the manufacturing of the panel is made in the factory and after the transport and positioning of this panel in the definite place using a munck truck. The results obtained in all stages of evaluation showed a proper performance to the system, reaching the minimum levels required in the applicable standards. It should be noted that fire safety assessments were not considered in this study; it could be the focus of future assessments in order to clarify all doubts regarding the potential of the system presented.

Key words: construction system, prefabricated panel, performance evaluation, housing

1. Introduction

The search for new construction technologies and industrialized execution processes has been the alternative found by construction companies that intend to reduce costs, maintaining acceptable standards of quality and performance of housing units.

According to Oliveira and Mitidieri Filho (2012) [1], the concept of sustainable development fosters the idea of designing the building not only for construction and use, but also for its final phase, including the concept of deconstruction, dismountability, and recyclability, in addition to the Design Life (VUP) and Global Cost.

In this scenario, buildings composed of prefabricated reinforced concrete panels, mainly slender panels, stand out for their convenience regarding the processes of transportation, assembly, and, if necessary, disassembly and recycling, given that the elements that comprise them favor these aspects.

Currently, the method that employs prefabricated panels is used in the manufacture of internal and external vertical fences of housing buildings, and it may have a structural function or serve only as fence system and room partitions.

As presented in this study, the panels are produced in factories capable of rigorously controlling the production phases of the elements and quickly adjusting potential deviations. A common type of concrete was used, i.e., without incorporation of air or addition of fibers; the thickness specified in the project

Corresponding author: Gisleine Coelho de Campos, Doctor in Civil Engineering; research area/interest: geotechnical engineering. E-mail: gisleine@ipt.br.

is eight centimeters. The concrete process may occur in metallic forms positioned on a vibrating table or on concrete tracks.

The typologies evaluated were isolated and twinned single-storey houses and submitted to the performance tests specified in ABNT NBR 15575-4 (2013), particularly for thermal comfort, acoustic, structural, watertight, among others tests. This study did not consider fire safety evaluations, which may be the focus of future evaluations in order to clarify any and all doubts in relation to the performance potential of the system presented herein.

2. Material and Methods

This evaluation is composed by the realization of project analyses, inspections in works during the execution phase and finished buildings, inspections in industrial units, as well as observing the results of characterization tests of the materials used and performance tests.

The intention was to prove the minimum conditions of livability, comfort, and durability of the buildings evaluated based on Guideline SINAT 002-Rev. 02 (2016) and Performance Standard ABNT NBR 15575-4 (2013). Further observations were carried out between 2012 and 2015, and the inspections were focused in the cities of Astorga/PR and São João Batista/SC.

The construction system is intended for building walls for housing units. The system is composed of massive prefabricated reinforced concrete panels, eight centimeters thick, compressive strength f_{ck} greater than or equal to 25 MPa, and specific mass amounting to (± 50) kg/m^3. No fibers or air incorporation are added to the concrete. In this construction system electro-welded meshes type Q-138, steel CA60 are used presenting sections with area of 1.38 cm^2/m, spacing between wires of 100 mm, and wire diameter of 4.2 mm.

Some use conditions and limitations may be mentioned, such as:

- Prefabricated reinforced concrete panels for use in walls cannot be totally or partially demolished because they have a structural function; and
- The construction system is limited to environmental aggressiveness classes I and II, rural and urban respectively.

After assembling the forms, the demolding agent is applied and the frame is positioned, executed with electro-welded screens and steel bars in the reinforcements, close to the places where there are concentrations of forces, according to the structural design of each building.

Following the assembly of the rebar, the components of the electrical installations (conduits and switch and socket boxes) and the spacers are positioned to ensure the covering of the rebar. The hydraulic installations are not embedded; they are positioned in shafts, enabling periodic maintenance procedures.

The concrete application in prefabricated panels is always carried out horizontally and can be performed in two ways: in metallic forms positioned on a vibrating table for consolidation or in concrete tracks, where the metallic form is positioned and locked, restricting the area of application of the concrete and forming the type of panel to be produced. In this case, the consolidation is carried out by means of an immersion vibrator.

After 24 hours of concrete application, the demolding process commences, provided that the concrete has a minimum compressive strength of 12 MPa, and for each development the project must define the specific strength value of the concrete. The forms are then washed for use in another operational cycle.

The curing of the concrete panels used in the construction system is performed by sprinkling with water at least three times a day, during three days after the concrete application. Fig. 1 shows rebars positioned in the forms and the concrete application of the panel performed on the vibrating table for consolidation (Fig. 1).

Fig. 1 Rebars positioned and panel concrete application.

3. Panel Transportation and Assembly

The panels are transported and assembled *in situ* with the aid of a munck truck, which performs the lifting, moving, and positioning of the panel at the location specified by the project. Before fitting the panels, a mortar (1:3 trace) is applied to the interfaces between the panels and the foundation element. Some projects specify protruding steel rebars or metal inserts for corner connections, where after the joining of these elements by welding, a corrosion protection is applied (usually a painting with zinc-rich epoxy) and later release of the grout.

After the panel is placed in the definite location, with the aid of the munck truck, the plumb is inspected and the shoring is made with metal struts.

The alignment is obtained through the raft grooves. Next, the locking occurs between panels with type "C" clamps. These struts and locking clamps will only be removed three (3) days after grouting corner connections.

Fig. 2 shows the panels shored in the work and the details of the piece used and its dimensions (Fig. 2).

Joints are made to ensure the tightness of the facade water, especially in the areas of connections between adjacent structural panels, a procedure to which a depth limiter is inserted to occupy all the space between plate joints to prevent the leakage of the sealant and help compact the product by confinement. Afterwards, the sides and surface of the plates are cleaned and an elastic sealant of polyurethane is applied.

In the base areas of the panels that are in direct contact with the foundation element, cement-based waterproofing agents are applied in a strip of 1 m height throughout the perimeter of the building; then the acrylic sealer is applied on the entire surface, followed by acrylic-based Latex paint. Dry areas of the internal walls will be painted with a sealer and then painted again with PVA-based Latex paint. In wet areas (bathroom and laundry), the ceramic coating is used.

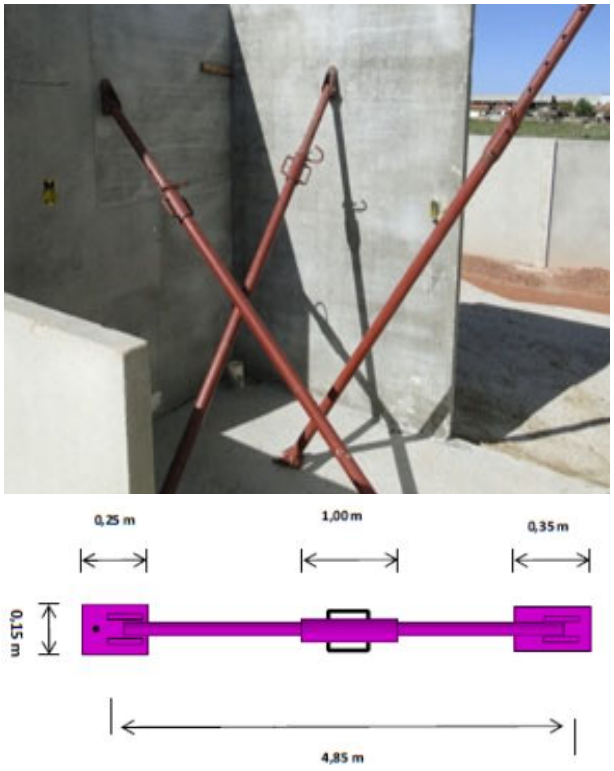

Fig. 2 Shoring and panel locking.

Fig. 3 shows buildings consisting of prefabricated reinforced concrete panels eight centimeters thick, finished and available for delivery to the owner (Fig. 3).

4. Technical Performance Evaluation

The technical evaluation presented in this study considered criteria regarding structural performance, watertightness, thermal performance, acoustic performance, durability, and maintainability. Criteria regarding quality control specific to the construction system were also considered.

4.1 Structural Performance

The characteristic strength specified for the concrete used in prefabricated concrete panels is equal to or greater than 25 MPa, as proven in concrete characterization tests performed in a laboratory installed in the plant.

Fig. 3 View of finished buildings.

The structural configuration is given by the composition of the structural panels responsible for building stability. The conclusion of the structural conception analysis performed by the estimating engineer and presented in the structural calculation memory suggests that the structural panels used as walls of the proposed construction system may receive the permanent actions and overloads expected for single-family and isolated single-storey houses, transferring them to the foundations in order to allow safety, stability, and the conditions of use, as long as the specific foundations design has been met.

In order to certify compliance with the criteria of Guideline SINAT 002-Rev.02 (2016), soft and hard body impact tests were performed on pre-molded structural panels used as external and internal walls and also tests of actions transmitted by sudden door closures and soft body impact with 240 J energy, applied in the geometric center of the door skin, showing no displacement or tearing of the frame, nor rupture or loss of stability of the wall. The suspended load test was also carried out.

The proponent of new construction systems should always prepare specific structural projects for each development, verifying the overall stability of the building and its implementation. It should be emphasized that for each specific situation the proponent should conduct the land analysis and the specific projects of development foundations and structure.

4.2 Watertightness

Project analyses were carried out to evaluate compliance with the watertightness requirement of the wall system of external and internal moisture sources.

It is considered that the wall system meets rainwater tightness conditions due to its construction characteristics (prefabricated reinforced concrete panels, with fck = 25 MPa, and subsequent painting application) and the treatment with an acrylic-based waterproofing system, applied at the facade base with a

height of 1 m, counted from the floor slab, and also the application of ceramic coating on the walls of moist and wet areas. In some projects the sidewalk is an extension of the raft, with 60 cm width and 5 cm difference in elevation in relation to the internal floor of the building (Fig. 4).

The way the windows are fixed (screws and polyurethane sealing) meets the conditions for rainwater tightness in the interface area between the wall and the window. The watertightness of the internal walls in contact with water for use and washing is considered satisfactory, also because of the construction characteristics of such wall (reinforced concrete walls with f_{ck} = 25 MPa and application of ceramic coating). With respect to the watertightness of the joints (interfaces) between walls and internal and external floors, the projects of each development should provide floor trims and difference in elevation between the external and internal floors to minimize the contact of the water on the floor with the base of the wall. An acrylic-based waterproofing system is also applied to the floor slab to prevent moisture from capillary rise of the soil. The joints between facade panels (connections of the structural panels) were evaluated based on a project analysis, presenting satisfactory performance in relation to watertightness. It is recommended to perform the tightness test of the facade panels in the laboratory, before and after the thermal shock test, in order to prove the performance of the system, especially in areas of joints.

4.3 Thermal Performance

Computational simulations were performed with the Energy Plus software to evaluate the thermal performance of buildings that use the system that is object of this study. The simulations considered climate zones Z2 and Z3, contained in ABNT NBR 15,220 (2005) for the typologies of isolated and twinned single-storey houses and according to each type of architectural project.

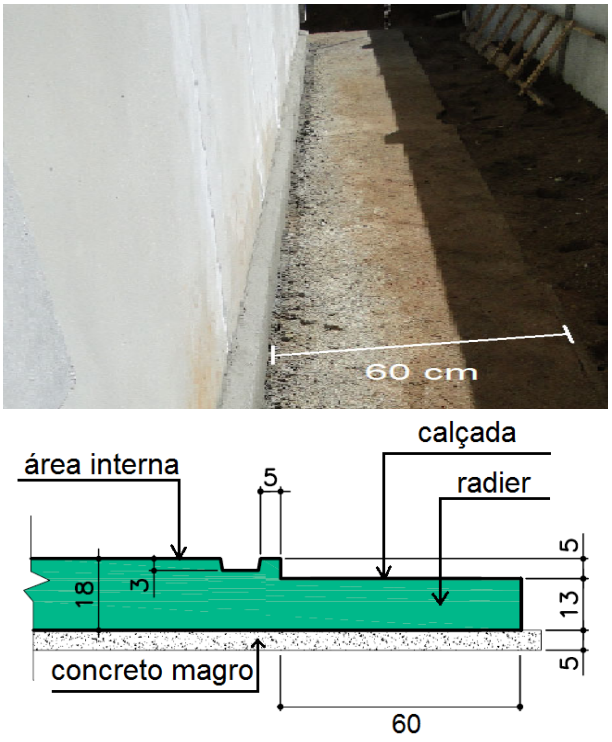

Fig. 4 Detail of the sidewalk pointing out the dimensions.

The typologies analyzed had areas between 60 m² and 78 m² and with ceiling height of 2.70 m; the covers evaluated were roofs with ceramic tiles or fiber cement, on attic and lining consisting of PVC boards 10 mm thick and concrete slab 10 cm thick. Considering the conditions established in Guideline SINAT 002-Rev.02 (2016), as well as the considerations mentioned in this study, the construction systems meet the thermal performance criteria. For other projects and other bioclimatic zones, specific analyses are recommended.

For the evaluation of the thermal performance the following parameters were considered: Absorbance to solar radiation of the external surface of the walls equal to: 0.3 (light colors), 0.5 (medium colors), and 0.7 (dark colors), listed in Guideline SINAT 002-Rev.02 (2016).

As an example, Table 1 presents a summary of the possible colors to be used in facades for the bioclimatic zones analyzed, which are the conditions to meet the isolated single-storey house typology with two and

three bedrooms, with ceramic roof tiles and PVC lining.

4.4 Acoustic Performance

The housing unit must meet the minimum criteria presented in Guideline SINAT 002–Rev.02 (2016). In a test performed, the acoustic performance presented satisfactory results, meeting the criteria for sound insulation provided by facade and ceiling elements. The acoustic performance evaluation was performed in a finished building (field test), considering the noise class II specified in ABNT NBR 15575-4 (2013).

The characteristics of one of the buildings tested are: area of 71.20 m²; facade wall composed of reinforced concrete panels 80 mm thick; "sliding" windows; two glass sheets 8 mm thick and with no shutter. The doors and door frames are made of wood and the ceiling is formed by roof with wooden structure, ceramic tiles (15 mm thick and density of 1700 kg/m³) and lining consisting of PVC boards (10 mm thick). Table 2 presents the synthesis of the results obtained.

Table 1 Necessary conditions for single-storey houses with the respective project typologies, to meet the requirements of Guideline Sinat 002-revision 2 [2].

Typology of the evaluated project	Bioclimatic zone	Color of the external finish of the facade walls			
		Standard condition (a)	With shading (b)	With ventilation (c)	With shading and ventilation (d)
Single-storey house with 2 dorm rooms	2	light or medium	light or medium	light or medium	light or medium
	3	light	light or medium	light or medium	light or medium
Single-storey house with 3 dorm rooms	2	light or medium	light or medium	light or medium	light or medium
	3	light	light	light	light or medium

(a) standard condition: rooms with ventilation only by infiltration through gaps in windows and doors, at a rate of one renewal of the ambient air volume per hour (1.0 Ren/h) and windows without shading;
(b) shading condition: external or internal sun protection that prevents direct sunlight from entering or reduces the incidence of global environmental sunlight by 50%;
(c) ventilation condition: ventilated environment at a rate of five renewals of the ambient air volume per hour (5.0 Ren/h);

Table 2 Summary of the results of the acoustic performance test, considering noise class II [3].

Fencing	$D_{2m,nT,w}$ (dB)	Required criteria (dB)	NOTE
Facade Front Dorm Room 1	26	≥ 25	It meets the minimum performance level
Facade Back Dorm Room 2	25		

4.5 Durability and Maintainability

Project analyses and tests were performed to evaluate the requirements considered important for the durability of the wall system at issue. The cement consumption, the environmental aggressiveness class, the compressive strength of the concrete, and the water-cement ratio were verified to ensure meeting the minimum quality of the concrete. The system of prefabricated reinforced concrete panels uses concrete with at least 300 kg/m^3 of cement, water-cement ratio ≤ 0.60, which is classified in concrete class C25 and in classes I and II of environmental aggressiveness. The nominal cover (cnom) for concrete panels is 25 mm, considering Class II of environmental aggressiveness, for fck = 25 MPa.

The project considers the preponderant aging and deterioration mechanisms related to concrete and rebars, specifying the characteristic of the concrete used in the construction system, complying with Guideline SINAT 002-Rev.02 (2016). Spacers are also used to obtain a nominal cover of 30 mm for the screen (Q138) composed of two 4.2 mm wires and centralized; these spacers are installed every 600 mm throughout the rebars, ensuring the minimum cover specified.

For each new development, an alkali-aggregate reaction test should be performed to support the choice of materials to be used in the concrete. In the case of the

construction system under analysis, as it is made up of concrete walls that have a structural and fencing function, the Design Life (VUP) specified for the structure is 50 years, which is the same for internal and external vertical fences. Guideline SINAT 002-Rev.02 (2016) is met regarding heat and thermal shock action since they are elements with homogeneous construction characteristics (solid concrete walls). Also, they have presented satisfactory results in the tests performed. The test was performed according to the specifications, following the dimensions of the specimens (2.40 m in length by 2.70 m in height) and the representation of the construction system, containing the joints between panels.

The maintainability was evaluated by ITA (Technical Evaluation Institution), considering the content of the Operation, Use, and Maintenance Manual of the building, prepared by the technology proponent, particularly analyzing the items related to the construction elements that compose or interfere with the prefabricated concrete wall system, specifying the precautions for the use and maintenance of the concrete wall system, including the definition of inspection schedules and the anticipation of wall painting procedures and frequency, replacement of components of hydraulic and electrical installations, among others.

5. Quality Assurance

Audits were carried out in manufacturing units and in works executed with the construction system of prefabricated concrete panels, verifying the quality control of the production process and compliance with Guideline SINAT 002-Rev.02 (2016). In the initial audit performed by the Technical Assessment Institution, the aspects of control described below were verified. Such aspects should be continuously controlled by the technology proponent.

- Receipt of materials and components (rebars and concrete — tests to verify the consistency and compressive strength of concrete at the demolding time and at 28 days);
- Sequences and quality of the production steps (cleaning and geometric control of the formwork; positioning and covering of the rebars; pouring of concrete; demolding, and curing);
- Sequence and quality of the assembly of frames and finishes such as ceramic tiles, waterproofing, painting, and texture application; and
- Sequence and quality in the assembling process of joints between panels.

The controls are based on technical documents that provide quality control of the projects, the receipt of materials, and wall molding. The technology proponent is responsible for the development of these technical control documents and for their application during the execution of the works, which was verified in the audited works.

The documents that prove the technological control of concrete and the traceability of information were also analyzed. One hundred percent of the batches of concrete delivered to the construction site are checked for consistency and compressive strength at the following times: 24 hours, 7 days, and 28 days. This control is done by an external technological control laboratory, and the tests are duly accredited. For the steel, the verification control of the product quality certificates is performed.

The control frequency and sampling of the materials that compose the reinforced concrete panels that are object of this construction system are:

- Constituent materials of reinforced concrete at each receiving batch (cart) for Cement (compressive strength, fineness, and blaine); Aggregates (granulometry and powder material); and Additive (product type and validity control);
- Concrete in fresh state at each application (reception, sampling, and slump);

- Concrete in hardened state at each molded specimen (curing and compressive strength test).

6. Final Comments

This study presented the potential for meeting the performance requirements of buildings composed of internal and external vertical fences produced with prefabricated reinforced concrete panels, especially with regard to their thickness of eight centimeters. Furthermore, the quality control criteria recommended for the proposed construction system were presented, which are aimed at ensuring compliance with the Design Life (VUP).

The project analyses and the results obtained in the tests performed suggested compliance with the applicable requirements of ABNT NBR 15575-4 (2013), with at least a minimum performance level.

Considering the above, the construction system addressed is understood to confer livability to the user, building durability, and that the fire safety assessments can be performed to clarify any and all doubts regarding the potential of the system presented herein.

The data presented in Table 3 shows the items evaluated, the criteria adopted, and the results obtained in relation to the analysis performed.

Table 3 Items evaluated, criteria adopted, and results obtained.

Item evaluated	Evaluation criteria	Results obtained	Required standard criteria	Performance level obtained
Structural performance	Guideline SINAT 002–Rev.2 (2016) - item 4.2.1	It meets ELU, ELS, impacts, and suspended load	According to item 3.1 of Guideline SINAT 002 rev.2	All items evaluated meet the minimum performance levels that are expected.
Watertightness	ABNT NBR 15575-4 (2013) item 10.1.1	VVE considered waterproof in the project analysis	According to item 3.3 of Guideline SINAT 002 rev.2	
Thermal performance	Guideline SINAT 002-Rev.2 (2016) item 4.2.4.2 and ABNT NBR 15.220 (2005)	It meets Z2 and Z3	According to Table 1	
Acoustic performance	ABNT NBR 15575-4 (2013) item 12.2.1.2	26 dB	≥ 25 dB	
		25 dB		
Durability and maintainability	Guideline SINAT 002-Rev.2 (2016) - item 4.2.6	It meets the VUP	≥ 50 years	

References

[1] Oliveira, Luciana Alves; Mitidieri Filho annd Claudio Vicente, O Projeto De Edifícios Habitacionais Considerando A Norma Brasileira De Desempenho: Análise Aplicada Para As Vedações Verticais, 2012, access on: May 11, 2017, available online at: http://www.revistas.usp.br/gestaodeprojetos/article/view/51022/55089.

[2] Roriz Engenharia Bioclimática, S/S LTDA (São Paulo), *Avaliação dos Níveis de Desempenho Térmico de Edificações Habitacionais com Paredes em Concreto*, São Carlos: Roriz, 2013, p. 15.

[3] Apoio Acústico (São Paulo), *Avaliação de Desempenho Acústico de Fachadas em Casa Isolada em Canelinha-SC.* (112nd ed.), Canelinha: Apoio Acústico, 2013, p. 31.

Modern Environmental Science and Engineering (ISSN 2333-2581)
September 2019, Volume 5, No. 9, pp. 811-820
Doi: 10.15341/mese(2333-2581)/09.05.2019/004
Academic Star Publishing Company, 2019
www.academicstar.us

Evaluation of Remedial Works for a Spillway on Landslide-dammed Lakes by an Earthquake: A Case Study in the Jiufengershan Landslide

I-Hui Chen[1], Kuo-Ching Chang[2], Yu-Chin Chen[2], and Miau-Bin Su[1]

1. Department of Civil Engineering, College of Engineering, National Chung Hsing University, Taiwan

2. Department of Soil and Water Conservation, National Chung Hsing University, Taiwan

Abstract: This study applied digital elevation models of different periods and long-term field monitoring data to compare elevation changes of a spillway for remedial works of landslide-dammed lakes in the Jiufengershan landslide. Digital aerial photogrammetry and LiDAR techniques were used to rebuild orthophotos and digital elevation models in the area from 1998 to 2015 in order to review the changes of deposit and erosion in topographies and profiles of the spillway. Through many torrential rainfalls in the past, it was particularly effective for the spillway and related remedial works to suppress the production and flow of collapse debris from banks of the spillway channel. It is the most important for spillway remedial works to remain the stabilization of two dammed lakes. Overall, average sediment amount of the two dammed lakes from 2007 and 2018 was only 0.33 m per year so the performance of the spillway would be well successful for the stabilization of the dammed lakes and the landslide area.

Key words: landslide-dammed lake, spillway, landslide remedial works, digital elevation model

1. Introduction

This paper employed digital elevation models (DEMs) of different periods and long-term field monitoring data to compare elevation changes of a spillway and water-level variations of landslide-dammed lakes in the Jiufengershan landslide by the 1999 Chichi earthquake. Many landslide-dammed lakes were often transitory to keep their integrity because the flow of water in a dammed lake could easily spill over the top of a landslide dam in which unconsolidated debris may rapidly be eroded and cut; then, it could cause the dam to break down in a few hours so that occurred a catastrophic flood disaster [1]. The author indicated 91% of landslide dams failed within 1 year of formation based on 63 cases from literature and past experience. Thus, it is necessary for the safety of residents in the downstream to remediate the dammed lakes against failure disasters.

For emergency treatments of landslide-dammed lakes, excavated spillway is a fast and simple method which is used for the overflow discharge of a dammed-lake and the mitigation of potential disasters caused by the breakage of landslide dams [2-4]. Other methods include drainage by intake structure, siphon pipes, pump systems, tunnel excavation and diversions [5-8].

The case study of the research is in the Jiufengershan landslide by the Chichi earthquake in September 1999 in Taiwan, which caused two landslide-dammed lakes. There are two main emergency measures for the landslide and two dammed lakes. First, one of emergency mitigative measures was an innovative method, namely temporary geotextile dams of debris-filled shipping containers, in the end part of

Corresponding author: I-Hui Chen, Dr.; research areas/interests: landslide monitoring, GIS. E-mail: ian.cih82@gmail.com.

deposit area in order to increase strength of the slope stable and avoid headward erosion. The other emergency measure was an excavated spillway of dammed lakes that was an emergency drainage channel so as to discharge the overflow of dammed lakes and decrease the storage volume of two lakes. After emergency mitigative measures for dammed lakes, Remedial works of a permanent spillway needed to be undertaken so as to retain the two dammed lakes. There were a slit-type sabo dam, several columnar-type submerged dams, groundsill works and some check dams in the spillway from 2000 to 2008.

For the performance evaluation of the spillway, digital aerial photogrammetry and LiDAR techniques were used to rebuild orthophotos and DEMs in the area from 1998 to 2015 in order to review the changes of deposit and erosion by profiles of the spillway and to evaluate lake-surface variations of dammed lakes by long-term monitoring data. Meanwhile, echo sounding survey was employed for detailed visualization and analyses of topography changes and sediment amount of lake bottoms [9]. Consequently, the echo sounder technology was used to calculate sediment changes and water storage volume of the two dammed lakes so that the performance and effectiveness of the spillway can be assessed.

2. Jiufengershan Landslide

A case study is located at the Jiufengershan landslide in Taiwan by the Chichi earthquake in September 1999, as shown in Fig. 1. The area of the landslide is 195 ha and the amount of the collapse is 35 million cubic meters that blocked two creeks, namely Jiutsaihu and Sezaikeng streams, and caused two dammed lakes. The area of the Jiutsaihu and Sezaikeng dammed lakes is 4.4 ha and 6.4 ha, respectively. Since 2003, there has been a monitoring landslide project in the Jiufengershan landslide with some monitoring equipment, including extensometers, inclinometers, groundwater lever gauges, etc.

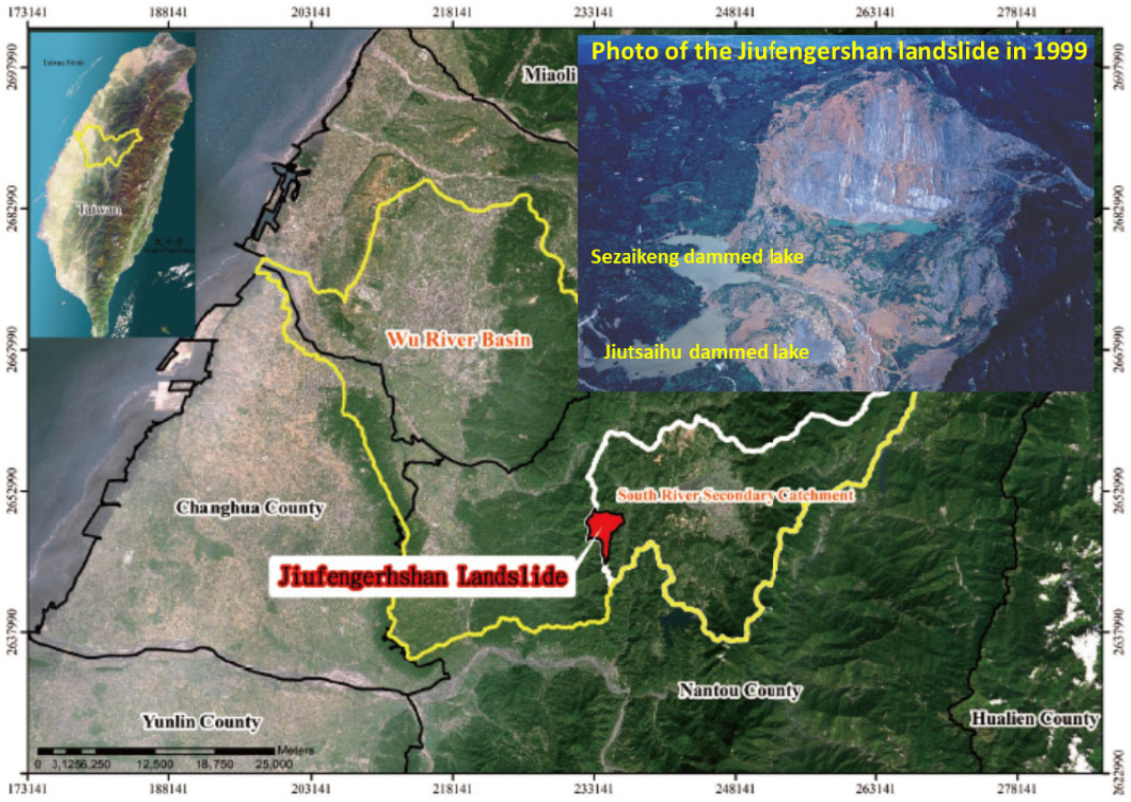

Fig. 1 Location of the Jiufengershan Landslide

The geology of the landslide is underlain mainly by Miocene sedimentary rocks where the strike is N36°E and the dip is 21°SE with an N-S trending synclinal axis of Daanshan syncline in the eastern part; the geologic formation of the syncline axis is the Kueichulin Formation which unconformably contacted with the underlain Changhukeng Shale; the lower formations include Miocene strata of Shihmen Formation [10], as shown in Fig. 2.

With regards of two dammed lakes, the surface elevation of the Jiutsaihu and Sezaikeng lake was 585 m and 577.5, respectively, as the earthquake occurred. The detailed data of two lakes is shown in Table 1. Furthermore, the greatest depth of the Jiutsaihu and Sezaikeng lake was estimated about 29 m and 37.5 m, respectively, before completed spillway.

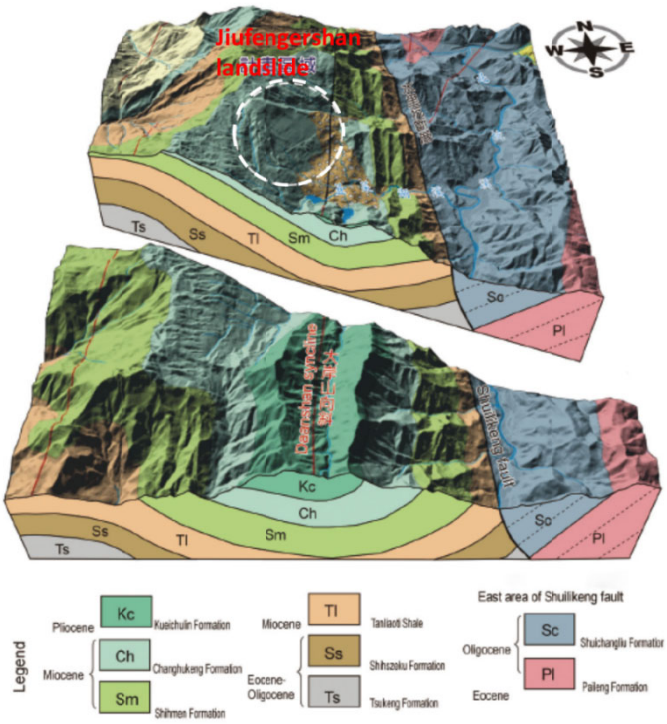

Fig. 2 3D Geological Structure in the Jiufengershan landslide.

Table 1 Comparison of elevations, depths and volumes of two landslide-dammed lakes.

	Jiutsaihu dammed lake	Sezaikeng dammed lake
Area (ha)	4.43	6.48
	Before completed spillway	
Elevation (m)	585	577.5
Maximum depth of lake (m)	29	37.5
Storage volume (m^3)	678,000	1,089,700
	After completed spillway	
Elevation (m)	575.89	570.05
Maximum depth of lake (m)	15	29
Maximum lake-level rise while a heavy rainfall (m)	1.2	4

For long-time monitoring the lake surfaces of the Jiutsaihu and Sezaikeng lakes in Fig. 3 and Fig. 4, the elevations of lake surfaces dropped to 575.89 m and 570.05 m, respectively, after completed spillway. From rainfall and lake-surface monitoring data of typhoon events in September 2015, the highest water levels of the Jiutsaihu and Sezaikeng lakes was 577.1 m and 574 m which went up approximately 1.2 m and 4 m, respectively. As a result, it is successful to control water surface levels of two dammed lakes while the spillway completed.

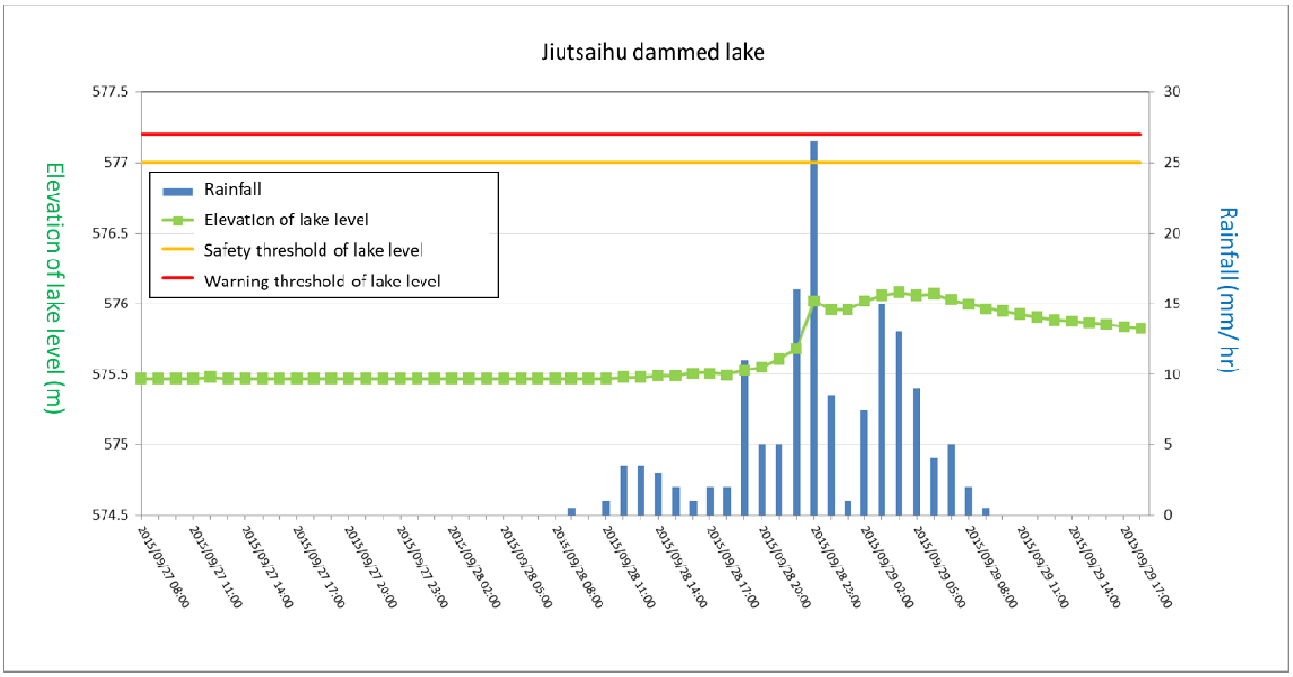

Fig. 3 Relationship between rainfall and elevation of lake level in the Jiutsaihu dammed lake.

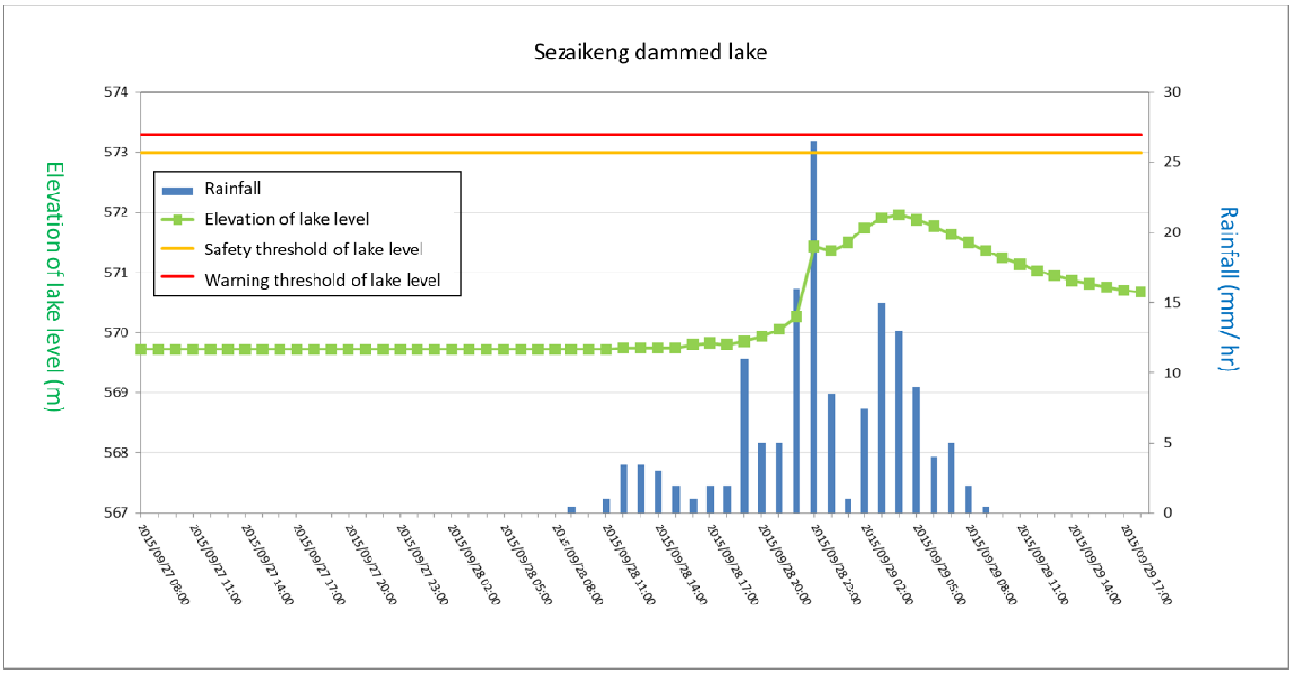

Fig. 4 Relationship between rainfall and elevation of lake level in the Sezaikeng dammed lake.

3. Remedial Works of the Landside and Dammed Lakes

3.1 Emergency Treatment

Dammed lakes were vulnerable to catastrophic failure by overtopping and breach, landslide emergency treatments involved in the potential failure of these dams need to be carried out for protection of relative people's living and property. Thus, there were two items of remedial works for the landslide and two dammed lakes.

First, one of emergency mitigative measures was an innovative method, namely temporary geotextile dams of debris-filled shipping containers, in the end part of accumulation area in order to increase strength of slope stable and avoid headward erosion. The measure of debris-filled shipping containers was the first for the slope toe loading of a landslide in Taiwan whose height, width and height were 122.7 m, 8.2 m and 7.5 m, respectively, and the aims of the measure were for four functions as marked in Fig. 5(1) (they are: ① slope stable, ② slope toe loading, ③ headward erosion control, ④ protection of stream bank).

The other emergency measure is a spillway of dammed lakes that is an emergency drainage channel with 1450 m in length and 8 m in depth in order to discharge the overtopping of dammed lakes and decease the storage volume of two lakes in October 1999, as shown in Fig. 5(2)

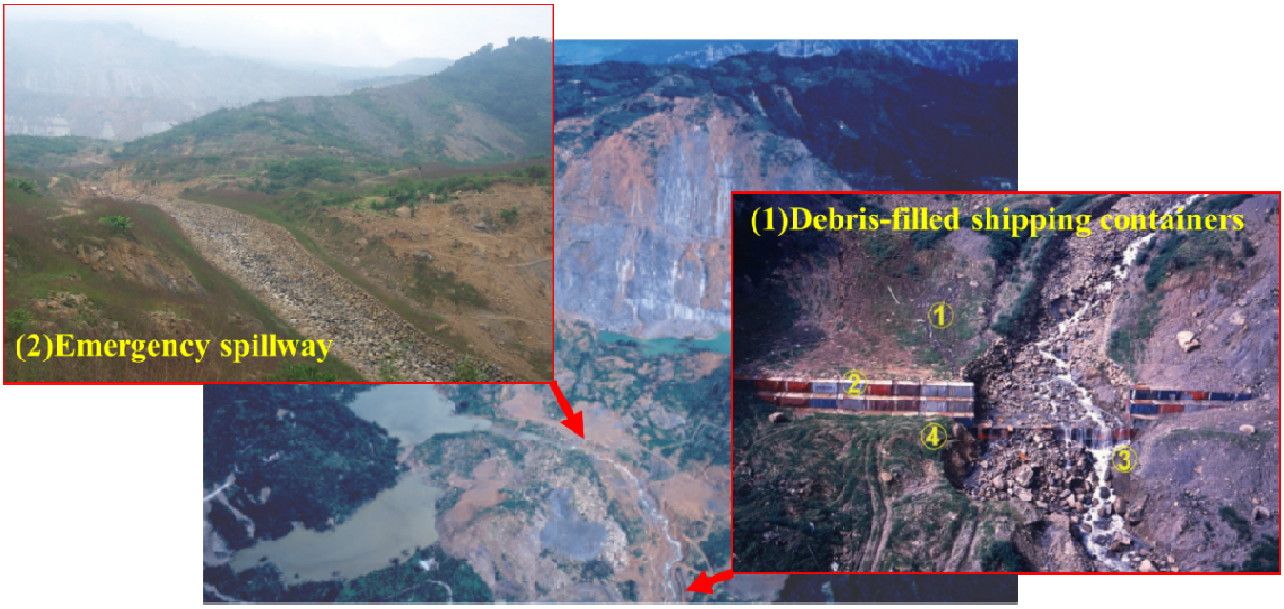

Fig. 5 Locations and photos of emergency treatments in the landslide

3.2 Soil and Water Conservation Treatment

After emergency mitigative measures of dammed lakes, it is important for remedial works of a permanent spillway so as to avoid severely incised channel, losing a lot of debris and dammed-lake failure. One of the remedial works was a slit-type sabo dam that was located at 1K+230m from the overflow outlet of the spillway in 2000. The aim of the dam was for a direct barrier to debris flows which could occur. The location of the sabo dam is shown in Fig. 6.

The slit-type sabo dam divided two constructions including a main dam and auxiliary dam, of which the lengths and heights were 131 m and 15.5 m, and 84 m and 8 m, respectively. The sabo dam that categorized as a permeable structure is one of popular methods currently used for debris flow prevention [11, 12]. The dam can effectively block huge boulder as well as

debris from upstream while allow smaller-grain debris and stream flow to be released into downstream channel.

The other remedial works were 20 columnar-type submerged dams on the spillway so as to increase the stabilization of channel bed and decrease fast headward erosion of the spillway in 2003 (Fig. 6). The size of a single submerged dam is 42m in length and 5 in height. The column diameter is 1 m and the spacing in 3 rows is all 1m. In contrast with traditional dams, this dam was more permeable from its bottom to all other parts which was suitable for the special geology in the Jiufengershan landslide, so 20 columnar-type submerged dams were immediately designed and implemented. After that, remedial works of check dams was performed to enhance the bed stability of the spillway from 2008 to 2013 (Fig. 6).

4. Performance Evaluation of Spillway Works

4.1 Landform Changes with Photogrammetry and LiDAR Survey

Digital aerial photogrammetry and analysis tools of ERDAS IMAGINE were used to rebuild orthophotos and DEMs for different periods before and after the 1999 Chichi earthquake, as shown in Fig. 7. According to the topographic analysis in Table 2, the average depth of the landslide is 34 m with a collapse volume of 34.92 million cubic meters and a deposit volume of 36.58 million cubic meters.

Fig. 6 Location of spillway works in the landslide

Table 2 Relative areas and volumes of collapse and deposit in the landslide area.

Type	Area (ha)	Debris volume (m^3)	Maximum elevation change (m)
Collapse	102.5	34,923,400	-85
Deposit	92.5	36,585,000	+108
Sum	195		

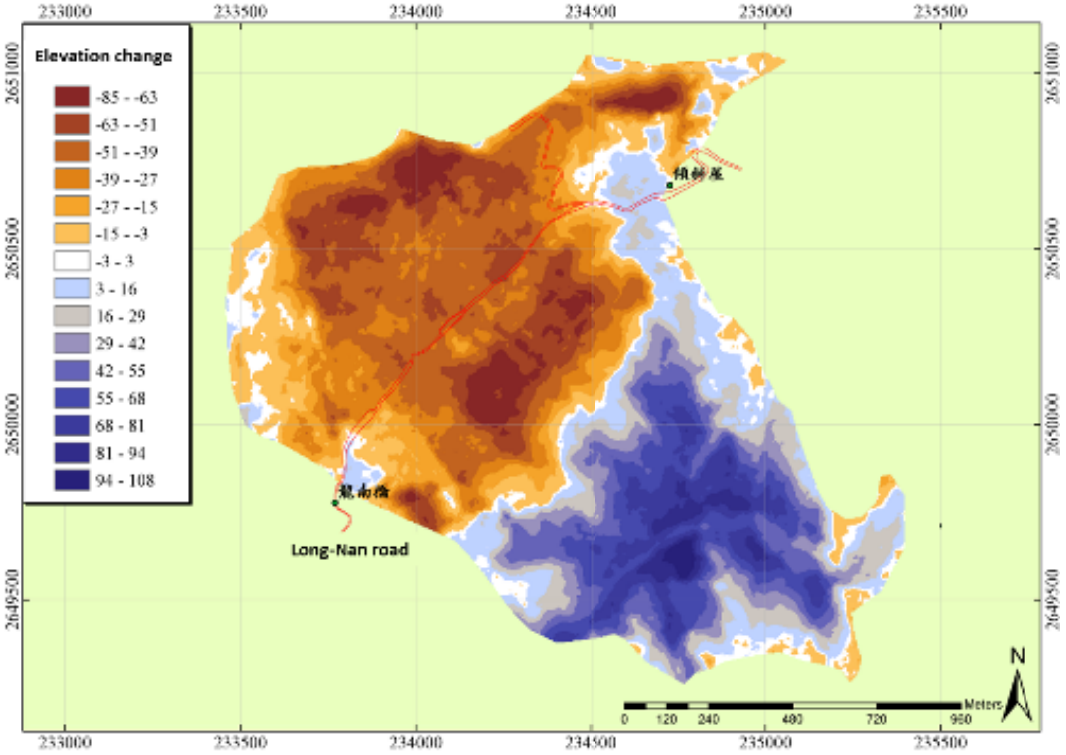

Fig. 7 Landform change between 1998 and 2002 (collapse is in brown color; deposit is in blue color).

There was LiDAR data to make DEM for this area after 2004. The data of DEMs in 2004, 2011 and 2015 for the landslide can be compared with ground surface changes in three dimensions and help to understand area and volume changes.

The data of DEMs was built in 2004, 2011 and 2015. The results of elevation changes illustrate the differences in elevations from 2004 to 2015 in the landslide, as shown in Fig. 8(1) which illustrates that erosion area is in blue color and deposit area is in red color between 2004 and 2015 in which the landslide volume is estimated about 267,000m3 with a maximum erosion depth of 27 m and maximum deposit depth of 24 m. However, the elevation variation was smaller from 2011 to 2015 in Fig. 8(2).

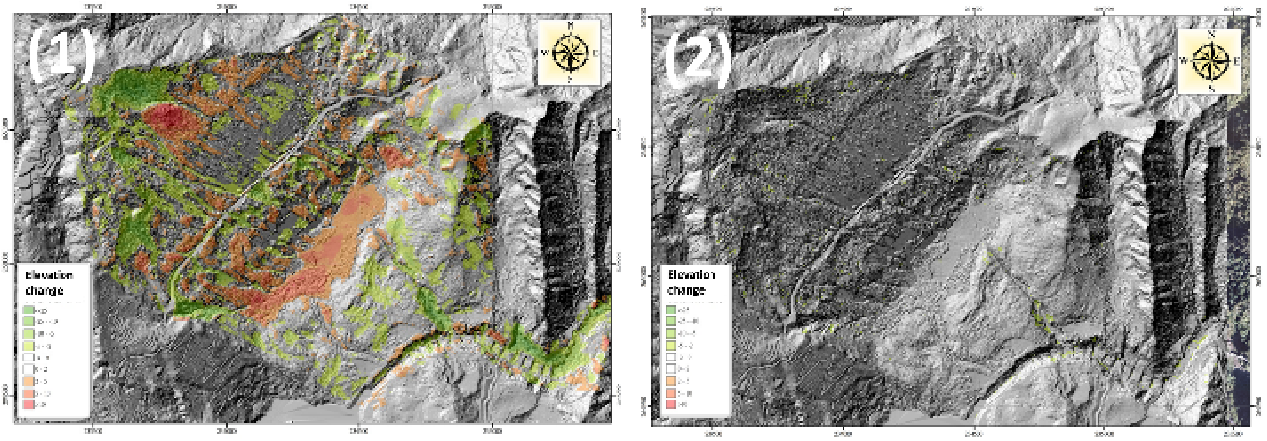

Fig. 8 (1) Landslide change between 2004 and 2015; (2) Landslide change between 2011 and 2015 (Erosion area is in green color and deposit area is in orange color).

4.2 Profile Changes of the Spillway with Photogrammetry and LiDAR Data

DEMs of the area were built by the data of photogrammetry in 1998, 2002 and 2005. Then, profiles of the Jiutsaihu stream before and after the 1999 Chichi earthquake were drawn using the data of DEMs in Fig. 9 which shows elevation changes of the stream bed before and after the earthquake in which the maximum landslide depth is 87 m at 2 K+250 of the profile line. It is clear for the profiles that there was an erosion phenomenon at 3 K+500 of the upstream and a deposit area occurred from 0 K+775 to 1 K+365 at the downstream that was possibly caused by excavated spillway or collapsed debris of the upstream.

Other DEMs of the area were built by the data of LiDAR in 2004, 2011 and 2015 with the grid precise of 5 m. Then, profiles of the spillway were drawn by using the data of DEMs in the three periods, as shown in Fig. 10 where locations of remedial works, including a sabo dam, 20 columnar-type submerged dams and check dams were plotted.

Fig. 10 illustrates that there was a significant downcutting in the elevation change by 20 meters between 0 K+870 m and 1 K+80 m in the spillway from 2004 to 2011, which caused falling and damage of some columnar-type submerged dams. Nevertheless, the elevation changes gradually remained stable from 2011 to 2015 after remedial check dams and groundsills from 2008. The other point is that the sabo dam effectively blocked the massive debris against its flowing to downstream. All spillway works could have a capacity of debris pool by 6 million cubic meters. Dammed-lake failure and debris flow did not occur in the landslide area while all spillway works completed.

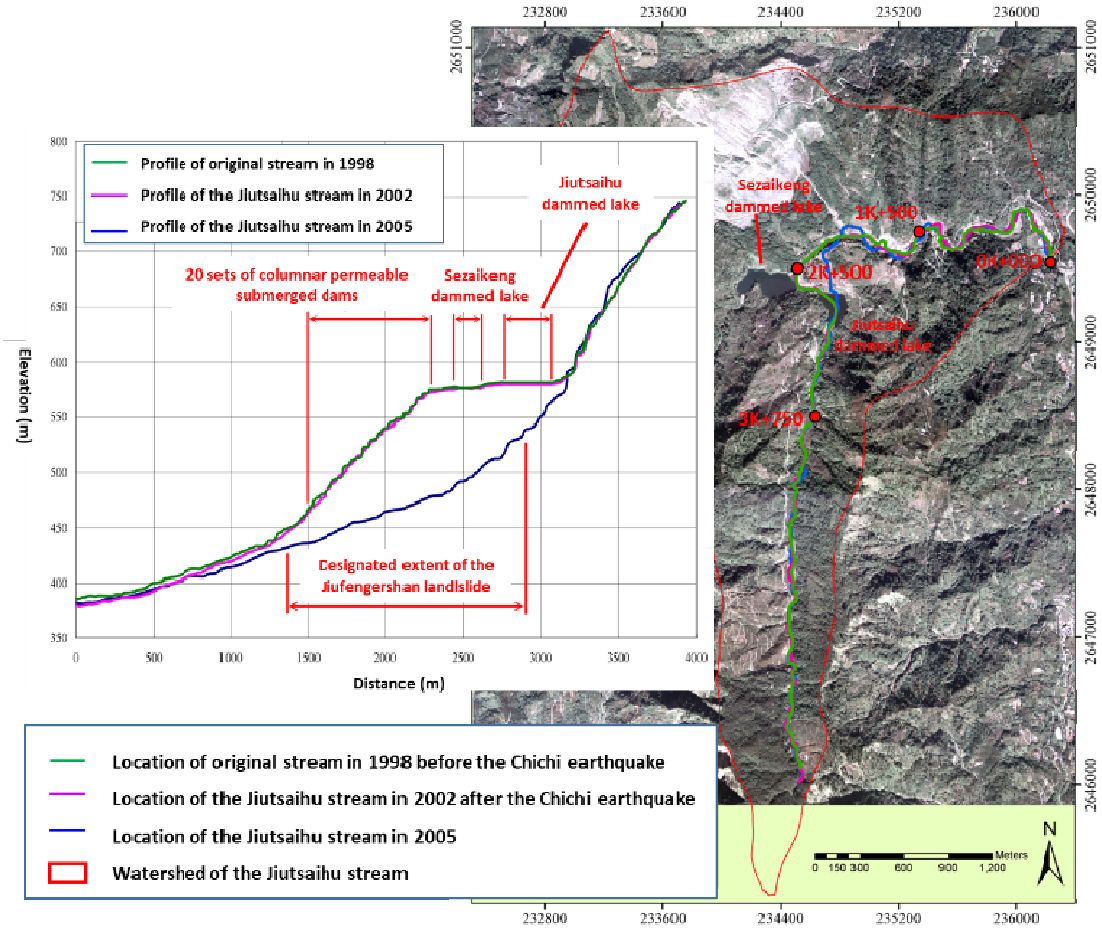

Fig. 9 Location and profile of the Jiutsaihu stream before and after the Chichi earthquake.

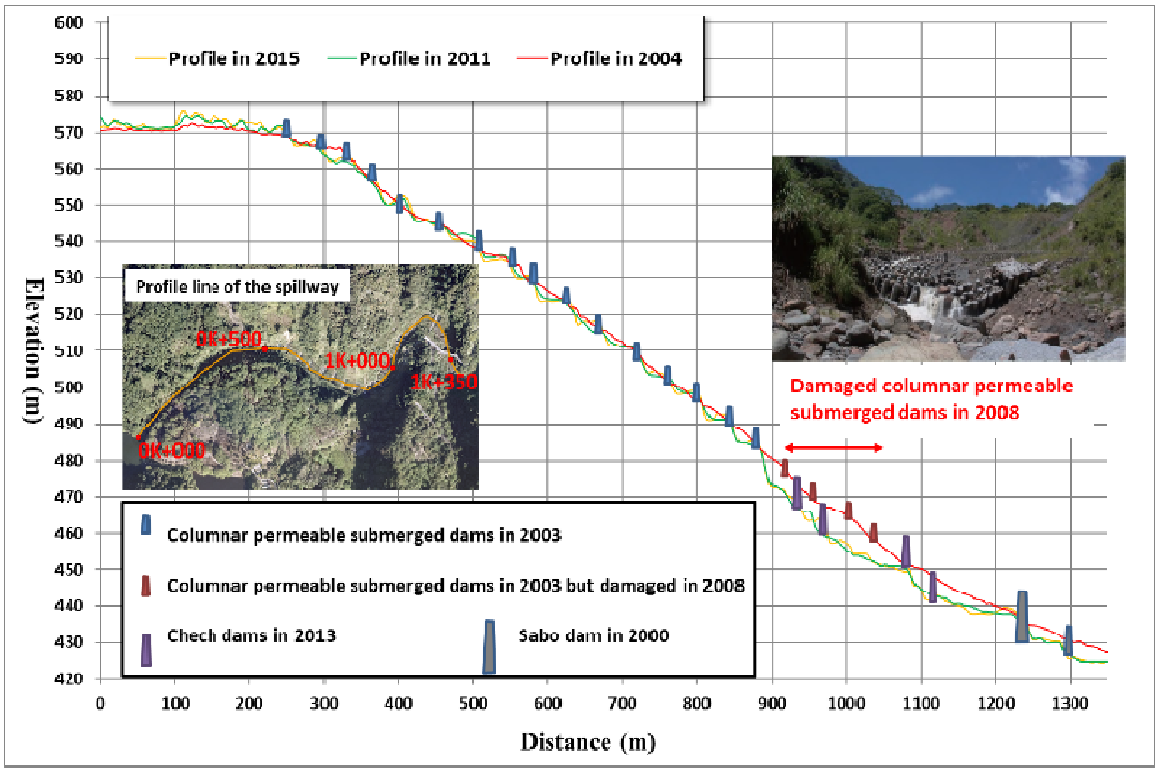

Fig. 10 Elevation changes of the spillway for different periods.

4.3 Echo Sounding Surveys for Two Dammed Lakes

Echo sounder, GPS, and total-station theodolite were used for surveys of depth of the water in two dammed lakes in 2007 and 2018. Data from the echo sounder was used to generate maps depicting elevation of the surface and bathymetry of each lake so each lake bottom elevation and water volume can be determined.

Sediment thickness can be calculated by differences of lake bottoms between 2007 and 2018. The data of sediment thickness and water volume was useful in estimating the long-term average sediment accumulation and water volume changes in the two dammed lakes, as shown in Table 3. Comparing to initial lake surface and water storage volume before spillway works in 1999, there was a significant drop in lake surface elevation by approximately 8 m after 2007. In particular, water storage volumes of the two lakes dramatically decreased, which was helpful for stability of the two dammed lakes. The thickest lake sediments were observed at approximately 3.7 and 3.1 m in the two lakes, respectively, from 2007 to 2018. The long-term average sediment accumulation rate can be calculated at approximately 0.33 m/y.

Table 3 Results of echo sounding survey for two dammed lakes in 2007 and 2018.

	Date	Lake Elevation		Changes of Lake bottom (m)	Maximum depth of lake (m)	Storage volume (m^3)
		Lake surface (m)	Lake bottom (m)			
Sezaikeng dammed lake	1999	577.5	---	---	37	1,089,700
	2007	570	540	3.7-m sediment amount	30	---
	2018	570.7	543.7		27	440,000
Jiutsaihu dammed lake	1999	585	---	---	29	678,000
	2007	576	559	3.1-m sediment amount	17	---
	2018	576.4	562.1		14.3	110,000

Overall, the spillway and related remedial works which had cost about 12 million USD were particularly effective suppress the production and flow of collapse debris in the bed and bank of the spillway channel through many torrential rainfalls and typhoons from 2004 to 2015. The most important performance of the spillway is to remain the stabilization of two dammed lakes.

4. Conclusion

For the performance evaluation of the spillway works in the Jiufengershan landslide, it is successful for these works to drop the elevation of water surfaces in two dammed lakes by 8.28 m and to control changes of water storage volume and sediment amount in the two lakes. Generally, 91% of 63 global barrier lakes broke down within a year after having formed [1]. As a result, it is valuable for the spillway in the landslide that two dammed lakes can be maintained and there was no severe disaster in the past.

Comparing to elevation changes of the spillway by DEMs of different periods with photogrammetry and LiDAR techniques, the average depth of the landslide area was 34 m with a collapse volume of 34.92 million cubic meters and a deposit volume of 36.58 million cubic meters while the Chichi earthquake occurred. Then, there were significant elevation changes in the spillway down-cutting by 20 m between 0 K+870 m and 1 K+80 m from the outlet of the lake between 2004 and 2011. The elevation changes in the spillway caused some submerged dams damaged. However, the elevation changes gradually mitigated from 2011 to 2015 after some check dams were completed. Using echo sounding surveys, average sediment amount of the two dammed lakes from 2007 and 2018 was only 0.33 m per year.

Finally, the most important performance of the spillway and remedial works is to remain the stabilization of the two dammed lakes and the landslide area.

References

[1] R. L. Schuster, *Landslide Dams: Processes, Risk, and Mitigation*, ASCE, 1986.

[2] T. Li, R. L. Schuster and J. Wu, Landslide dams in south-central China, in: *Landslide Dams: Processes, Risk, and Mitigation*, ASCE, 1986, pp. 146-162.

[3] X. Q. Chen, P. Cui, Y. Li and W. Y. Zhao, Emergency response to the Tangjiashan landslide-dammed lake resulting from the 2008 Wenchuan Earthquake, China, *Landslides* 8 (2011) 91-98.

[4] K. B. Delaney, S. G. Evans, The evolution (2010-2015) and engineering mitigation of a rockslide-dammed lake (Hunza River, Pakistan): Characterisation by analytical remote sensing, *Engineering Geology* 220 (2017) 65-75.

[5] J. W. Sager and D. R. Chambers, Design and construction of the Spirit Lake outlet tunnel, Mount St. Helens, Washington, in: L*andslide Dams: Processes, Risk, and Mitigation*, ASCE, 1986, pp. 42-58.

[6] J. A. Code and S. Sirhindi, Engineering implications of impoundment of the Indus River by an earthquake-induced landslide, in: *Landslide Dams: Processes, Risk, and Mitigation*, ASCE, 1986, pp. 97-110.

[7] D. C. Hansen and R. L. Morgan, Control of Thistle Lake, Utah, in: *Landslide Dams: Processes, Risk, and Mitigation*, ASCE, 1986, pp. 84-96.

[8] C. P. Cameron, K. D. Cato, C. C. McAneny and J. H. May, *Geotechnical Aspects of Rock Erosion in Emergency Spillway Channels*, Department of the Army, Waterways Experiment Station, Corps of Engineers, Geotechnical Laboratory, 1986.

[9] B. K. Odhiambo and S. K. Boss, Integrated echo sounder, GPS, and GIS for reservoir sedimentation studies: Examples from two Arkansas Lakes, *Journal of the American Water Resources Association* 40 (2004) 981-997.

[10] K. J. Shou and C. F. Wang, Analysis of the Chiufengershan landslide triggered by the 1999 Chi-Chi earthquake in Taiwan, *Engineering Geology* 68 (2003) 237-250.

[11] Q. Xu, X. M. Fan, R. Q. Huang and C. Van Westen, Landslide dams triggered by the Wenchuan Earthquake, Sichuan Province, south west China. *Bulletin of Engineering Geology and the Environment* 68 (2009) 373-386.

[12] H. Cedergren, *Seepage, Drainage & Flow Nets*, McGraw Hill, 1989.

Modern Environmental Science and Engineering (ISSN 2333-2581)
September 2019, Volume 5, No. 9, pp. 821-826
Doi: 10.15341/mese(2333-2581)/09.05.2019/005
Academic Star Publishing Company, 2019
www.academicstar.us

Modern School Architecture: Analysis of the Educational Research Center Applied in Maceió, Alagoas, Brazil

Camila Matos de Oliveira Silva, Dilson Batista Ferreira, Jéssica Caroline Rodrigues de Lima, Leila Vieira Torres, and Morgana Maria Pitta Duarte Cavalcante

Faculty of architecture and urbanism, Federal University of Alagoas, Maceió, Alagoas, Brazil

Abstract: The concept of park school, conceived by Anísio Teixeira, consisted of an ambitious project of reformulation of the teaching planned to become a national model both in terms of its pedagogical profile and in terms of its physical viability, becoming in an important landmark of modernist architecture. Following this pattern, the Applied Educational Research Complex (CEPA) emerged in 1958 in the city of Maceió in the state of Alagoas, Brazil, transforming the school architecture of the city and being long considered the largest educational complex in Latin America. In this context, the present work had as objective to make a study about the modern school architecture and an analysis of the projective strategies adopted in the Educational Complex of Applied Research (CEPA) in Maceió. A qualitative study was carried out, by means of theoretical foundation and case study, by the accomplishment of technical visit, photographic survey and design analysis, carried out at the Maria José Loureiro State School, component of the Complex. It was concluded that the Educational Complex consists of a strong example of the modern movement in architecture, with the presence of architectural elements intrinsic to this style, and also by the social concepts inherent to the model of Parque Escola. Understanding this way, its importance, still today, for the state of Alagoas.

Key words: "school park", modernism, study of form, architecture, project

1. Introduction

The present article intends to make a study of the modern school architecture, and an analysis of the projective strategies adopted in the Educational Complex of Applied Research (CEPA) in Maceió, capital of the state of Alagoas, Brazil.

The methodological procedures adopted in this study were elaborated based on qualitative research, through theoretical foundation and elaboration of a case study in the Educational Complex of Applied Research (CEPA), having as sample the Maria José Loureiro State School and Moreira e Silva State School2. A technical visit, photographic survey and design analysis were carried out based on the methodologies used by Cavalcante [1] for project analysis that addresses disciplinary and interpretative aspects; also observing the composition of the elements used in the façade, with reference to the principles of Ching [2]. Attending to the sectorization, partitioning and access; to the party; thermal comfort and the geometry of facades and volume. The language of the building was also observed, identifying its dominant design strategies.

Corresponding author: Camila Matos de Oliveira Silva, Doctor; research area/interest: conception, construction and adequacy of inhabited space. E-mail: oscamilamatos@gmail.com.

2. Theoretical Foundation

2.1 Modernism in School Architecture in Brazil

The Modern Movement in Brazil generated a new aesthetic phase that integrated tendencies fixed in the

valorization of the reality of the country, suggesting a liberation of the symbolic tie of the classic architecture visualized in the previous period. It was sought to produce school buildings with modulated and optimized spaces that would serve the emergent urban-industrial society [3].

Buffa and Pinto [4] point out that the attribute of simplicity conferred to plants, generally composed of long corridors with rooms on both sides, is more concerned with the use of ventilation, as well as the conditions of insulation and sound insulation. According to Segawa [5] the constructions were of low cost in structures of reinforced concrete and closing in masonry with preoccupation in sizing of circulations and with standardized finishes.

The precepts of rationality and functionality of modern architecture suited the economic interests of the state, and with this the new schools arose with simplicity of volumes, disembedding of ornamentation and use of modulations.

In the state of Alagoas, public education was marked by the CEPA — Educational Center of Applied Research inaugurated between the years of 1958 and 1971 in Maceió. This complex, made up of eleven schools, was designed by the architects Diógenes Rebouças and José Bina Fonyat and strongly influenced by the concept of School Park idealized by Anísio Teixeira. CEPA has long held the position of largest educational complex in Latin America, and is still considered one of the largest in the country [6].

2.2 The Theory of Form

The shape, according to Ching [2], is related to the sense of mass or three-dimensional volume and can be referenced both to the internal structure and to the outer profile, as well as the unit as a whole. The volume can refer to both spaces contained and defined by the planes of the walls, floor and ceiling, as well as space occupied by the mass of a building. The shape, size, color, texture, position, orientation and visual inertia are important properties of the shape, which can be affected by the different conditions and are observed by the individuals. Still according to the author, circulation is seen as the movement through the spaces of a building, responsible for its connection, influencing the perception of its forms and environments through its elements. Already Cavalcante [1] says that the language of the building is established in the interconnection with plurality, with the diversity of architectures and their temporal and spatial contexts. Thus, we take into account the design strategies used to generate the adopted parti.

3. Results and Discussion

Two school units of the CEPA Educational Complex, the Maria José Loureiro State School, directed to elementary education, and the Moreira e Silva State School, which attends secondary and high school students, were analyzed. Both schools count on classrooms, room of direction, coordination and teachers, library, auditorium, laboratories of informatics and sciences, cafeteria, covered patio and green area.

3.1 Modernist Language

The design of the Maria José Loureiro School has architecture with modernist features, without ornamentation, and pure forms can be found, such as the use of rectangular and circular geometric elements in both the floor plan and the façade presentation. The Escola Moreira e Silva presents the same characteristics, having as exception only the circular element, having exclusively rectangular geometric forms. Both schools rely on the presence of vertical linear elements, and the use of brises and cobogos (Figs. 1 and 2).

The recreation area of the Maria José Loureiro School presents a raised concrete box under the pilotis, which provides visual permeability and lightness, resulting in free living, living, and rest spaces (Fig. 3). Elements such as patios that give continuity between the interior and exterior can be found in both schools,

as well as the presence of rhythm in the openings of the doors and use of the full and empty ones, giving them physical characteristics of the modernist school (Fig. 4).

Fig. 1 Cobogós and brises elements on the façade of the State School Maria José Loureiro.

Fig. 2 Cobogós and brises elements on the façade of the State School Moreira e Silva.

Fig. 3 Recreational area of Maria José Loureiro school.

Fig. 4 Green area of Moreira e Silva school.

3.2 Sectorization, Compartmentalization and Accesses

The schools have only ground floor and are divided into six sectors: pedagogical area, educational area, recreational area, green area, services and toilets. In the Maria José Loureiro School, the pedagogical area has irregular shaped environments, due to the circular shape that makes up the structure of this block, while the classrooms have rectangular shapes and are accessed by an extensive corridor without openings. The green and recreational areas are covered by covered and uncovered spaces that have irregular contours (Fig. 5).

In the Moreira e Silva School, the sectors are distributed separately throughout the perimeter of the same, being located in corridors that interconnect them, having openings for the discovered patios. The green areas covered by the courtyards and the recreational area with covered patio and multi-sport gymnasium have regular forms and occupy the largest area of the terrain (Fig. 6).

The accesses of the schools occur in different ways because the Escola Maria José Loureiro is at a high level to the one of the street, being necessary the access by stairs and a more extensive and oblique ramp (Fig. 7). The access to the Moreira e Silva School is carried out only by a simple and straight ramp since its entrance is near the same level of the street (Fig. 8).

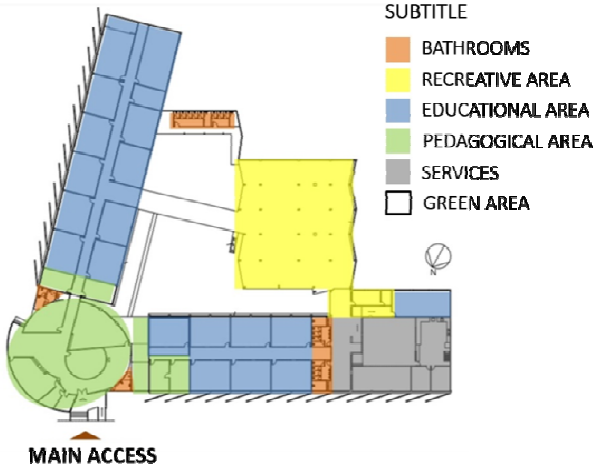

Fig. 5 Ground plan of the Maria José Loureiro State School with the sectorization [9].

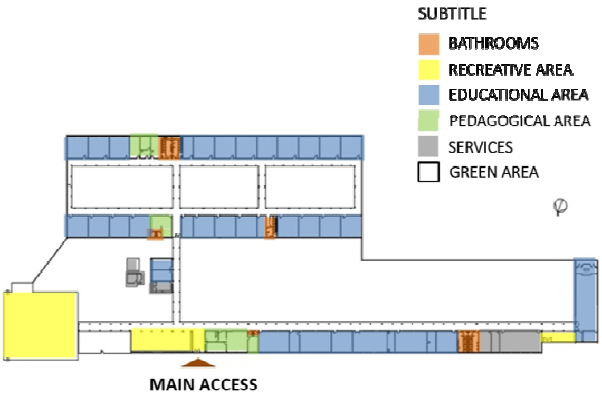

Fig. 6 Ground plan of the Moreira e Silva State School with the sectorization [9].

Fig. 7 Access to school entrance Maria José Loureiro.

Fig. 8 Access to school entrance Moreira e Silva.

3.3 Parti, or Design Concept

When analyzing the lower levels of the schools, it was possible to perceive the existence of a linear organization, because they have repetitive spaces and similar in terms of size, form and function. It is also possible to find principles of order such as symmetry and rhythm (Figs. 9 and 10).

In the Maria José Loureiro School, the pedagogical area, besides having a superior hierarchical level in relation to its function, has a prominent position due to its circular shape, being different from the others, and also serves as a connecting element between the two blocks of rooms of class. The balance and symmetry can be seen in this project, by tracing an imaginary axis diagonally from the center of the pedagogical area, providing a bilateral symmetry (Fig. 11).

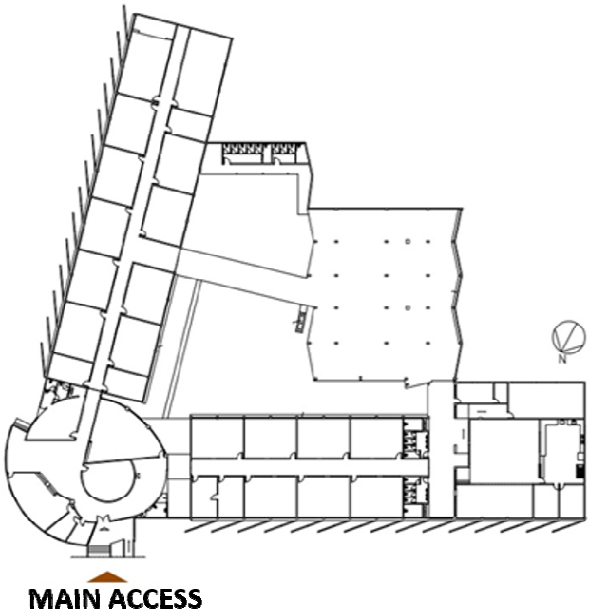

Fig. 9 Ground plan of the school Maria José Loureiro [9].

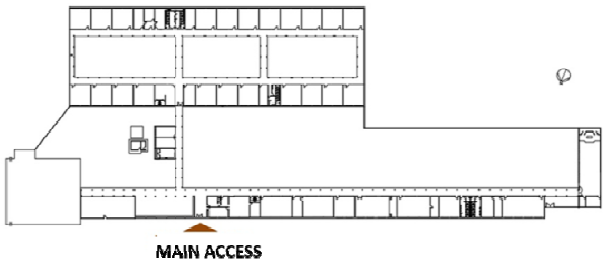

Fig. 10 Ground plan of the school Moreira e Silva [9].

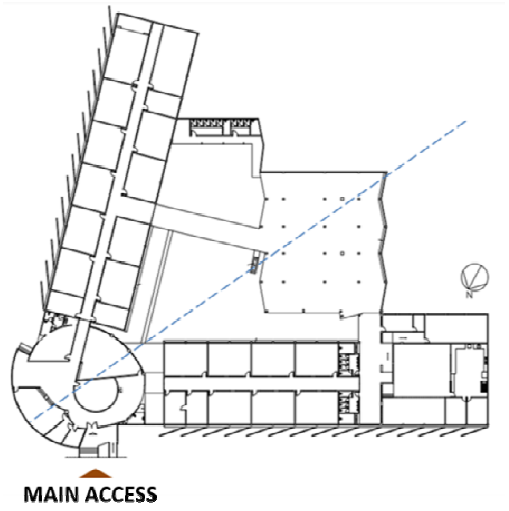

Fig. 11 Ground plan with axis of the Maria José Loureiro State School [9].

The internal circulations of the Maria José Loureiro School that give access to the classrooms are made up of parallel and opaque planes, with insufficient size and illumination, providing a sense of closure along the corridors (Fig. 12). The circulations of the Escola Moreira e Silva are broad and open, presenting a sense of freedom (Fig. 13).

3.4 Comfort

When analyzing the project of the Maria José Loureiro school, it is observed that the building was implanted in the terrain aiming at better thermal comfort for the students, because block 1, which has more classrooms, is contemplated by the southeast and east. As a solution to the problems caused by the sunshine, the architects designed, together with the facades of blocks 1 and 2, concrete bricks, which were strategically directed to protect the direct incidence of solar rays without blocking ventilation (Fig. 14).

Fig. 12 and 13 Circulation of Maria José Loureiro and Moreira e Silva schools, respectively.

In the Moreira e Silva school, it was noticed that the implantation of the school in the field favored the last block of rooms. This school has potential for cross ventilation resulting from the presence of open aisles and windows in classrooms. As in the other school, elements that reduce problems due to sunlight were used (Fig. 15).

3.5 Geometry of Facades and Volume

The Maria José Loureiro School has three facades, the asymmetrical main facade being composed of an entrance located in the circular block, displaced to the

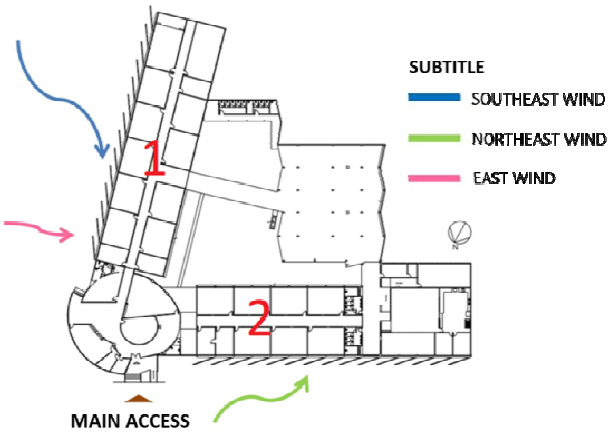

Fig. 14 Ground plan with wind flows of the Maria José Loureiro State School [9].

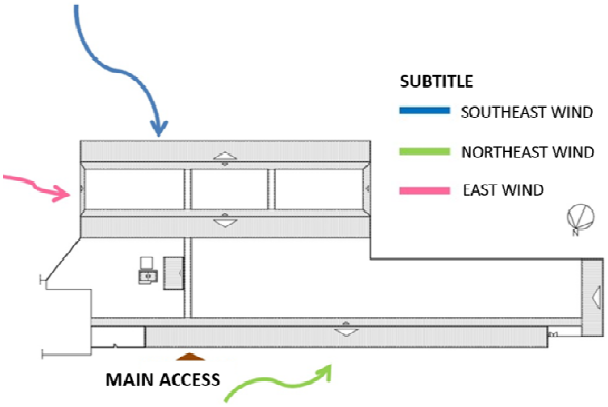

Fig. 15 Ground plan with wind flows of the Moreira e Silva State School [9].

Fig. 16 Main façade of the Maria José Loureiro school.

Fig. 17 Main façade of the Maria José Loureiro school.

left of the building, and also by a series of vertical brises that occupy the other part of the facade, transmitting dynamicity and communicating an idea of verticality to it (Figs. 16 and 17).

As far as volumetry is concerned, the exploration of geometric forms can be seen from a cylindrical element that interconnects two rectangular blocks. Although it is composed of rigid geometric shapes, the addition of brises gives an idea of movement to the whole.

4. Final Considerations

From the theoretical foundation on the modernist school architecture it was observed that the transformations in the scope of the architecture consist in cultural and political reflexes of the society of the period explored. In the case of the schools analyzed, it can be seen that these in fact consist of strong examples of the modern architecture movement, not only through the presence of architectural elements intrinsic to this style, but also through the social concepts that led to the elaboration of the complex.

References

[1] M. M. P. D. Cavalcante, D. B. Ferreira, J. Lima, C. M. O. Silva, and L. V. Torres, Modern school architecture: Analysis of the Educational Center of Applied Research in Maceió-AL, *National Encounter of Technology of the Environment Built* 17 (2018).

[2] Ching Francis D. K. Arquitetura, *Form, Space and Order*, São Paulo: Martins fontes, 1998.

[3] Azevedo Giselle Arteiro Nielsen, School architecture and education: A conceptual model of interactionist approach, Ph.D. Thesis in Sciences in Production Engineering, Federal University of Rio de Janeiro, Rio de Janeiro, 2002, p. 236.

[4] Buffa Ester and Pinto Gerson de Almeida, *Architecture and Education: Organization of Space and Pedagogical Proposals of Escola Escolares Paulistas, 1893-1971* (1st ed.), São Carlos: EdUFSCar, INEP, 2002, p. 174.

[5] Segawa Hugo, *Architectures in Brazil 1900-1990*, São Paulo: Publisher of the University of São Paulo, 1997, p. 224.

[6] Alaniz Erika Porceli and Fernandes Fabrícia Dias da Cunha de Moraes, School architectural patterns and expansion of elementary education in the early 20th century in Brazil, *Electronic Journal of Education* 10 (2016) (3) 87-103, accessed on 15 Mar. 2018, available online at: http://www.reveduc.ufscar.br/index.php/reveduc/article/view/1543/516.

[7] Carvalho Telma Cristina Pichioli, Inclusive School Architecture: Building spaces for early childhood education, Ph.D. thesis in Architecture and Urbanism, University of São Paulo, 2008, p. 342.

[8] Manhas Adriana Capretz Borges da Silva, Manhas Max Paulo Giacheto, Silva Lucas Queiroz and Lima Taiane Gonçalves, To know to preserve: the documentation of school complexes in Maceió (AL) in an architectural portal of historical, technical and artistic interest, in: *9th Seminar Docomomo Brasil — Interdisciplinarity and Experiences in Documentation and Preservation of Recent Patrimony*, Brasília, Anais electronic, 2011, accessed on: Jan 21 2018, available online at: http://docomomo.org.br/wp-content/uploads/2016/01/172_M02_RM-ConhecerParaPreservar-ART_AdrianaManhas.pdf.

[9] ALAGOAS, Secretary of State for Education – SEDUC, School projects in AutoCad format, Maceió, 2002.

Modern Environmental Science and Engineering (ISSN 2333-2581)
September 2019, Volume 5, No. 9, pp. 827-836
Doi: 10.15341/mese(2333-2581)/09.05.2019/006
Academic Star Publishing Company, 2019
www.academicstar.us

Design and Manufacturing of a System That Generates Renewable Energy from A Permanent Magnet Generator

Tripodi R.[1,4], Cowes D.[2,3], Montenegro S.[1,4], Ganiele M.[1,4], Alcantar S.[1,4], Lucio G.[1,4], Arcone D.[3], Daverio N.[3], Pereira C.[1,4], Moreno M.[3], and Ponzoni L.[4]

1. Ingeniería Ambiental, [b]Ingeniería de Sonido, Universidad Nacional de Tres de Febrero, Argentina

2. Proyecto ICES GDTyPECNEA, Argentina

3. Comisión Nacional de Energía Atómica, Argentina

4. Proyecto Aerogenerador Social, Universidad Nacional de Tres de Febrero, Argentina

Abstract: The most efficient electric generators to use in low power wind turbines are those of permanent magnets, this being one of the most expensive components of wind turbine. In this work, a prototype of a synchronic generator of axial flow was designed and built, based on Neodymium-Iron-Boron permanent magnets to be installed in low power wind turbines (less than 0.5 KW). The work was based on the following premises: 1) Designing and specification of the electrical and mechanical components of the generation system for wind turbines. 2) Building the power generation system, 3) Realizing tests and measurements of the constructed prototype. All the parts of the generator (rotor, stator, AXIS, base and coils) were designed and built using the following machinery: pantograph, grinder, bench drill, bench sander, tin soldering iron, winder, industrial dryer, rotating lathe. The result was a three-phase axial generator with 12 pairs of poles, with 24 magnets located in a rotor of 165 mm diameter and 9 coils connected in a star shape, offset by 40 degrees from one another. The tests yielded a maximum voltage test of 7.6 Volt at 500 rpm, obtaining a linear relationship between voltage and rotational speed. Although, this design is very low power, its construction allowed to obtain the necessary experience and knowledge-know how- for the development of future electric generators for low power wind turbines in the alar profile research group.

Key words: permanent magnet, generator, stator, rotor, wind turbine

1. Introduction

The model of the current economic development around the world is based on the intensive use of fossil energetic resources mainly in the underdeveloped countries.

These fuels are not renewable, they are finite and so the reservoirs are depleted progressively.

On the other hand, their extraction, processing, and combustion increase the proportion of greenhouse effect and release toxic gases to the atmosphere.

In order to find a solution to this problem, a Project called “social wind turbine” has been created. The aim of the Project is to develop wind turbine of horizontal axis, low-powered and manufactured from reused materials to be installed in poor communities. In order to achieve this goal, a wind turbine prototype has been manufactured and installed in the National University de Tres de Febrero in Villa Lynch. This prototype will be used to adjust the design variables. This project has been approved by the university (Code 32/17 521).

The aim of this project is to design and manufacture the electrical energy generator system in a laboratory scale. To make it reproducible, the design has some features: easy manufacture, assembly, installation and operation. Making the prototype more accurate will give poor communities access to safe and reliable electric power.

Corresponding author: Romina Noelia Tripodi, Environmental Engineer; research area/interest: wind energy. E-mail: rominatripodi1991@gmail.com.

2. Materials and Methods

The paper starts with the design of the generation system. At this stage, equations, criteria, materials and assumptions necessary to get the design variables are presented.

A permanent magnet generator has been proposed to turn the mechanic energy obtained into electrical energy.

In this type of generator, the magnetic flux goes through the coils in a parallel direction to the axis device. This device consists of two rotors and one stator. Both rotors are joined by a longitudinal axis and the stator is installed in a fixed base. The copper wire coils are in the stator, there the tension is generated by the magnetic field rotors. The magnets are displayed to let the magnetic flux go from one rotor to another. The magnetic flux goes through the coils as the rotors turn round. In this way, the sinusoidal voltage is induced in the coils [1]

For the development stage, the paper "Axial Flux Permanent Magnet Generator Design for Low Cost Manufacturing of Small Wind Turbines" [2] was used as a reference. After the realisation of the calculations in the design stage, the values for the manufacturing of the laboratory scale generator were obtained as shown in the data Table 1.

2.1 Number of Poles and Coils

The number of poles in a generator is directly related to the frequency of the voltage we want to generate. The nominal frequency determines the pole pairs *p*, and so the total number of magnets.

$$p = \frac{120\, f_{nom}}{n_{nom}} \quad (1)$$

$$0.5 = \frac{2Q}{3p} \quad (2)$$

The permanent selected magnets are rectangular and of Neodymium-Iron-Boron (NdFeB). It is possible to reuse the magnets in the hard discs to reduce the cost in the manufacturing generation system and at the same time to positively contribute to the environment.

Table 1 List of symbols [1].

ai	pole arc to pole pitch ratio
Bmg	magnetic flux density on magnet surface (T)
Bp	peak value of the fundamental component of airgap flux density (T)
Br	remanent magnetic flux density (T)
Cpmáx	maximum power coefficient
Cq	heat coefficient (W/cm^2)
dc	copper diameter (mm)
Din	generator inner diameter (mm)
Dout	generator outer diameter (mm)
Ef	electro-magnetic force (V)
fnom	generator nominal frequency (Hz)
G	mechanical clearance gap (mm)
Hc	coercive field strength (A/m)
hm	permanent magnet thickness (m)
hr	back iron thickness (m)
IAC	nominal AC current (A)
IACmax	maximum AC current (A)
Jmax	maximum current density (A/mm^2)
kd	inner to outer radius ratio
kf	coil fill factor
ksat	saturation factor
la	active length (m)
laug	average coil length (m)
lec	end-turn length (m)
Is	generator inductance (mH)
N	generator RPM
Nc	number of turns per coil
nnom	nominal RPM
Nphase	number of turns per phase
P	number of pole pairs
Pair	aerodynamic power (W)
Pnom	generator nominal power (W)
PCU	ohmic losses (W)
pcu	copper density (kg/m3)
Q	number of coils per phase
Q	total number of coils
Rc	coil resistance (Ω)
Rin	inner radius (m)
Rout	outer radius (m)
R turb	wind turbine diameter (m)
Sc	copper crosection (mm^2)
SPM	permanent magnet surface area (m^2)
tw	stator axial thickness (m)
vw	wind speed (m/s)
wc	coil side width (m)
wm	permanent magnet radial width (m)
H	generator efficiency
λopt	optimum tip speed ratio
μ0	vacuum permeability (Wb/(A·m))
μrrec	recoil permeability
P	air density (kg/m^3)
ρcu	electrical resistivity of copper (Ω m)
Φmax	maximum magnetic flux (Wb)
ωe	electrical speed (elec.radians)

The number of coils (Q) can be calculated from the Eq. (2). The appropriate pole pair for coil combinations for a three-phase system is shown in Table 2.

Table 2 Pole-coil combinations [1].

8-6	12-9	16-12	20-15	24-18

The combination 12-9 was used. The coils will be connected in a three- phase system using a star connection. The coils should be separate by 120° electric degrees regarding the other phase.

2.2 Axial Dimensions of the Generator

The Axial dimensions of the generator include the mechanical clearance gap (*g*), the thickness of the stator (*tw*), the thickness of the rotor discs (*hr*), and the thickness of the magnets (*hm*) as shown in Fig. 1.

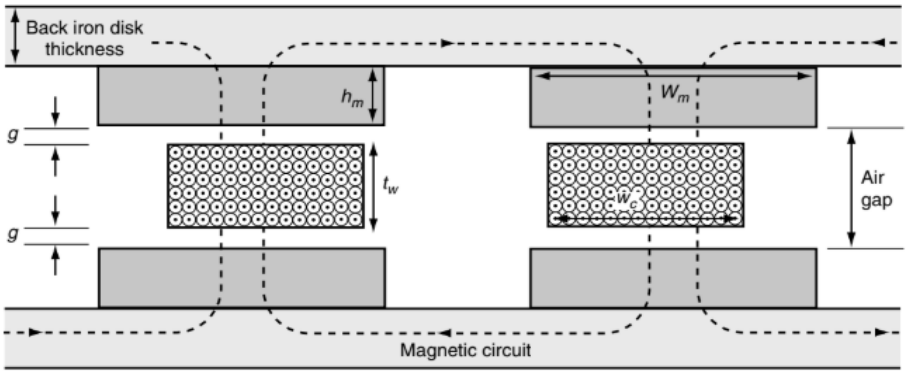

Fig. 1 Axial dimensions of the generator (rotor disks and magnets, stator coils and clearances).

The mechanical clearance gap (*g*) is one mm.

Magnets Dimensions

thickness (h_m): 3 mm; width (w_m): 10 mm; length (l_a): 20 mm

2.3 Rotor Disc Thickness

The rotor discs thickness that makes the rotors should be reduced to as much as possible to avoid increases in the total weight of the generator, but at the same time it should not be reduced too much in order to withstand the attractive magnetic forces pulling the two rotors discs together and thus ruining the mechanical clearance gap damaging the generator.

Also magnet saturation is possible in the iron disc if it is chosen too thin. Nevertheless we can use a general rule which indicates that the thickness of the rotor should be the same as the thickness of the magnets. The diameter selected for the rotors is 16.5 cm.

2.4 Axial Coil Thickness (t_w)

The *tw* can be calculated through the equation 3 which results from the analysis of the magnetic circuit while assuming no magnetic flux density leakage. The magnetic flux density near the magnet surface B_{mg} is usually set about *br/2*, where the remanent magnetic flux density *Br* and coercive field strength *hc* are characteristic values of the magnet that are related to its grade and can be easily extracted from neodymium magnet data sheets. Other variables are k_{sat} = 1 due to the coreless stator and μ_0 the vacuum permeability.

$$B_{mg} = \frac{Br}{2} = \frac{B_r}{1+\mu_{rrec}\frac{(g+0.5t_w)}{h_m}k_{sat}} \quad (3)$$

$$\mu_{rrec} = \frac{1}{\mu_0}\frac{B_r}{H_c} \quad (4)$$

Due to the fact that the magnets are NdFeB N40, the equation can be rewritten for the stator thickness (t_w) as:

$$t_w = 2h_m - 2g \quad (5)$$

$$t_w = 2\ (3\ mm) - 2(1\ mm) = 4\ mm$$

2.5 Number of Turns per Coil (N_c)

Using basic equations for the electromagnetic induction and assuming an almost sinusoidal magnetic flux density, the required turns per coil can be

calculated using Eq. (6).

$$\Phi_{max} = B_{mg} * w_m * l_a \quad (6)$$

$\Phi_{max} = 0.64T * 0.01m * 0.02m = 1.28\times10^{-4}$Wb

The number of turns per coil *Nc*, is calculated using 7 where k_w is a winding coefficient equal to 0.95, *Q* is the number of coils per phase, *n* is the *RPM* at cut-in and ef is the corresponding induced voltage during the the cut-in.

$$N_c = \frac{\sqrt{2}E_f}{q*2\pi*k_w*\Phi_{máx}*n*\frac{p}{120}} \quad (7)$$

$$Nc = \frac{\sqrt{2}*12V}{3*2\pi*0.95*1.28\text{x}10^{-4}\text{Wb}*160rpm*\frac{12}{120}}$$

$$Nc = 462.74\ vueltas$$

2.6 Coil Width (w_c)

Given the number of turns per coil N_c and the axial stator thickness t_w, the coil leg width w_c is calculated in 8 for a value of the heat coefficient *cq* that is equal to 0.3 W/cm^2 and where $I_{ACmáx}$ is the maximun generator current and *p* is the electrical resistivity of copper.

$$w_c = \frac{I_{AC\,máx}*N_C}{\sqrt{\frac{2*cq*k_f*t_w}{\rho}}} \quad (8)$$

The fill factor *(kf*) of the coils could be about 0.55 due to the fact that construction of the coils is manually done.

2.7 Heat Coefficient cq and Maximun Current Density J_{max}

Along with the heat coefficient *cq*, the maximun current density J_{max} of the winding must be cosidered as shown in 14.

This is possible after realising the Eq. (9) for I_{ACmax} where in the place of I_{AC}, I_{ACmax} is used which is the maximun current used produced momentarily in a gust of wind which is 10% more powerful than the nominal potential P_{nom}. So 15 has to be calculated for the copper cross-sectional area.

$$I_{ACmáx} = \frac{1.1*P_{prom}}{3*E_{fnom}*\eta} \quad (9)$$

To know the value of I_{AC} it is necessary to calculate E_{fnom}, which is obtained from the following equation:

$$E_{fnom} = \frac{n_{nom}}{n_{cutin}} * E_{fcutin} \quad (10)$$

$$E_{cutin} = \frac{E_f+1.4}{\sqrt{3}*1.35} = \frac{12\ V+1.4}{\sqrt{3}*1.35} = 5.74\text{ V} \quad (11)$$

$$n_{nom} = \frac{60*v_w*\lambda_{nom}}{2\pi*R_{turb}} = \frac{60*10\frac{m}{s}*7}{2\pi*1.5m} = 445.63\text{ rpm} \quad (12)$$

$$n_{cutin} = \frac{60*v_{cutin}*\lambda_{cutin}}{2\pi*R_{turb}} = \frac{60*3\frac{m}{s}*8.75}{2\pi*1.5m} = 167.11\text{ rpm} \quad (13)$$

As it is shown in the Eqs. (11), (12) and (13) it was assumed an E*f* of 12 V, a minimun wind speed of 3 m/s and a nominal wind speed of 10 m/s. On the other hand, a value of λ_{cutin} of 8.75 was used, a value of λ_{nom} *of 7* and *a* R_{turb} of 1.5 m.

$$E_{fnom} = \frac{445.63\ rpm}{167.11\ rpm} * 5.74\ V$$

$$E_{fnom} = 15.28\ V$$

Supposing that η = 0.9 then the value of $I_{acmáx}$ can be calculated

$$I_{ACmáx} = \frac{1.1 * 35\ V}{3 * 15.28\ V * 0.9} = 0.933\ A$$

Once the value of $I_{ACmáx}$ is known, the side width of the coil can be calculated with the Eq. (8).

$$w_c = \frac{0.933\ A * 462.74\ rpm}{\sqrt{\frac{2 * 3000\frac{W}{m^2} * 0.55 * 0.00371428m}{0.0000000168\ \Omega\text{ m}}}}$$

$$w_c = 0.01598\ m$$

A standard approach for the design of the small wind turbine would be a value for the current density of 6A/mm^2 without this value being restrictive. The structure of the generator, with the rotating discs working as fans cooling the winding system allows high current density values.

$$J_{máx} = \frac{I_{ACmáx}}{S_c} \quad (14)$$

2.8 Copper Diameter (d)

The copper cross-sectional area *sc* and the diameter of the copper wire dc which will be used, it is obtained from Eq. (15) and (16) respectively.

$$s_c = \frac{k_f*w_c*t_w}{N_c} \quad (15)$$

$$s_c = \frac{0.55 * 0.01598\ \text{m} * 0.00371428\text{m}}{462.74\ rpm}$$

$$s_c = 7{,}0569\text{x}10^{-8} m^2$$

$$d_c = \sqrt{\frac{4 * s_c}{\pi}} \quad (16)$$

Substituting the value *sc* in the previous equation, the value of the copper wire diameter is obtained.

$$d_c = \sqrt{\frac{4 * 7{,}0569\text{x}10^{-8} m^2}{\pi}}$$

$$d_c = 2.997x10^{-4} m$$

With the result obtained in Eq. (15) $J_{máx}$ of the Eq. (14) is obtained.

$$J_{máx} = \frac{I_{ACmáx}}{S_c} = \frac{0.933\ A}{7{,}0569\text{x}10^{-8} mm^2}$$

$$J_{máx} = 13221102.75\ \frac{A}{mm^2}$$

The form of the coils: It is a general rule that the inner form of the coils has to have the same dimensions as the magnets

The generator radio: Using all the variables obtained previously, the diameter of the steel discs can be calculated.

$$R_{in} = \frac{(2Q * w_c) + (p * w_m)}{2\pi} \quad (17)$$

$$R_{in} = \frac{(2 * 9 * 0.01598521181\ \text{m}) + (12 * 0.01\ m)}{2\pi}$$

$$R_{in} = 0.0648\ \text{m}$$

$$D_{out} = D_{in} + 2l_a \quad (18)$$

$$D_{out} = (2 * 0.0648\ \text{m}) + (2\ * 0.02\text{m})$$

$$D_{out} = 0.1697\ \text{m}$$

2.9 Generation System Manufacturing

2.9.1 Materials (Table 3)

2.9.2 Machinery (Table 4)

Table 3 Materials and dimensions.

Parts	Components	Quantity	Dimensions
Rotor	Magnets	24	l_a: 20 cm w_m:10 cm h_m: 3 mm
	Low carbon steel plate	2	D_{out}: 165 mm h_r: 3 mm
Stator	Paraffin	250 g	-
	Copper wire	500 g	d_c: 0.3 mm
	Tape	-	-
Axis and Base	Wood plank	1	Long: 170 cm *Width:* 20 cm *Thickness:* 4 cm
	Ball bearings	2	Diameter (in): 12 mm *Diameter (out)*: 32 mm
	Threaded rod	1	Diameter (out):12 mm
Others	Nut	8	Diameter (in): 12 mm
	Screws	11	Diameter: 4 mm
	Washers	8	Diámeter (in): 12 mm

Table 4 Machinery and application.

Machinery	Application
Pantograph	Circular cutting of steel plates for the rotor
Grinder	Edge rounding
Drill press	Circular cutting of acrylic plates and wood drilling
Pencil soldering iron (low power)	Cable welded
Oscilloscope	Obtaining the sinusoidal curves
Gaussimeter	Magnetic field measurement
Rotating lathe	Shaft rotation
Industrial dryer	Paraffin casting
Winder	Winding of copper wire

2.10 Stator Manufacturing

The stator manufacturing started with the winding up of the copper wire of 0.3 mm diameter. This was realised with a winder which possess a turns counter and let us set different speeds for the winding up.

A device that works as a winding mold was developed; it allows to keep the right dimension of the coil (thickness and width) and it also gives it the right size as shown in the Fig. 2.

As it was mentioned in the design stage, the inner form of each coil has to be the same as the form of the magnets that's why an acrylic mold was inserted.

(a)

(b)

Fig. 2 (a) Winding process, (b) Inside of the coil.

The winding process was done at different speeds based on the forms the coils were taking and it finished when the device showed 462 turns. Twelve coils were made and nine were selected. The coils whose inductance values were similar, were selected.

Then the coils were placed in a rectangular plastic mold and covered with paraffin. A circumference was realised manually. This circumference was devided in 9 parts to ensure the right place of the coils. Then a neutral circular wire was placed in the center of the mold and the initial ends were joined to each coil. Once the ends were linked, the three-phase connection started.

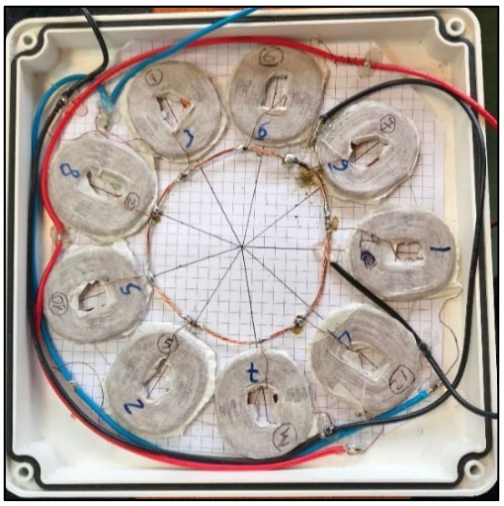

(a)

(b)

Fig. 3 (a) Three-phase connection, (b) Stator embedded in paraffin.

The coils 1, 2, 3 constitute the first phase (blue wire), 4, 5, 6 the second phase (red wire) and 7, 8, 9 the third phase (black wire). Later 250 paraffin grams were heated until it became liquid and this was put in the mold to form the stator.

The result was a stator of 19.6 cm wide, 19.6 cm long and 6.1 cm thick.

2.11 Rotors Manufacturing

For the manufacturing of the rotors, a low carbon steel plate was used. The plate was cut with a pantograph and two discs (165 mm in diameter and 3 mm thick) were obtained. Every measurement was calculated in the design stage.

Three drillings were made in each disc. One in each centre (12 mm in diameter) and the other two were made to join both discs so that they could reach the same speed. The location of the twelve magnets was drawn to fix them in the right position, well aligned. After that the magnets were inserted alternatively.

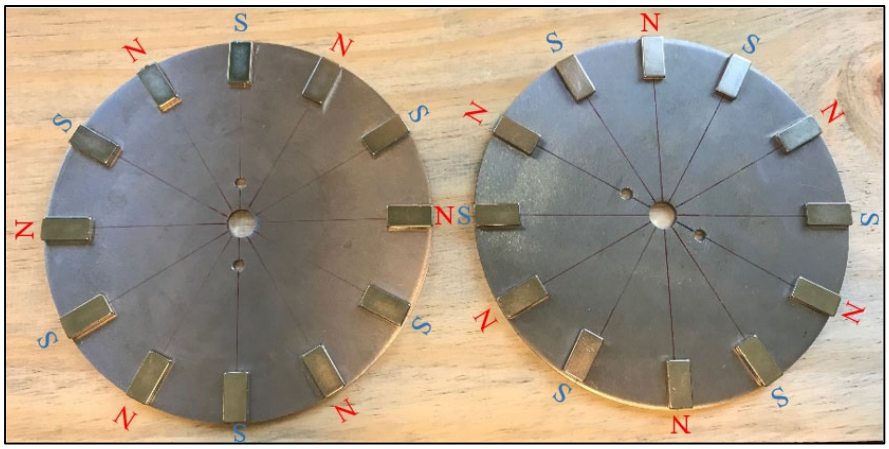

Fig. 4 Rotors with permanent magnets.

2.12 Assembly and Installation

Once the rotors and the stator were built, the Assembly of the Generation System was started. The rotors were placed on a longitudinal axis and the stator (between the two rotors) on a fixed base. Also one of the phases was connected to 4 led lights to check the operation of the generator.

2.13 Costs

For the manufacturing of the energy generator system based on permanent magnets, reused materials were used. Not all the materials were reused because of the lack of time to collect them.

2.14 Measurement of the Magnetic Field

For the measurement and detection of the electromagnetic fields a Gaussmeter was used to measure the magnetic influence produced by the permanent magnets. The unit of measurement obtained was kG. Before the measurement of magnetic field, the equipment was calibrated.

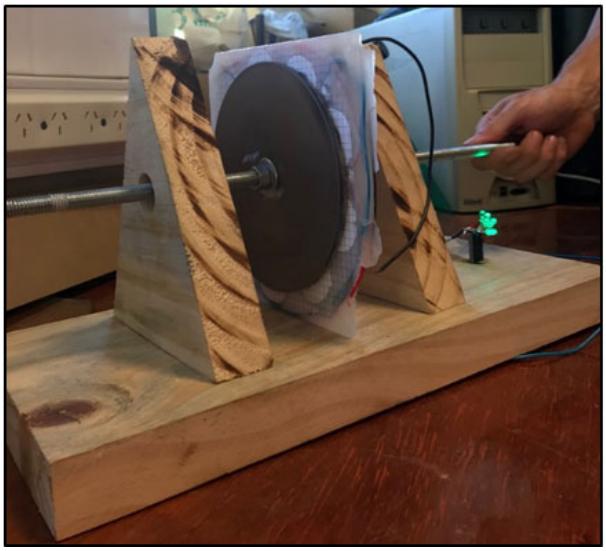

Fig. 5 Permanent magnet generator.

Table 5 Costs of manufacturing.

	Components	Quantity	Cost / Obtaining
Rotors	Neodymium-Iron-Boron (NdFeB) magnets	24	$383
	Steel plates	2	Reused
Stator	Paraffin	250g	$42
	Copper wire	500g	$371
Axis and base	Wood plank	1	Reused
	Threaded rod	1	Reused
	Ruleman	2	$100
Others	Nuts	8	Reused
	Washers	8	Reused
	Screws	11	Reused
Total	----------	----------	$896

Once the equipment was calibrated, the sensor was put on the magnets and the measurement was realised. The value of the magnetic field obtained was -2.63 kG at the temperature of 24ºC.

2.15 Resistance and Inductance of the Phases

Once the manufacturing of the stator was finished, the values of R and L of each phase were measured at 100 hz.

2.16 Sinusoidal Curve

A three-phase system is the set of three monophases which are outphased at 120º.

2.17 Electrical Tests

To measure the tension and the revolutions per minute (rpm) the generator was connected to a voltmeter and a tachometer. Consequently an axis was joined to a drill to make it turn around to measure at different speeds.

2.18 Tension vs RPM

To obtain the graph of tension with load based on the rpm, one phase was connected to three resistors of 1 ohm each. Knowing that the power is Tension^2/Resistance, it was multiplied by three to get the delivered power to the three loads.

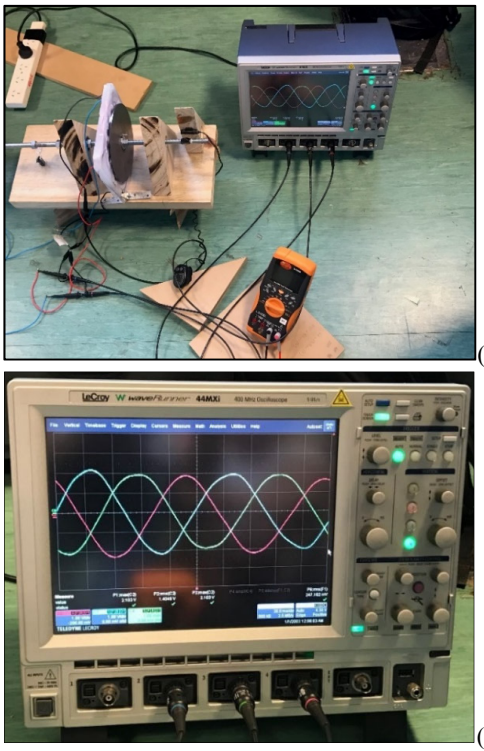

(a) (b)

Fig. 6 (a) Connecting the generator to the oscilloscope, (b) Sinusoidal curve.

Table 6 RPM vs. voltage.

Data	Rpm	Volt (V)	Power (W)
1	25	0.456	0.6238
2	138	0.4789	0.6880
3	145	0.4653	0.6495
4	147	0.4892	0.7179
5	149	0.4813	0.6949
6	151	0.4891	0.7177
7	162	0.6404	1.2303
8	213	0.7746	1.8000
9	236	0.7869	1.8576
10	240	0.7822	1.8355
11	243	0.7912	1.8780
12	246	0.9067	2.4663
13	266	0.9297	2.5930
14	286	0.953	2.7246
15	290	0.9224	2.5525
16	295	0.9425	2.6649
17	311	1.0594	3.3670
18	333	1.09	3.5643
19	338	1.0966	3.6076
20	343	1.1003	3.6320
21	360	1.345	5.4271
22	413	1.4111	5.9736
23	449	1.4287	6.1236
24	459	1.4759	6.5348
26	472	1.5359	7.0770
27	493	1.6091	7.7676
28	500	1.5999	7.6790
29	515	1.5446	7.1574
30	493	1.4975	6.7275
31	486	1.5626	7.3252

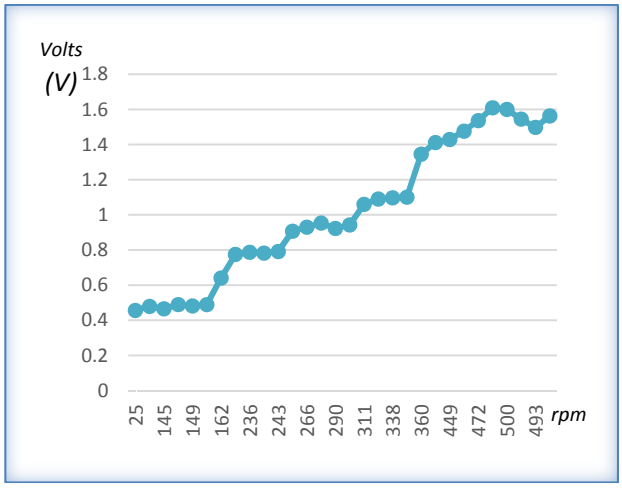

Fig. 7 Volts vs. rpm.

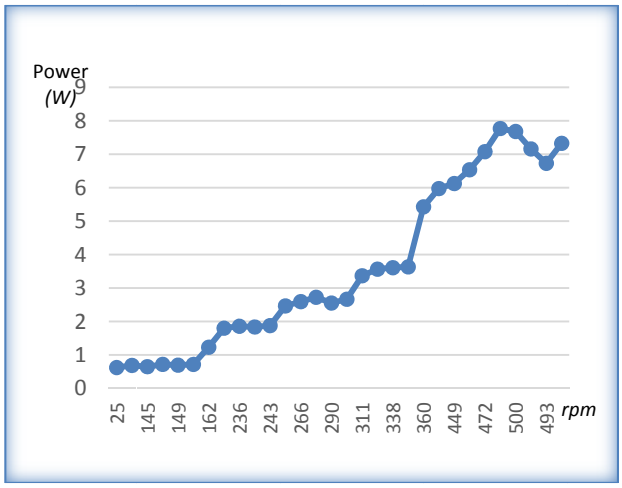

Fig. 8 Potencia vs rpm.

The maximun voltage obtained was 1.6091 V at 493 rpm giving out the maximun power of 7.76 W.

3. Results and Discussion

The generation of energy based on the application of the Faraday-Lenz law using permanent magnets is a good alternative to be installed in the wind turbine prototype located in Villa Lynch.

The current development from its proposed small scale represents a potential solution to the crisis that is currently overwhelming us around the world in reference to exhaustion of the natural resources and the global warming.

The stages of design, manufacturing and measuring done during the current work meant an incentive to continue doing research on the exploitation of wind resources.

This development let us identify the methods which better adapt to low budgets and short time lapses in the manufacturing.

It is clear that the power achieved with this prototype is not enough to meet the energy needs of the university. However, considerable quantities of energy could be obtained by increasing the scale and by optimizing the operation variables in future developments.

3.1 Aspects to Improve

It is important to use the appropriate materials to keep the main features and structural integrity intact. Next, some aspects of the generator are detailed to be improved, which will be useful to optimize the design variables.

Stator: A 3D printer is a good alternative for the manufacturing of the stator. A good option for the winding process is to use a precision coiler so as not to get a lot of space between the copper overlapping layers. Thus, the width of the coils will be reduced approaching the design values

Rotors: The use of the most quantity of magnets in the rotor can mean an important improvement for the generator because the magnetic field would be intensified.

Base and ball bearings: A good choice for the base would be the use of a satellite panel with honeycomb structure because it is resistant and light. However, it is difficult to acquire this material. The support of the ball bearing can be obtained from a 3D printer to reduce its size and weight.

3.2 Future Works

The development of the energy generation system based on permanent magnets was very important to know in detail the design and manufacturing process of these types of generators. Based on this work, the necessary adjustments will be made so that the generation system to be installed in the prototype located in Villa Lynch will not have mechanical or

electric defects before it starts operating.

From this starting point, a future job will be to implement the proposed aspects to improve and then to propose a storing energy system through batteries. Once this system is optimized, the installation of this device in the university is the next step. To get more energy, solar panels can also be installed.

References

[1] K. C. Latoufis, G. M. Messinis and N. D. Hatziargyriou, Wind Engineering (4 ed.), Vol. 36, 25 de julio de 2012, Atenas: Universidad Técnica Nacional de Atenas. Recuperado el 4 de noviembre de 2018, available online at: http://journals.sagepub.com/doi/abs/10.1260/0309-524X.36.4.411

[2] P. B. Rosenman, Diseño de Aerogeneradores con imanes permanentes para aplicaciones en electrificación rural. Santiago de Chile: Universidad de Chile Facultad de Ciencias Físicas y Matemáticas, Departamento de Ingeniería Eléctrica, agosto de 2007.

Modern Environmental Science and Engineering (ISSN 2333-2581)
September 2019, Volume 5, No. 9, pp. 837-848
Doi: 10.15341/mese(2333-2581)/09.05.2019/007
Academic Star Publishing Company, 2019
www.academicstar.us

Temporary Effect of Mining on Breathing and on the Physicochemical Conditions of Soil

Giovanny Ramírez Moreno[1, 2], Harley Quinto[3], Lady Vargas Porras[1, 2], and J. Orlando Rangel Ch.[4]

1. Institute of Environmental Research of the Pacific, Research Group of Knowledge, Management and Conservation of the Ecosystems of Chocó Biogeográfico, Colombia

2. Institute of Natural Sciences, National University of Colombia, Chocó, Colombia

3. Faculty of Biology Science, Choco Technological University, Quibdó, Colombia

4. Biodiversity Research Group, Institute of Natural Sciences, National University of Colombia, Bogotá, Colombia

Abstract: The physicochemical variables and the respiration of the soil were characterized in the areas of 5, 15 and 30 years of post-mining recovery and a reference forest. We used 15 plots of 200 m^2 (4 × 50), in each of the successional stages (area of early succession, forest of late succession and reference forest) for a total of 60 plots. The results showed that after the mining, the contents of OM, total N, Al and clay were increased; while, the concentrations of available P and sand decreased. The edaphic availabilities of Ca, K, Mg, CICE and silt increased during the intermediate stages of succession, and were reduced in the reference forest, while the variables indicating edaphic microorganism activity (H, CH_4 and CO_2) were high in all the scenarios evaluated. It was concluded that after 30 years of recovery the K, Ca and Mg have their greatest availability in the soil and that with the advance in plant succession the availability of total N and MO increases due to the recovery of the forest increases the accumulation of aerial and subterranean vegetation biomass, which increases the accumulation of OM of the soil, given the balance of income and expenses due to production and decomposition of organic waste (litter) of the forest. It is evident that with open-pit mining in tropical rainforests, pedogenesis and soil development begins again, with the attenuating of not favoring the natural ecological recovery.

Key words: soil, mining, breathing, physicochemical conditions

1. Introduction

Soils are fundamental components of tropical forest ecosystems [1]. Since, according to their physicochemical characteristics, they determine plant diversity, ecological succession, net primary productivity, nutrient recycling and the role of forests in mitigating global climate change [2-7]. However, these ecosystem components are strongly threatened by the destruction and degradation of habitats, which generate significant negative impacts on their ecological functioning [8]. In particular, open-pit mining is one of the main anthropogenic activities that causes losses and significant degradation of tropical soils. Open-pit mining of metals is a harmful process against tropical soils; since, in the exploitation process, the vegetation cover and the edaphic substrate covering the exploited mineral deposit are removed [9, 10]; As a result, soil aggregates are eroded, texture is changed, moisture content is reduced, nutrients are leached, the substrate is contaminated with toxic waste (mercury), vegetation is reduced and associated ecological processes are affected [9-11]. Also, after the mining activity the residual material is accumulated forming small mounds, characterized by having very low fertility and presenting, in the upper part, coarse textures (gravels and coarse sands), with very little

Corresponding author: Lady Vargas Porras, Doctorate in Biology; research area/interest: aquatic pollution, water ecosystems, limnology, environmental management. E-mail: lvargas@iiap.org.co.

moisture content and low proportions of silt, clays and organic matter (MO), due to the process of water dragging and deposition in the lower parts of the mound [12]. Therefore, a mosaic of soil substrates and plant communities are generated in different successional stages, differentiated according to the time and intensity of the disturbance [9].

When open-pit mining is carried out, the soil is totally exposed (without surface horizons, nor forest cover) and the nutrients are easily lost by leaching [10], this situation accentuates the infertility of the soil and hinders plant succession and recovery [12, 13]. Given that mining has strong impacts on the edaphic system, it is essential to develop restoration processes to recover the ecological functions developed by tropical soils [10, 12-14]. In particular, soil type, microbial activity, texture and availability of nutrients have a primary effect on the recovery of soils in degraded areas 12, 13, 15]; consequently, in order to effectively execute restoration programs it is necessary to know how the physicochemical properties of the soil change in successional ecosystems degraded by mining.

It has been hypothesized that in tropical soils, in initial successional stages, there is a limitation by nitrogen (N), which over time is mitigated due to the colonization of atmospheric N2 fixative plants [16]; in turn, this N fixation is limited by the availability of P and humidity. Therefore, as the succession progresses, this limitation is reduced [15, 17]. Unlike N, P levels in the soil tend to be high in the first successional stages, and over time it tends to decrease its availability, due to losses by leaching and immobilization in Fe and Al sesquioxides [18-20]. However, some studies that evaluate the edaphic parameters in different successional stages show that the nutrients present different dynamics that differ from the hypothesis proposed [21-23]; For example, Werner (1984) [21] showed that some minerals increase temporarily and then decrease (Fe, Al, H, MO, total N), some fluctuate (NH4-N, PO4-P) and others decrease (Ca, Mg, K, Mn). While, Li et al. (2013) [23] observed that with the passage of time in the succession there were no significant changes in total P and soil NH4-N. Which, evidences that each ecosystem presents different environmental conditions that condition the ecological succession and consequently the restoration of degraded areas; likewise, these investigations denote uncertainties and lack information in this regard.

The biogeographic Chocó region is considered one of the most biodiverse and endemic hotspots on the planet [24]. However, in these ecosystems, rural communities constantly conduct gold and platinum open-pit mining [25, 26]. According to the Ministry of Mines and Energy of Colombia, as of 2011, ≈ 268,821 hectares of forest have been granted for this activity [27, 28]; likewise, according to the IIAP (2001) [29] about 360 hectares of natural forest are destroyed each year as a result of this activity [29]. This produces soil degradation, pollution and considerable losses of diversity [30]. Given this situation, and with the purpose of evaluating the hypotheses about the dynamics of nutrients in tropical successions [21, 23, 31], we set out to evaluate the physicochemical properties of soil in successional ecosystems degraded by mining in forests of the biogeographical Chocó.

2. Materials and Methods

2.1 Study Area

The present study was conducted in the San Juan mining district, in the Jigualito corregimiento, belonging to the municipality of Condoto, in the department of Chocó, Colombia. The town of Jigualito is located at an altitude of 74 masl; it limits to the North with Guarapito by the highway that leads to Chiquichoqui, to the South with Novita by the watershed between the rivers Tamaná and Opogodó, to the East with Opogodó, to the West with the Tigre by the streams El Tigre and Luis (City Hall of Condoto 2004). The average annual rainfall of the area is 8000 mm per year, the relative humidity is 90%, the soils are mostly Ultisols, and the life zone corresponds to tropical rain forest [32, 33]. According to Valoyes

(2017) [34], the area presents a landscape contrast because it still contains areas with a dense vegetation cover without anthropic intervention, where variables such as topography and climate converge, which model the landscape between 100-250 m of altitude. On the well-drained slopes there are species such as Brosimum utile (HBK) Pittier, Huberodendron patinoi Cuatrec, Campnosperma panamensis Standl, Oenocarpus minor Mart, Mauritiella macroclada (Burret) Burret, Carapa guianensis Aubl., Cespedesia spathulata (Ruiz and Pav.) Planch, Euterpe precatoria Mart, Vismia macrophylla Kunth, Saccoglotis procera (Little) Cuatrec, Iriartea deltoidea Ruiz and Pav, palmares of Wettinia quinaria (OFCook and Doyle) Burret, mixed with Welfia regia H.Wendl., Socratea exorrhiza (Mart.) H. Wendl., And Oenocarpus bataua (Mart.) At the level of the arboreal stratum, and Geonoma cuneata H. Wendl. ex Spruce, at the level of the shrub layer among other species [35].

2.2 Selection of Sampling Sites

With information from the people of the community of Jigualito who were exclusively dedicated to mining in the area; In addition, with the support of the Community Councils of Condoto, Rio Iró (COCOMACOIRO), and the town of Jigualito, and finally with the support of the Mayor's Office of Condoto, three areas were defined with different stages (or elapsed times) and/or post-intervention chronosequences by gold and platinum open-pit mining. In this sense, an area with recent disturbance was defined (Area of early succession with 5 years of recovery), another area with an intermediate time of recovery (Area of late succession with 30 years), and finally a secondary Forest. In each of these areas, the physicochemical characteristics of the soil were measured to observe and quantify the changes that occur in edaphic systems after mining activity.

2.3 Area of Early Succession (5 Years)

Located at coordinates 1043965 N, 1047797 W, corresponds to a forest recently intervened by mining activity, with a soil devoid of organic matter, without defined horizons, composed mainly of gravel, with a micro topography with intermediate undulations, surrounded by artificial lagoons (channels resulting from mining activity). The area has little vegetation, a process of primary succession was observed where the dominant flora is composed of herbaceous species consisting mainly of Gramineae (Andropogon bicornis L., Cyperus luzulae (L.) Rottb.), Legumes (Mimosa pudica Mill.) , Rubiáceas (Borreria latifolia (Aubl.) K. Schum) and Melastomatáceas (Aciotis sp, Nepsera aquatica (Aubl.) Naud) among others and some species of woody plants in seedling and juvenile state, which are dispersed and close to the matrix [34, 35].

2.4 Forest of Late Succession (> 30 Years).

Located at coordinates 07641582 N and 0502416 W; corresponds to a forest of late succession, presents a moderate micro topography with undulations in the terrain. The soil lacks a defined structure, it is composed of gravel left by the mining activity, which is nourished by the litter product of the biomass that the trees present in the area contain. The vegetation is dominated by Cespedesia spathulata, accompanied by other pioneering species such as Cecropia peltata, Cecropia sp, Conostegia micrantha (with variable heights that exceed 15 m and DAP ≥10 cm) [34, 35].

2.5 Reference Forest

It is located at coordinates 7641063 N, 0501424 W, corresponds to an area of intervened forest, with advanced succession process where mining activity has not been practiced; it presents soils with a homogenous topography, poorly drained, with a defined structure and a defined organic layer; The vegetation of the area is made up of varied species whose composition and structure is dominated by tree species, some of them from intervened areas, but dominate species of the original composition [34, 35].

2.6 Establishment of Plots

We used 15 temporary research plots of 200 m^2 (4 × 50) each, in each of the successional stages (Area of Early Succession, Forest of Late Succession and Secondary Forest Reference); for a total of 45 sampling plots. These plots were established between 2013 and 2016; and in turn, they were divided into five squares of 4 × 10 m (40 m^2) considered as registration units; in which soil samples were taken for this study.

2.7 Soil Analysis

To evaluate the fertility of areas degraded by mining, composite soil samples were used, taken at the four corners and in the center of the grid (4 × 10 m), and then unified, collected at 20 cm depth, previously removing the leaf litter and organic material thereof; In each of the three successional stages, 15 composite samples of soils will be taken, giving a total of 45 samples; Samples were analyzed for the texture, pH, MO content and nutrient content (N, P, K, Ca, Mg), in the Biogeochemistry laboratory of the National University of Colombia Medellin Headquarters, using the techniques that are referenced then: the texture with the Bouyoucos technique, the pH in water (1: 2) with Potentiometer, the MO content with the Walkley and Black technique, the total N with the Micro-Kjeldahl technique, the P was extracted by the method of Bray II and determined with ascorbic acid in UV-VIS spectrophotometer, the nutrients Ca, Mg, and K were extracted with 1M ammonium acetate, neutral, and determined by atomic absorption [36].

2.8 Statistic Analysis

Measures of central tendency and dispersion of the data were calculated. To compare the soil fertility (texture, MO, pH, Al, N, P, Ca, K, Mg, CICE) of the three successional stages in areas degraded by mining, the nonparametric tests of Kruskal Wallis were used because they were not they fulfilled the assumptions of normality and homogeneity of variances of the data, evaluated with the Bartlett's and Hartley's tests. By means of principal component analysis (PCA), the physicochemical variables (acidity, MO, nutrient content and texture) of the soil in each one of the scenarios or successional stages were related multilineally. The analyzes were carried out with the Statgraphics Centurion XV [37] and The R Project for Statistical Computing programs (www.r-project.org/).

3. Results

3.1 Soil Fertility

In the areas degraded by open-pit mining, it was observed that the soils show extreme acidity in different stages of ecological succession (5, 15 and 30 years), with greater acidity in the reference area. Aluminum concentrations were low in the early stages of recovery of degraded areas, but in the reference forest, their content was significantly high, reaching values close to toxicity (2.41 cmolc kg^{-1}) (

Table 1). The contents of Ca, K, Mg and CICE were low in the first years after mining (5 and 15 years), then increased significantly with the passage of time, until reaching intermediate and high values (30 years); finally, concentrations in the reference forest tend to be low again. On the other hand, the available soil content is very high in the mines, but decreases drastically with the passage of time, to such an extent that in the reference forests its content is very low. The contents of total N and organic matter are low in the areas degraded by mining, but show considerable increases with the passage of time after mining, with the highest values in the reference forest. A similar trend shows the percentages of silt and clay in the soil, which are very low in the intervened areas, but increase their concentration in the reference forest. The sand content was high in the areas of 5, 15 and 30 years, and shows a reduction in the reference forest (

Table 1). In summary, it was observed that after the mining, the contents of OM, total N, Al and clay increased; while, the concentrations of available P and sand decreased. On the other hand, the edaphic availabilities of Ca, K, Mg, CICE and silt, increased

during the intermediate stages of succession, and then decreased in the reference forest (

Table 1).

When evaluating the changes in the physicochemical characteristics of the soils after the degradation by mining, it was observed that the edaphic concentrations of total MO and N were limited during the first 30 years of recovery. Contrary to this, the amount of available P was high in the initial stages (5 and 15 years) after mining, and decreased significantly with the succession. The concentrations of Ca, K and Mg were very low in the initial stages, after 30 years they increased their availability considerably, while in the reference forest the edaphic quantities were smaller. The observed trends in nutrient availability (Ca, K and Mg) were also evidenced in the pH, the CICE and the percentage of soil silt. Finally, the edaphic concentrations of Al and clay increased significantly with the recovery of the ecosystem; while, the sand content decreased.

The PCA showed an underlying gradient determined by age after abandonment, where elements such as organic matter and nitrogen showed a marginal increase with the age of abandonment among the mines, but a drastic increase between them and the reference forest (Fig.). In summary, the soil variables measured in the areas of 5, 15, 30 years and the reference area varied among themselves, and indicated that the areas intervened together have sandy soils and are poorer in nutrients when compared with the soil in the reference forest. Specifically, variables such as phosphorus, pH, magnesium and calcium were related to each other and were higher in the areas of 5, 15 and 30 years than in the reference forest, while nitrogen and organic matter presented positive relationships and were manifested with greater magnitude in the reference forest. The rest of the measured variables did not vary significantly between successional environments (

Table 1).

Table 1 Physical and chemical characteristics of the soil in sampling plots in mines of 5, 15 and 30 years after the abandonment and reference forest in Condoto, Chocó, Colombia.

Variable	Escenario																Kruskal-Wallis	
	5 años				15 años				30 años				Bosque referencia					
	Media	Min	Max	DE	Media	Min	Max	DE	Media	Min	Max	DE	Media	Min	Max	DE	H	*P*
A	69.6	56.0	84.0	10.8	57.5	57.0	58.0	0.71	46.8	28.0	58.0	11.4	64.4	28.0	90.0	20.6	0.70	0.12
L	19.6	10.0	34.0	9.1	18.5	18.0	19.0	0.71	36.0	28.0	42.0	5.10	21.2	8.00	38.0	9.67	8.74	**0.03**
Ar	10.8	6.0	16.0	3.6	24.0	24.0	24.0	0.01	17.2	12.00	30.0	7.56	14.4	2.00	34.0	11.3	3.98	0.26
pH	4.4	4.0	4.7	0.3	4.8	4.7	4.8	0.07	4.60	4.20	5.40	0.48	4.06	3.80	4.30	0.18	11.6	**0.008**
N	0.2	0.1	0.3	0.1	0.2	0.2	0.2	0.05	0.20	0.06	0.27	0.09	0.64	0.36	1.05	0.25	15.9	**0.001**
MO	0.8	0.1	1.5	0.6	1.8	1.7	1.8	0.07	6.82	3.70	9.00	2.20	12.8	4.40	23.8	7.78	14.6	**0.002**
Al	1.4	0.6	2.1	0.6	1.5	1.4	1.5	0.07	1.38	0.34	2.16	0.69	2.12	1.05	3.43	0.75	4.74	0.19
Ca	0.4	0.2	1.0	0.3	0.3	0.3	0.3	0.01	3.22	0.80	5.50	1.92	0.13	0.08	0.27	0.06	16.3	**0.001**
Mg	0.3	0.1	0.4	0.1	0.4	0.4	0.4	0.01	1.63	0.34	3.20	1.13	0.24	0.12	0.47	0.11	10.9	**0.01**
K	0.05	0.03	0.1	0.03	0.3	0.3	0.3	0.01	0.18	0.07	0.28	0.08	0.14	0.06	0.31	0.07	13.1	**0.004**
CIC	2.2	1.5	2.9	0.7	2.3	2.2	2.4	0.14	6.40	2.40	9.50	2.78	2.65	1.40	3.90	0.83	7.47	0.06
P	29.2	19.0	44.0	9.7	17.0	16.0	18.0	1.41	18.2	7.00	37.00	12.2	2.10	1.00	3.00	0.74	17.1	**0.001**

3.2 Biological Activity of the Soil

The variables indicating the biological activity of the soil (H, CH_4 and CO_2) showed statistically significant differences between the sampling scenarios, in this sense, in general terms the activity was higher in the reference forest and in the area with 15 years of recovery (Table 2). However, from the biological point of view, it is important to note that the biological activity of the soil is high from early stages of succession, in particular, all the variables that indicate

activity of edaphic microorganisms were high in all the scenarios evaluated (Table 2, Fig.). The previous trend was maintained even throughout the entire measurement time of the indicator variables (Fig.).

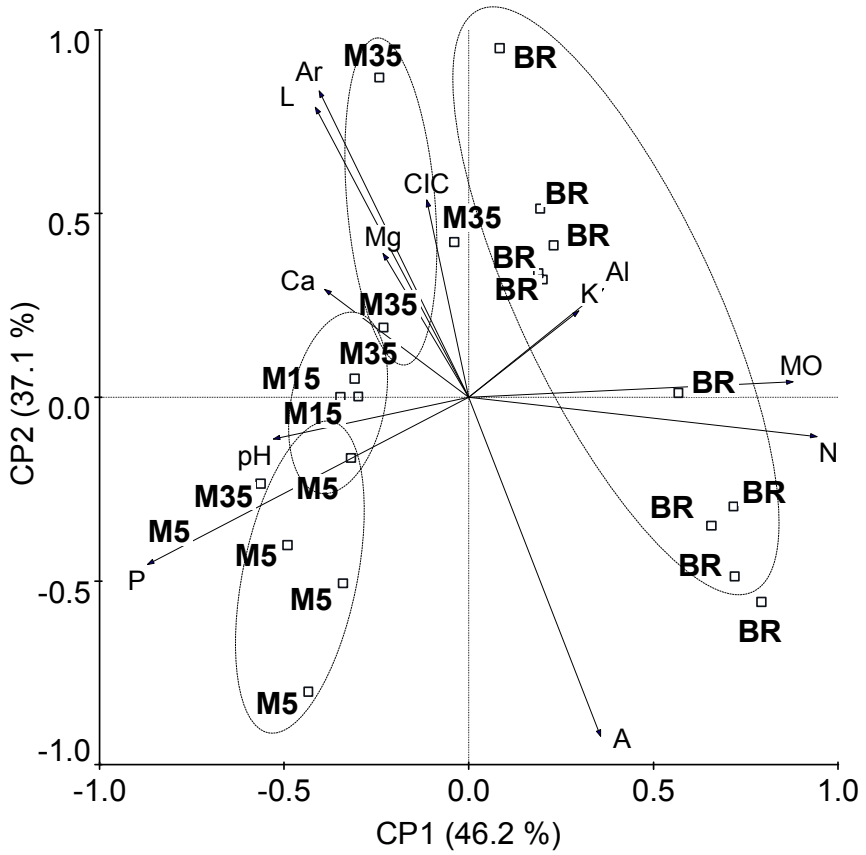

Fig. 1 Principal components analysis (PCA): physical and chemical characteristics of the soil in sampling plots in mines of 5, 15 and 30 years after abandonment and reference forest in Condoto, Chocó, Colombia.

Table 2 Indicator variables of biological activity in the soil of mines and reference forest in Condoto, Chocó, Colombia.

Escenarios	Variables		
	H	CH_4	CO_2
5 años	567.5±37.7	479.7±29.6	394.3±28.2
15 años	698.9±27.6	604.0±33.4	558.8±36.6
30 años	543.3±31.9	505.4±35.9	400.2±37.1
BR	686.7±21.8	564.6±14.3	497.1±10.8
$F_{3,11364}$	19831.9	10351.1	19842.5
P	< 0.0001	< 0.0001	< 0.0001

4. Discussion

Changes in soil acidity in areas degraded by mining: Areas degraded by open-pit mining with different recovery times in Jigualito, Condoto (Chocó), presented extremely acid soils (Table 1, Fig.). This corroborates the extreme acidity previously recorded in tropical rain forests in the localities of Bajo Calima, Opogodó, Pacurita and Salero, in the Chocó Biogeográfico [33, 38]. Furthermore, these observations confirm the tendency of acid soils mentioned in several studies carried out in tropical humid forests [2, 32, 39-41].

The extreme acidity in tropical soils is mainly generated by the leaching of basic cations (Ca, Mg, K

and Na) and the accumulation of acid cations (Al and H) due to environmental factors such as high precipitation [42, 43]; likewise, due to the influence of other factors such as the high content of MO that releases carbonic acids that acidify the soil, and the symbiotic fixation of N_2 that liberates H + ions that increase soil acidity [43]. Therefore, it can be stated that, in areas degraded by mining in the biogeographic Chocó, variations in the concentration of cations, MO and total N, possibly explain in greater proportion the changes in soil acidity levels. In the successional stage that presented lower acidity (after 30 years of recovery), the highest availability of cations (K, Ca and Mg) was also registered.

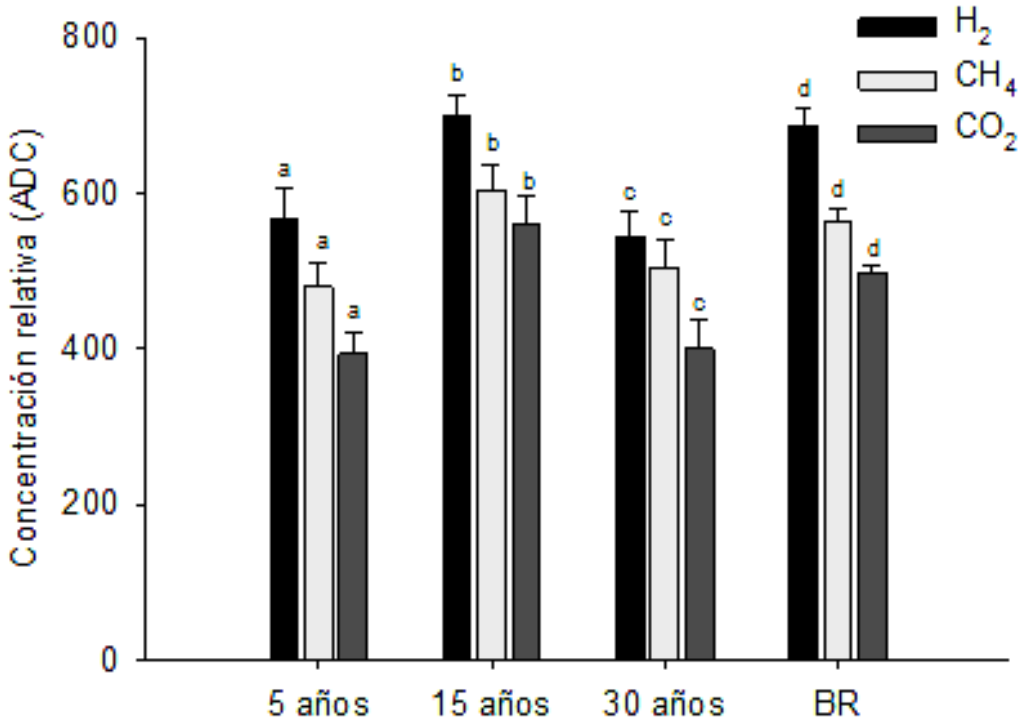

Fig. 2 Biological activity of soil in mines and reference forest in Condoto, Chocó, Colombia.

However, the trends in soil acidity of areas degraded by mining were different from those recorded by Li et al. (2013) [23] who observed greater edaphic acidity in successional stages characterized by having soils rich in OM and minerals (K, Zn, Cu, Fe) in tropical forests of China [23]. Also, the results of the present study were different to those mentioned by Werner (1984), who observed that pH levels remained relatively constant through plant sequences following deforestation processes in tropical forests of Costa Rica. These differences in edaphic acidity with plant succession after anthropic interventions of different tropical rainforests [4], show that pH levels are very sensitive to local edaphic conditions (nutrients, MO, humidity, etc.); and that, in addition, due to its sensitivity it would not be a good edaphic predictor in terms of restoration of degraded ecosystems, especially those degraded by open-pit mining.

Changes in the content of Aluminum, Calcium, Potassium and Magnesium in the soil in areas degraded by mining: The reference forest presented the highest concentration of Al soil (Table 1, Fig.), which, evidences a possible toxicity that is frequent in these geographical zones, which are similar with the high mineral levels registered in the soils of localities like Bajo Calima, Salero and Pacurita, in the biogeographical Chocó [38, 44]. The reason why it increases the Al soil with the succession in areas degraded by mining, is surely because when open-pit mining is carried out, the mechanical action of the

backhoes on the ground and subsoil, expose fragments of igneous and metamorphic rocks that by weathering processes they gradually release minerals (Al, Fe, S, P, Mg, K, etc.) to the residual soil [9, 10, 12]. A large part of these minerals, released to the ground by weathering, are rapidly leached by intense rains [36, 45, 46]; However, the concentration of Al tends to increase, possibly due to the fact that its leaching rate is lower than that of the other minerals [36]. In addition, the Al may be in soluble forms in the soil solution, interchangeably absorbed on the surface of the negatively charged clays, complexed by the OM of the soil, and/or precipitated as a secondary mineral in the form of oxide and hydroxide in the soil, which explains its high availability in extremely weathered soils such as Ultisols and Oxisols [36]; similar to what occurs in clay soils with high aluminum content in the Chocó Biogeographic [47].

In tropical areas that have suffered anthropogenic disturbances, soil nutrients increase their availability during the initial and intermediate stages of succession; but later, they reduce their concentration in the advanced stages of ecosystem development [4, 21, 31, 48]. Particularly, in areas degraded by mining in Jigualito, after 30 years of recovery, K, Ca and Mg presented their greatest availability in the soil (Fig.); However, when comparing the content of these minerals in the ground of the reference forest, a decrease in their concentration is noted. Possibly, by the absorption and immobilization of cations in the vegetable biomass of the forest, which represents one of the main mechanisms of conservation of limiting nutrients [4, 49, 50]. These patterns of increases and reductions in the concentration of nutrients in areas degraded by mining are similar to those registered in soil development processes (pedogenesis) and primary succession, in which the availability of nutrients and soil fertility increase in the first stages of pedogenesis; but at the end of the succession, when a dynamic equilibrium is reached in the ecosystem, the concentration of nutrients decreases [31, 48]. Consequently, it can be concluded that, with open-pit mining in tropical rainforests of the biogeographic Chocó, an "edaphic rejuvenation" is generated.

Changes in the concentration of organic matter, total nitrogen and soil phosphorus in areas degraded by mining: it was evidenced that, with the advance in plant succession after mining, the availability of total N and OM in the soil increases. Particularly, the OM presented very high values and increased with the natural recovery time of the system. This increase is possibly due to the fact that the recovery of the forest increases the accumulation of aerial and subterranean vegetation biomass [23, 51], which increases the accumulation of OM of the soil, given that it is the result of the balance of income and expenses for the production and decomposition of organic waste (leaf litter) from the forest [44]. The high values of OM observed in areas degraded by mining have also been previously recorded in other tropical rainforests of the biogeographic Chocó [38, 52, 53]; which is probably due to the effect of high rainfall on the functioning of tropical forests; since, the high rainfall generates decrease in the foliar concentrations of N, P, Ca and Mg [45, 46, 52, 54], decreases the decomposer activity of microorganisms due to lack of oxygen [54, 55], it reduces the decomposition rate of organic matter [56], and therefore reduces the edaphic availability of nutrients [57]; as a result of the above, the content and time of replacement of the organic matter of the soil is increased [52], and explains the high contents of OM in areas degraded by mining after 30 years.

Finally, changes in soil concentrations of total N and P available in areas degraded by mining, showed increases and reductions, respectively. These trends corroborate the hypothesis that in tropical soils, in initial successional stages, there is a limitation by nitrogen (N), which over time is mitigated due to the colonization of atmospheric N_2 fixative plants [16]; in turn, this N fixation is limited by the availability of P and humidity. Therefore, as the succession progresses, the total N of the soil increases and its limitation for the

ecosystem is reduced [15, 17]. In addition, this hypothesis states that, unlike N, P levels in the soil tend to be high in the first successional stages, and over time tends to decrease their availability, due to losses by leaching and immobilization in Fe and Al sesquioxides [18-20]. In summary, it is evident that with open-pit mining in tropical rainforests of the biogeographic Chocó, pedogenesis and soil development begins again, with the attenuating of conditioning the natural ecological recovery.

Biological activity of soil in areas degraded by mining. The variables indicating the biological activity of the soil (H, CH_4 and CO_2) showed that in all the evaluated scenarios the microbial activity is high (Table 2), even in the mines poor in nutrients (Fig.). These results are possibly due to the fact that the activity of soil microorganisms is determined by various environmental variables such as temperature, humidity, acidity, clay content, soil alterations, quality and quantity of organic material, and characteristics of the microbial community, among others [58], which determine considerably processes like microbial respiration in edaphic ecosystems like those of the biogeographic Chocó. Specifically, the soils of the biogeographic Chocó evaluated in this study are characterized by high temperatures and humidity [32, 33], high contents of organic matter and acid soils (Table 2 and Fig.); which, favors microbial activity in these areas.

According to Mendiara (2012) [58], the main edaphic processes that influence the process of soil respiration are leaching, fragmentation and chemical alteration. In particular, soil fragmentation is a preponderant process in areas degraded by mining, and would explain to a large extent the high microbial activity in these edaphic ecosystems; since, with mining, accumulated residual material is generated forming small mounds; characterized by having coarse textures (gravels and coarse sands) in the upper part [9, 12]. In short, mining increases the amount of rock fragments and soils; consequently, such fragmentation of the soil creates new surfaces for microbial colonization and increases the proportion of the amount of residues that are accessible to the attack of microorganisms [58]; which would partially explain the high microbial activity of areas degraded by mining.

However, the highest microbial activity occurred in the reference forest and in the mines with 15 years of recovery (Table 2); which, possibly, is due to the combination of environmental factors (high humidity, temperature, organic matter) favorable for the activity of microorganisms [58]. Specifically, high humidity (90%) is produced in 15 year old mines due to the constant and heavy rains of the region, which favor microbial activity; likewise, high temperatures are a constant in these ecosystems, which are devoid of dense forest cover, the product of deforestation by mining, with which solar radiation is direct, which increases the temperature and favors the activity of microorganisms. This assertion is based on the point raised by Raich and Schlesinger (1992) [59], who consider that, on a global scale, soil respiration is influenced by average annual temperatures and precipitation, and the interaction between these two variables [59]. In addition, explain that soil temperature is one of the factors that has greater importance on the growth and survival of edaphic microorganisms. Since, as the temperature rises, chemical and enzymatic reactions are accelerated, so that the growth, metabolism, biomass and rate of microbial respiration increase considerably in the soil [58-60]. In addition to the above, these mines presented accumulations of organic matter (1.8%) as a result of the colonizing vegetation; which, favors the microbial activity. In short, the joint action of the high humidity (product of precipitation), the temperature (generated by direct solar radiation) and the accumulation of organic matter, is responsible for the high microbial activity recorded in the areas of early stages of succession (15 years); which may be similar to that recorded in the neighboring reference forests.

References

[1] P. W. Richards, *The Tropical Rain Forests: An Ecological Study* (2nd ed.), Cambridge: Cambridge University Press, 1996, p. 575.

[2] P. M. Vitousek, Litterfall, nutrient cycling, and nutrient limitation in tropical forests, *Ecology* 65 (1984) 285-298.

[3] D. A. Clark, S. Brown, D. W. Kicklighter, J. D. Chambers, J. R. Thomlinson, E. Holland and J. Ni., Net primary production in forest: An evaluation and sinthesis of existing field data, *Ecological Aplications* 11 (2001) (2) 356-370.

[4] M. Guariguata and R. Ostertag, Neotropical secondary forest succession: changes instructural and functional characteristics, *Forest Ecology and Management* 148 (2001) 185-206.

[5] C. C. Cleveland, A. R. Townsend, P. Taylor, S. Alvarez-Clare, M. Bustamante, G. Chuyong, S. Z. Dobrowski, P. Grierson, K. E. Harms, B. Z. Houlton, A. Marklein, W. Parton, S. Porder, S. C. Reed, C. A. Sierra, W. L. Silver, E. V. J. Tanner and W. R. Wieder, Relationships among net primary productivity, nutrients and climate in tropical rain forest: A pan-tropical analysis, *Ecology Letter* (2011) 1-9.

[6] H. Quinto and F. Moreno, Net primary productivity and edaphic fertility in two pluvial tropical forests in the Chocó Biogeographical Region of Colombia, *PLoS ONE* 12 (2017) (1): e0168211, doi: 10.1371/journal.pone.0168211.

[7] Intergovernmental Panel on Climate Change (IPCC), *Climate Change 2014: Synthesis Report*, Contribution of Working Groups I, II and III to the Fifth Assessment Report of the Intergovernmental Panel on Climate Change Core Writing Team, R. K. Pachauri and L. A. Meyer (Eds.), IPCC, Geneva, Switzerland, 2014. 151 pp.

[8] R. B. Primack, *A Primer of Conservation Biology* (4th ed.), Sinauer Associates, Inc. Sunderland. MA., 2008, p. 349.

[9] W. A. Diaz and S. Elcoro, Plantas colonizadoras en áreas perturbadas por la minería en el Estado Bolívar, Venezuela, *Acta Botánica Venezuela* 32 (2009) (2) 453-466.

[10] Environmental Law Alliance Worldwide (ELAW),. *Guidebook for Evaluating Mining Project EIAs*, Eugene, U.S.A., 2010, p. 110.

[11] K. D. Holl, Tropical moist forest, in: Perrow M. R. and A. J. Davy (Eds.), *Handbook of Ecological Restoration*, Vol. 2, Restoration in Practice. Cambridge University Press, 2002, pp. 539-558.

[12] I. E. Chacón, *Pequeña y mediana minería aluvional. Oro y diamante. Tomo II*, Universidad de Oriente, Núcleo Bolívar, Fundaudo, Ciudad Bolívar, 1992.

[13] R. L. Chazdon, Tropical forest recovery: Legacies of human impact and natural disturbances, *Perspectives in Plant Ecology, Evolution and Systematics* 6 (2003) (1) 51-71.

[14] L. R. Walker, J. Walker and R. J. Hobbs, *Linking Restoration and Ecological Succession*, Springer, New York, NY, USA, 2007.

[15] L. R. Walker and R. del Moral., Lessons from primary succession for restoration of severely damaged habitats, *Applied Vegetation Science* 12 (2008) 55-67.

[16] L. R. Walker, Nitrogen fixers and species replacements in primary succession, in: Miles J. & D. W. H. Walton (Eds.), *Primary Succession on Land*, Blackwell, Oxford, UK, 1993, pp. 249-272.

[17] C. C. Cleveland, A. R. Townsend, D. S. Schimel, H. Fisher, R. W. Howarth, L. O. Hedin, S. S. Perakis, E. F. Latty, J. C. Von Fischer, A. Elseroad and M. F. Wasson, Global patterns of terrestrial biological nitrogen (N_2) fixation in natural ecosystems, *Global Biogeochem Cycles* 13 (1999) (2) 623-645.

[18] T. W. Walker and J. K. Syers, The fate of phosphorus during pedogenesis, *Geoderma*15 (1976) 1-19.

[19] P. A. Sanchez, *Properties and Management of Soils in The Tropics*, Wiley-Interscience Publications, New York, New York, USA, 1976, p. 618.

[20] P. Vitousek, S. Porder, B. Z. Houlton and O.A. Chadwick, Terrestrial phosphorus limitation: Mechanisms, implications, and nitrogen-phosphorus interactions, *Ecological Applications* 20 (2010) (1) 5-15.

[21] P. Werner, Changes in soil properties during tropical wet forest succession in Costa Rica, *Biotropica* 16 (1984) (1) 43-50.

[22] G. Jia, J. Cao., C. Wang and G. Wang, Microbial biomass and nutrients in soil at the different stages of secondary forest succession in Ziwulin, northwest China, *Forest Ecology and Management* 217 (2005) 117-125.

[23] Y. Li, F. Yang, Y. Ou, D. Zhang and J. Liu et al., Changes in forest soil properties in different successional stages in Lower Tropical China, *PLoS ONE* 8 (2013) (11) e81359, doi: 10.1371/journal.pone.0081359.

[24] N. Myers, R. A. Mittermeier, C. G. Mittermeier, G. A. B. da Fonseca and J. Kent, Biodiversity hotspots for conservation priorities, *Nature* 403 (2000) 853-858 doi: 10.1038/35002501.

[25] J. M. Rivas, A. K. Palomeque, N. L. Berardinelli and L. Hinestroza, Afectación del derecho al medio ambiente sano en la Comunidad de Condoto-Chocó por el otorgamiento de títulos mineros a empresas multinacionales, *Pensamiento Jurídico* 42 (2015) 213-240.

[26] H. Valois-Cuesta, Sucesión primaria y ecología de la revegetación de selvas degradadas por minería en el Chocó,

Colombia: bases para su restauración ecológica, Tesis doctoral, Universidad de Valladolid, España, 2016.

[27] MINMINAS (Ministerio de Minas y Energía), 2012. Censo Minero Departamental 2010-2011, Ministerio de Minas y Energía. República de Colombia, Bogotá DC, 2012, p. 40, Descargado el 30 de abril de 2016, available online at: https://www.minminas.gov.co/censominero.

[28] UPME-MINMINAS (Unidad de Planeación Minero Energética del Ministerio de Minas y Energía), Indicadores de la minería en Colombia, Versión preliminar. Subdirección de Planeación Minera, Ministerio de Minas y Energía. República de Colombia. Bogotá DC., 2014, p. 127.

[29] Instituto de Investigaciones Ambientales del Pacífico (IIAP), *Informe Técnico Aspectos Mineros en el Chocó*, Informe de Proyecto, Quibdó, Colombia, 2001.

[30] G. Ramírez and E. Ledezma, Efectos de las Actividades Socio-económicas (Minería y Explotación Maderera) Sobre los Bosques del Departamento del Chocó, *Revista Institucional Universidad Tecnológica del Chocó* 26 (2007) 58-65.

[31] L. O. Hedin, P. M. Vitousek and P. A. Matson, Nutrient losses over four million years of tropical forest development, *Ecology* 84 (2003) (9) 2231-2255.

[32] D. Malagon, C. Pulido, R. D. Llinas, C. Chamorro and J. Fernández, Suelos de Colombia, Origen, Evolución, Clasificación, Distribución y uso, Instituto Geográfico Agustín Codazzi. Subdirección de Agrología, Santa fe de Bogotá – Colombia, 1995, p. 632.

[33] H. Quinto and F. H. Moreno, Precipitation effects on soil characteristics in tropical rain forests of the Chocó biogeographical region, *Revista Facultad Nacional de Agronomía Medellín* 69 (2016) (1) 7813-7823, doi: 10.15446/rfna.v69n1.54749.

[34] Z. Valoyes, *Efectos de la actividad minera de oro y platino a cielo abierto sobre los bosques de terrazas y colinas bajas en Condóto-Chocó. Tesis de Maestría en Ciencias Ambientales*, Corporación Académica Ambiental. Universidad De Antioquia. Medellín, Colombia, 2017, p. 122.

[35] M. G. Ramírez, Estudio de las comunidades de Palmas en dos regiones fitogeográficas del Chocó-Colombia. Trabajo de grado para optar al título de Magister en Ciencias-Biología Línea Biodiversidad y Conservación, Universidad Nacional de Colombia, 2010.

[36] N. W. Osorio, *Manejo de nutrientes en suelos del Trópico* (2nd ed..), Editorial L. Vieco S.A.S. Medellín, Colombia, 2014, p. 416.

[37] Statistical Graphics Corp, StatgraphicsPlusCenturium Version 5.1, 2002, available online at: http://www.statgraphics.com.

[38] D. Faber-Langendoen and A. H. Gentry, The structure and diversity of rain forests at Bajo Calima, Chocó Region, Western Colombia, *Biotropica* 23 (1991) (1) 2-11.

[39] S. W. Buol, F. D. Hole and R. J. McCracken, *Génesis y Clasificación de Suelos* (Primera Edición), Editorial Trillas, S.A. México D.F. México, 1981, p. 417.

[40] P. M. Vitousek and R. L. Sanford Jr., Nutrient cycling in moist tropical forest, *Annual Review of Ecology and Systematics* 17 (1986) 137-167.

[41] J. S. Powers, K. K. Treseder and M. T. Lerdau, Fine roots, arbuscular mycorrhizal hyphae and soil nutrients in four neotropical rain forests: Patterns across large geographic distances, *New Phytologist* 165 (2005) 913-921.

[42] H. Jenny, *Factors of Soil Formation*, McGraw-Hill, New York, 1941.

[43] R. A. Sadzawka and R. R. Campillo, Problemática de la acidez de los suelos de la IX Región. I. Génesis y características del proceso, *Investigación y Progreso Agropecuario Carillanca* 12 (1993) (3) 3-7.

[44] F. H. Moreno and S. F. Oberbauer, Dynamics of soil carbón in primary and secondary tropical forests in Colombia, in: Bravo F., V. LeMay, R. Jandl, and K. von Gadow (Eds.), *Managing Forest Ecosystems: The Challenge of Climate Change*, Springer Science Business Media, 2008, pp. 283-296, 338.

[45] A. T. Austin and Vitousek P. M., Nutrient dynamics on a precipitation gradient in Hawaii, *Oecologia* 113 (1998) 519-529.

[46] L. S. Santiago, E. A. G. Schuur and K. Silvera, Nutrient cycling and plant-soil feedbacks along a precipitation gradient in lowland Panama, *Journal of Tropical Ecology* 21 (2005) (4) 461-470, doi: 10.1017/s0266467405002464.

[47] J. O. Rangel (Ed.), *Colombia Diversidad Biótica IV: El Chocó Biogeográfico/Costa Pacífica*, Instituto de ciencias Naturales, Universidad Nacional de Colombia, Bogotá, D.C., 2004.

[48] R. K. Peet, Community structure and ecosystem function, in: Glen Lewin, Peet R. K. and T. T. Veblen (Eds.), *Plant Succession: Theory and Prediction*, Chapman and Hall, London, UK, 1992, pp. 103-151, 352.

[49] Brown S. and A. E. Lugo, Tropical secondary forests, *Journal of Tropical Ecology* 6 (1990) (1) 1-32.

[50] F. S. Chapin III, P. A. Matson and H. A. Mooney, *Principles of Terrestrial Ecosystem Ecology*, Springer-Verlag New York, Inc. United States of America, 2002, p. 436.

[51] H. Quinto-Mosquera, J. Cuesta-Nagles, I. Mosquera-Sánchez, L. Palacios-Hinestroza and H. Peñaloza-Murillo, Biomasa vegetal en zonas degradadas por minería en un bosque pluvial tropical del Chocó Biogeográfico, *Revista Biodiversidad Neotropical* 3 (2013) (1) 53-64. doi: 10.18636/bioneotropical.v3i1.127.

[52] J. M. Posada and E. A. G. Schuur, Relationships among precipitation regime, nutrient availability, and carbon turnover in tropical rain forests, *Oecologia*. 165 (2011) 783-795.

[53] H. Quinto, M. H. Caicedo, L. M. Pérez and F. H. Moreno, Dinámica de raíces finas y su relación con la fertilidad edáfica en bosques pluviales tropicales del Chocó biogeográfico colombiano, *Revista de Biología Tropical* 64 (2016) (4) 1709-1719.

[54] E. A. Schuur and P. A. Matson, Net primary productivity and nutrient cycling across a mesic to wet precipitation gradient in Hawaiian montane forest, *Oecologia* 128 (2001) (3) 431-442, doi: 10.1007/s004420100671.

[55] E. A. Schuur, Productivity and global climate revisited: the sensitivity of tropical forest growth to precipitation, *Ecology* 84 (2003) 1165-1170.

[56] E. A. G. Schuur, The effect of water on decomposition dynamics in mesic to wet Hawaiian montane forests, *Ecosystems* 4 (2001) (3) 259-273, doi: 10.1007/s10021-001-0008-1.

[57] M. Kaspari, M. N. Garcia, K. E. Harms, M. Santana, S. J. Wright and J. B. Yavitt, Multiple nutrients limit litterfall and decomposition in a tropical forest, *Ecology Letter* 11 (2008) 35-43.

[58] S. Mendiara, *Efecto de los usos del suelo en la emisión de dióxido de carbono del suelo a la atmósfera en un Agroecosistema semiárido del Valle del Ebro*, España, Universidad de Vic, Escuela Politécnica Superior, 2012, pp. 16-18.

[59] J. W. Raich and W. H. Schlesinger, The global carbon dioxide flux in soil respiration and its relation to vegetation and climate, *Tellus* 44B (1992) 81-99.

[60] T. R. Sinclair, Mineral nutrition and plant growth response to climate change, *J. Exp. Bot.* 43 (1992) 1141-1146.

Modern Environmental Science and Engineering (ISSN 2333-2581)
September 2019, Volume 5, No. 9, pp. 849-853
Doi: 10.15341/mese(2333-2581)/09.05.2019/008
Academic Star Publishing Company, 2019
www.academicstar.us

Real-Time Optimal Energy Management for Hybrid and Plug-In Hybrid Electric Vehicles

Jian Dong, Zuomin Dong, and Curran Crawford

Department of Mechanical Engineering and Institute for Integrated Energy Systems, University of Victoria, Canada

Abstract: In this work, a systematic approach for real-time optimal energy management of hybrid electric vehicle (HEV) and plug-in hybrid electric vehicle (PHEV) has been introduced and validated through two HEV/PHEV case studies. Firstly, a new analytical model of the optimal control problem for Toyota Prius HEV with both offline and real-time solutions was presented and validated through Hardware-in-Loop (HIL) real-time simulation. Secondly, the new online or real-time optimal control algorithm was extended to a multi-regime PHEV by modifying the optimal control objective function and introducing a real-time implementable control algorithm with an adaptive coefficient tuning strategy. A number of practical issues in vehicle control, including drivability, controller integration, etc. are also investigated. The newly proposed real-time optimal control algorithm identifies the optimal operational mode and the corresponding torque split among each components at each time step. The control objective was to minimize the well-to-wheel energy use (PEU and GHG), where both the fuel and electric energy consumption was taken into account. The optimal torque split was computed based on Pontryagin's Minimum Principle. To reduce computational burden, the original 2 degree of freedom (DOF) powertrain control problem has been converted into a 1-DOF search algorithm in the optimization search. For practical implementation, an adaptive technique was utilized to update the equivalence factor based on battery SOC and current driving distance. The newly proposed fast PMP algorithm was investigated through Model-in-the-loop (MIL) simulation tests using the simplified vehicle model, showing improved PEU consumption by 3-5%, comparing to the baseline rule-based controller for which the battery SOC is just depleted at the end of the trip. The new algorithm was also validated on various driving cycles using both Model-in-Loop (MIL) and HIL environment. This research better utilizes the energy efficiency and emissions reduction potentials of hybrid electric powertrain systems, and forms the foundation for the developments of next generation HEVs and PHEVs.

Key words: hybrid electric vehicles, HEV, PHEV, real-time optimal energy management, HIL simulation, pontryagin's minimum principle

1. Introduction

Increasing concerns about environmental issues have made hybrid electric vehicles (HEVs) with considerably improved energy efficiency and reduced emissions a promising alternative to conventional Internal Combustion Engine (ICE) vehicles. The energy efficiency improvement of HEVs is partially due to their capability of recovering braking energy, and partially due to their ability to allow the ICE to operate at the high efficiency operation conditions with the additional degree of freedom from two energy sources on board of the vehicle, electrical energy storage system (ESS) and fuel tank. The presence of this additional degree of freedom, however, also demands an appropriate energy management strategy to exploit the optimal operation effectively.

Recently, plug-in hybrid electric vehicles (PHEVs), HEVs with oversized batteries that can be recharged using grid power at station, present an even more promising solution to greener vehicles due to their ability to further reduce the petroleum consumption and greenhouse gas (GHG) emissions by using grid

Corresponding author: Zuomin Dong, Ph.D.; research areas/interests: modeling, design optimization and real-time optimal control of advanced hybrid electric vehicles, marine vessels, fuel cell systems, and smart grids; meta-model based global optimization; application of intelligent systems; optimal 5-axis CNC tool path generation. E-mail: zdong@uvic.ca.

power generated from renewable energy sources and excess electric generation capacity at off-peak hours. The added part-time pure electric vehicle (PEV) mode supports better emissions control in highly populated urban areas and contributes to further improvement of powertrain efficiency. PHEVs also eliminate the problem of "range anxiety" associated to PEVs, because the ICE functions as a backup when the batteries are depleted, giving PHEVs driving range comparable to other vehicles with gasoline tanks.

2. Modeling, Optimal Control and Its Real-Time Validation for PHEV

2.1 PHEV Research Vehicle and Modeling of Its Multi-Regime PHEV Powertrain System

The prototype plug-in hybrid electric vehicle (PHEV) developed through the EcoCAR 2 program at the University of Victoria. The new PHEV was produced by re-engineering a 2013 Chevrolet Malibu donated by General Motors as the integration platform for advanced vehicle design to reduce emissions and environmental impact while retaining performance and consumer appeal.

The series-parallel multi-regime powertrain architecture of the PHEV is shown in Fig. 1. This architecture provides many substantial improvements over the production 2013 Malibu. The powertrain includes a powerful motor coupled to the engine through a belt system functioning as a belt-alternator-starter (BAS) at the front wheel, as well as a rear traction motor (RTM) and large battery. The battery and RTM make this architecture a full hybrid, giving it a significant electric-only range. This configuration was identified as having several advantageous operating modes. With the transmission set in neutral, the vehicle could essentially function as a series EREV, with the ICE charging the batteries through the BAS system. When additional power is required, or when it is more efficient to do so, the ICE and transmission could be used to propel the vehicle. For high-performance driving situations, the BAS

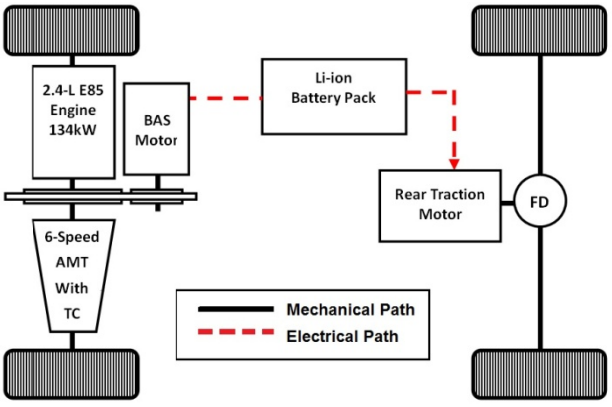

(a) Powertrain Archiecture

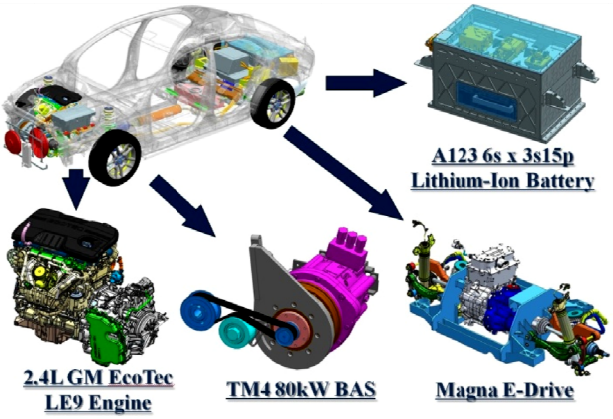

(b) Key Powertrain Components

Fig. 1 Series-parallel, Multi-regime Powertrain of the PHEV.

could provide a power-assist function to smooth out the torque curve of the ICE, and the RTM could add its power such that all available power sources propel the vehicle.

2.2 Forward-oriented Simulation Model

A forward-oriented vehicle model is shown in Fig. 2.

2.3 Rule-Based Controller Design for the Proposed PHEV Powertrain

A deterministic rule-based controller is developed first for the proposed PHEV powertrain, which will also serve as the baseline controller for the optimization-based controller that will be developed later to compare with. Depending on different driving situations, the Charge Depleting-Charge Sustaining (CDCS) rule-based controller produces simulation results as shown in Fig. 3 and Table 1.

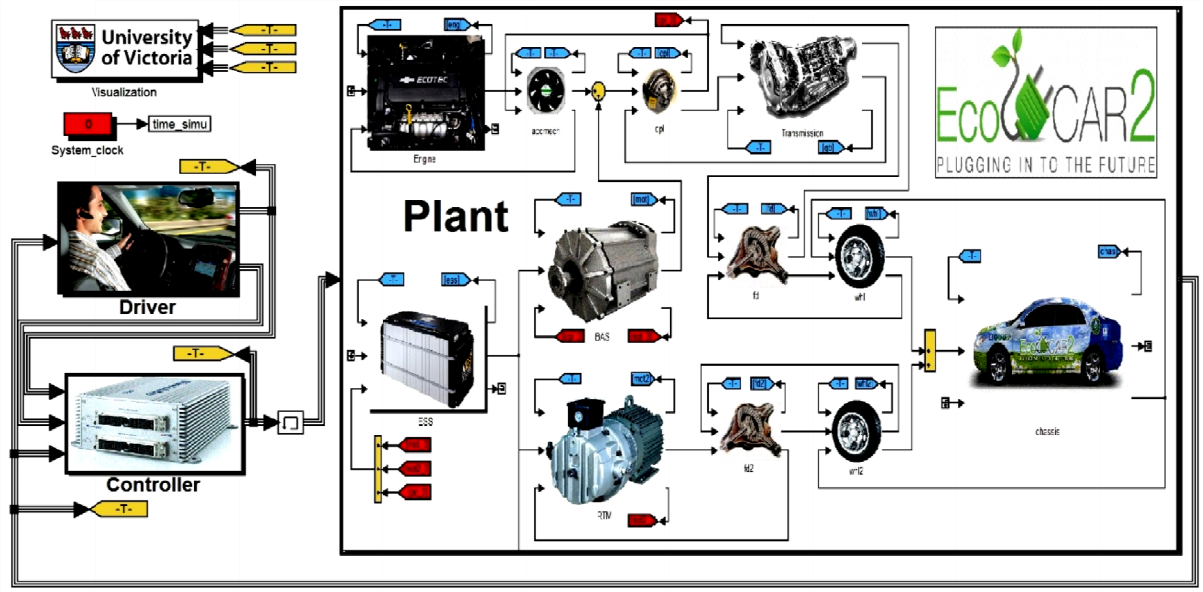

Fig. 2 Forward-oriented vehicle model in MATLAB/Simulink.

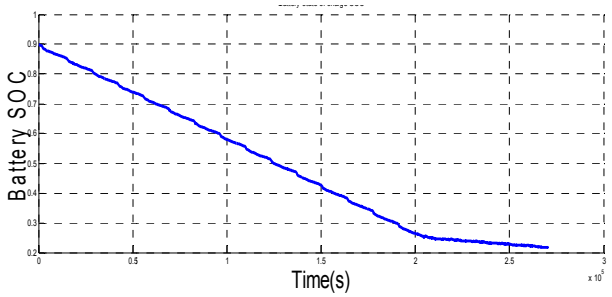

Fig. 3 Battery SOC result over 20*UDDS.

Table 1 Simulation results on 20*UDDS cycle.

(based on E85 fuel)	Results
Total Distance (miles)	148.32
Fuel Economy (MPG)	174.897
WTW GHG (g CO_2 eq/km)*	126.881
Initial SOC	0.9
Final SOC	0.2386
AER range (miles)	65.1147

3. Extension of the Proposed Real-Time Optimal Control Algorithm to PHEV

In this work, new formulation for the optimal control of the PHEV has been introduced, considering the amount of energy consumed and the well-to-wheel (WTW) greenhouse gas (GHG) emissions.

$$PEU_{WTW} = E_{fuel} \cdot \eta_{PEU,fuel} + E_{elec} \cdot \eta_{PEU,elec} \quad (1)$$

where E_{fuel} and E_{elec} are the per-kilometer amounts of fuel and alternating current (AC) electric energy (kWh/km) used. The WTW PEU factor η_{PEU} is used to relate fuel (or electric) energy use to the well-to-wheel petroleum energy use considering both upstream and downstream (at the vehicle).

$$GHG_{WTW} = E_{fuel} \cdot \eta_{GHG,fuel} + E_{elec} \cdot \eta_{GHG,elec} \quad (2)$$

where the WTW GHG factor η_{PHG} is used to relate vehicle energy use to the WTW amount of GHGs generated.

The new cost function for PHEV optimal control is thus redefined as follows:

$$\min\left\{J = \int_{t_0}^{t_f} [\dot{m}_{fuel}(t) \cdot \eta_{FSE} \cdot \eta_{PEU,fuel} + P_{bat}(t) \cdot \eta_{PEU,elec}]dt\right\} \quad (3)$$

Subject to various operational constraints

where $\dot{m}_{fuel}$ is the fuel consumption rate (kg/s) and P_{bat} is the battery DC electric power (kW) used at each time step. η_{FSE} is the fuel-specific energy by mass (kWh/kg), the value of which can be found in Table 6. T_{BAS} refers to the torque of the motor coupled with the BAS system and T_{RTM} refers to the torque of the rear traction motor.

The powertrain model described in 3.4 can be summarized as in the following two equations:

$$\begin{aligned}&(T_{eng}+T_{BAS}\cdot R_{belt}\eta_{belt}^{k})\cdot R_{tx}\eta_{tx}R_{fd}\eta_{fd}+T_{RTM}\cdot R_{rd}\eta_{rd}^{k}=T_{req}\\&P_{bat}=\eta_c{}^{m}(\eta_{BAS}T_{BAS}\omega_{BAS}+\eta_{RTM}T_{RTM}\omega_{RTM})\end{aligned}\quad(4)$$

The series-parallel powertrain has a degree of freedom of two. We chose battery power P_{bat} and rear traction motor torque T_{rtm} as the two independent control variables. To apply Pontryagin's Minimum Principle to the optimal control problem, we first have the Hamiltonian as follows:

$$\begin{aligned}H(P_{bat}(t),T_{rtm}(t),t)&=\dot{m}_{fuel}(P_{bat}(t),T_{rtm}(t),t)\cdot\eta_{FSE}\cdot\eta_{PEU,fuel}\\&+P_{bat}(t)\cdot\eta_{PEU,elec}-p(t)\cdot\frac{V_{oc}-\sqrt{V_{oc}^2-4R_{in}P_{bat}(t)}}{2C_{bat}R_{in}}\end{aligned}\quad(5)$$

where $p(t)$ is the costate.

The optimal control variables are determined such that the Hamiltonian is minimized at each time step:

$$\mathbf{u}^{*}(t)=[P_{bat}^{*}(t),T_{rtm}^{*}(t)]^{T}=\min_{\mathbf{u}(t)}H(\mathbf{u}(t),t)\quad(6)$$

For Prius, a 1D search has been conducted at each time step to get the optimal cost function (minimum Hamiltonian in this case). For this PHEV, a 2D search has to be carried out at each time step. The ultimate optimal point was the one that gave lowest cost (Hamiltonian) value.

The results of different optimal control strategies are given in Table 2 for comparison. The control algorithms have been implemented and tested on the dSPACE Hardware-in-Loop simulator as shown in Fig. 5. The Fast PMP optimal control method is practical and superior in fuel economy and GHG emission reduction.

The work was an extended study based on the EcoCAR2 development, where a 2013 GM Chevrolet Malibu was retrofitted into a PHEV to improve energy efficiency, reduce emissions while retaining and increasing performance. Following the model-based-design (MBD) process, two sets of plant model were developed: a simplified control-oriented plant model to allow initial conceptual validation of the optimal control algorithm and a more sophisticated

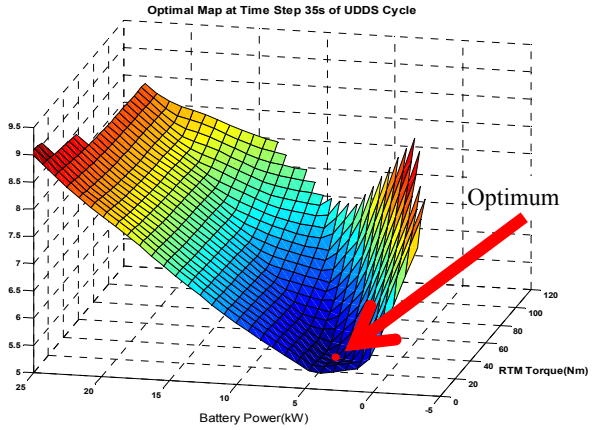

Fig. 4 Cost function at 35s step of UDDS cycle.

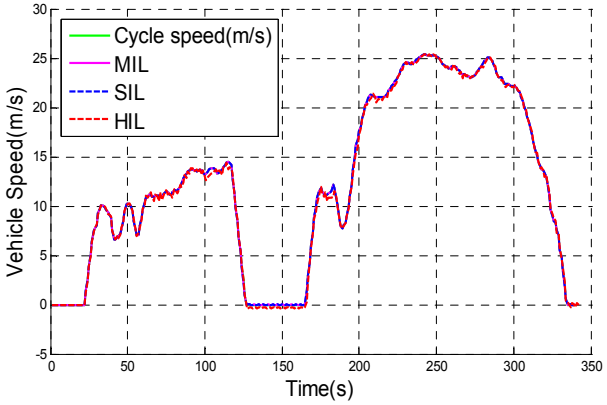

Fig. 5 Desktop simulation and HIL result.

4. Summary

Table 2 Fuel energy consumptions for different control strategies on the same UDDSx10 cycle.

	Fuel Economy MPG	WTW PEU (Wh PE/km)	Energy Consumption Improvement*	Computation Time** (Sample Time = 0.01s)
Mild-hybrid: Production Malibu	26.64	774	/	/
PHEV: Rule-based	47.98	101.96	(baseline)	10 min
PHEV: Slow PMP with fixed p	51.02	97.01	4.8%	6h
PHEV: Fast PMP with fixed p	50.69	97.319	4.5%	20 min
PHEV: Fast PMP with adaptive p	49.38	98.56	3.3%	20 min

* Compared to the baseline model. ** With same plant model and driver model, on a 32 GB, 4 core, 2.5 GHz computer.

implementation-oriented plant model based on dSPACE Automotive Simulation Models (ASM) tool, where I/O interface was the same as in the real vehicle.

Based on the above vehicle model, a real-time optimal control algorithm was developed, which identifies the optimal operational mode and the corresponding torque split among each components at each time step. The control objective in this study was to minimize the well-to-wheel petroleum energy use (PEU), where both the fuel and electric energy consumption was taken into account. The optimal torque split was computed based on Pontryagin's Minimum Principle. Since the powertrain system has a degree of freedom of two in terms of free control variables, a 2D search algorithm were initially developed to find the optimal point. To reduce the computational burden, the 2D search algorithm was further converted into a 1D-search algorithm based on optimization techniques. For practical implementation, an adaptive technique was utilized to update the equivalence factor based on battery SOC and current driving distance.

The proposed fast PMP algorithm was first investigated through Model-in-the-loop (MIL) simulation tests by using the simplified vehicle model. Simulation results have shown that the PMP algorithms have improved the PEU consumption by 3-5% when comparing to the baseline rule-based controller and the lowest PEU consumption was obtained when battery SOC is just depleted at the end of the trip. Among all algorithms, the fast PMP with adaptive costate p was the best one that has balanced both energy consumption, computation efficiency, and the ability for practical implementation, since only driving distance was needed for this algorithm.

After the control algorithm was validated in the MIL environment, it was then migrated to the more complex model and integrated with other system modules (such as subsystem diagnostic modules) in the rapid prototype controller (MicroAutobox II). The real-time performance of the developed controller was investigated through the rapid-prototyping controller HIL platform, where plant model was uploaded into dSPACE midsize real-time simulator and the controller model was uploaded into MicroAutobox II. HIL simulation has proved that the proposed control algorithm is able to run in real time and can track the driving cycle very well.

Modern Environmental Science and Engineering (ISSN 2333-2581)
September 2019, Volume 5, No. 9, pp. 854-859
Doi: 10.15341/mese(2333-2581)/09.05.2019/009
Academic Star Publishing Company, 2019
www.academicstar.us

Cluster Analysis of the Soil Physical Attributes under Soil Preparation Systems

Sálvio Napoleão Soares Arcoverde[1], Cristiano Marcio Alves de Souza[1], Weslley Rodrigues Santos[1], and Egas José Armando[2]

1. Federal University of Grande Dourados, Dourados, Brazil

2. Eduardo Mondlane University, Vilankulo, Mozambique

Abstract: The adoption of conservation management systems in sugarcane is still incipient in comparison to the conventional tillage system, due to a lack of scientific knowledge on its effects in soil quality, technological quality. This work aims to study the behavior of soil physical attributes of a Dystroferric Red Latosol under no-tillage and reduced soil preparation systems in sugarcane cultivation. In each soil preparation system, the systematic sampling grid was used, composed by 32 soil sampling points, in the 0.00-0.10 and 0.00-0.20 m layers. The attributes evaluated were: soil bulk density (SD), total porosity (TP), macroporosity (MA), microporosity (MI) and soil penetration resistance (PR). The data was submitted to Shapiro-Wilk normality test (value – $p \leq 0.05$) and was also verified the presence of discrepant points (outliers) considering the boxplot. Then, was performed the hierarchical grouping analysis, using Ward's method. The physical attributes are more similar in within the preparation system, suggesting differentiated effect of the soil preparation on the attributes in the layers 0.00-0.10 and 0.10-0.20 m. In general, the relationships between soil porosity attributes in both soil preparation systems are influenced by the clayey soil texture and consequently the high soil microporosity.

Key words: soil compaction; soil physical quality, no-tillage, reduced preparation

1. Introduction

Sugarcane is one of the most important crops in Brazilian agribusiness, since it has high potential for several purposes in agroindustry and cogeneration of electricity power. The increase in the demand for sugarcane products due to the growth of the Brazilian sugar and ethanol sector, which results in the expansion of sugarcane farming areas and investments in the construction of new plants, especially in the Center-South region. The adequate planning of the activities involved throughout sugarcane crop cycle, from the soil preparation to the harvest, is fundamental to meet the demand of the industry raw material both in quantity and quality. When soils are susceptible to compaction, such as clayey Latosols, are inserted in these productive systems, the development of degradation processes such as compaction and erosion occur. Thus, changes in soil structure and physical attributes has shown an increase in soil bulk density, soil resistance to penetration, and decrease of soil macroporosity, affecting the quality, limiting its properties such as aeration, availability and retention of water and nutrients, as well as restricting crops root development. Thus, it is necessary to carry out studies for better understanding of the changes caused by soil use aiming to maximize production and avoiding the degradation of agricultural soils, since they generate important information for soil management and conservation incorporated under intensive production processes. In the sugarcane production units it is necessary to understand the relationship between the

Corresponding author: Sálvio Napoleão Soares Arcoverde, Doctor; research area/interest: management soil, physical agricultural mechanization, agricultural precision sowing quality, soybean, mayze, sugarcane. E-mail: salvionapoleao@gmail.com.

soil management practices and the ability of the soil classes to increase the longevity of the cane plants and minimization processes of soil physical degradation. Including conservation management systems such as no-tillage and reduced tillage can be a sustainable alternative [1]. Hence, the multivariate analysis techniques enable to explain the maximum correlation between the soil characteristics and indicate the ones that most contribute to the characterization and/or alteration of the soil [2, 3]. Research has been applied to the multivariate techniques for soil quality analysis [1, 3-5]. Therefore, this work aims to study the behavior of physical attributes of a Dystroferric Red Latosol under no-tillage and reduced tillage in sugarcane cultivation.

2. Material and Methods

The trial was carried out in the municipality of Dourados, in the southern region of Mato Grosso do Sul, with the geographical coordinates 22°13'58"south latitude and 54°59'57" west latitude and 418 m altitude. The climate of the region is type Am, monsoon, with dry winter, and an annual average rainfall of 1500 mm, and annual average temperature of 22°C. The soil of the area is classified as Red Latosol Dystroferric, clay texture. The experimental area has been conducted in the last 14 years under cultivation of soybean and corn, in a system of succession and rotation of crops without soil mobilization. The area was divided into two subareas, composed by no-tillage and reduced tillage. In each preparation farming unit, the sugarcane cultivars were planted manually on 21 July 2016, in the density of 15 buds per meter. Eight sugarcane cultivars (RB965902, RB985476, RB966928, RB855156, RB975201, RB975242, RB036066 and RB855536) were planted in a completely randomized design with four replicates. The reduced preparation (RP) management system consisted of heavy harrowing. The operation was performed with an off-set disc harrower of 16 discs of 0.76 m in diameter (30") in each section, in the depth of 0.15 m. In the other hand, the no-tillage system consisted of mechanized control (weeding) of the weeds, and later, opening of grooves for planting. For this operation, it was used a straw crusher equipped with rotor of steel curved knives, working in high rotation and furrower to open the grooves for planting. For the preparation and opening of furrows for planting, a 4×2 power tractor was used in the 89.79 kW (122 hp) engine, 2200 rpm rotation, 3rd gear reduced, front tires 14.9-58 and rear 23.1-30, and mass of 4.51 Mg. In order to cover the furrows and crop management, a 4×2 TDA tractor with a power of 68.74 kW (92 hp), a rotation of 2200 rpm, a low gear, 7.50-18 and rear 18.4-34, and mass of 3.40 Mg; and a KO Cross-s 2000 sprayer, tires 9.5-24, 14 m bar and 1.40 Mg mass. Each experimental unit contained 55-meter long cane lines spaced 1.50 m (37.5 m^2), in a total of 32 experimental units per preparation. In each experimental unit, a soil sample with preserved structure was collected to determine the following soil physical attributes: soil bulk density, total porosity, soil macroporosity, soil microporosity and soil resistance to penetration (PR). The volumetric rings used to collect the soil were 0.0557 m in diameter and 0.0441 m high (107.45 cm^3), were wrapped in film paper and kept in a refrigerator after collection, aiming minimize the structural alteration and loss of sample water. The total porosity of the soil was obtained by the difference between the mass of the saturated soil and the mass of the dry soil in an oven at 110°C for 24 h; the microporosity of the soil determined by the tension table method with a water column of 60 cm in height. By the difference between total porosity and microporosity, macroporosity was obtained. Soil bulk density was determined by the mass of greenhouse dried soil at 105-110°C, values expressed as Mg dm^{-3} [6]. After reaching the equilibrium in the tension table, corresponding to the water column at 6 kPa, the PR was determined by means of an electronic penetrograph model MA-933, with a constant penetration velocity of 10 mm min^{-1}, a base diameter of the rod of 4 mm and conic angular tip at 30°, as standardized by ASABE [7].

For each attribute studied, the mean was calculated using the classical statistics. A multivariate technique was used by means of the hierarchical grouping analysis, calculating the Euclidean distance between the access among the ten attributes, using Ward's algorithm to obtain similar accessions groups. This analysis, aimed to verify the similarities between the attributes analyzed and the areas studied from homogeneous groupings represented in a dendrogram of similarity.

3. Results and Discussion

The Fig. 1 shows that, in the 0.00-0.10 m layer of soil with reduced tillage, attributes related to soil porosity, such as macroporosity (MA) and soil microporosity (MI) presented at least an unilateral outliers to the right side, also being observed a left sided for the total porosity (TP). In the 0.10-0.20 m layer, the same behavior was observed, however, with unilateral outliers to the right for TP, which also occurred for macroporosity under no-tillage. In both (0.00-0.10 and 0.10-0.20 m) layers, were observed outliers at the right either under no-tillage or reduced tillage (RT)for resistance to penetration (PR), while for the soil bulk density (SD) only left outliers under no-tillage in the 0.00-0.10 m layer was observed, and for the other layer there were no outliers in the data series for soil bulk density (Fig. 2).

After the removal of the outliers, all the soil physical attributes data presented normal distribution by the Shapiro-Wilk test (value – p ≤ 0.05) under the soil with no-tillage and reduced tillage. In Fig. 3a, when defining the cutting Euclidean distance point at11, the formation of two groups for the attributes in the two areas was verified: no-tillage and reduced tillage in the 0.00-0.10 m layer. Group 1 (G1) was composed by PR, SD and MI and in group 2 (G2) were TP and MA. In the 0.10-0.20 m layer (Fig. 3b), when defining the cutting Euclidean distance point(for G1 was composed by PR, SD, TP, MA and MI, while group 2 (G2) were PR, SD, MI, TP and MA.

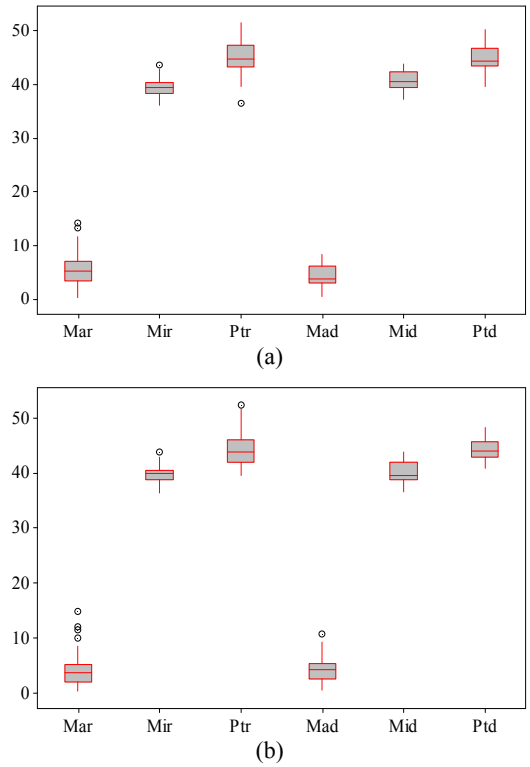

Fig. 1 ***Box-plots*** **of MAr, MIr, TPr, MAd, MId and TPd in the depth 0.00-0.10 m (a) and 0.10-0.20 m (b) under no-tillage and reduced systems.**

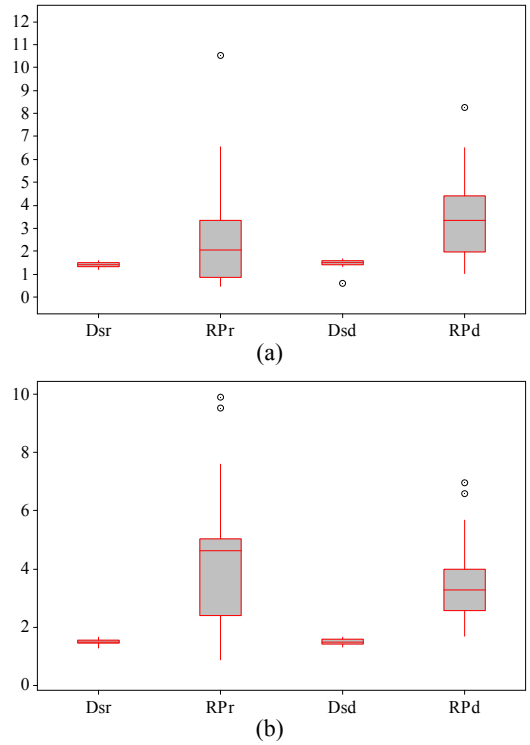

Fig. 2 ***Box-plots*** **of SDr, PRr, SDd and PRd in the depth 0.00-0.10 m (A) and 0.10-0.20 m (B) under no-tillage and reduced systems.**

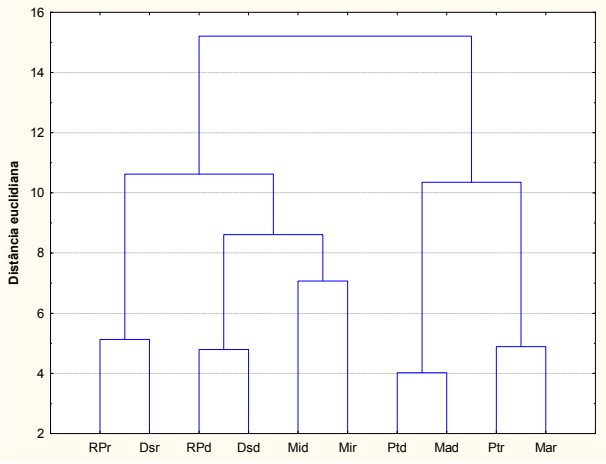

(a)

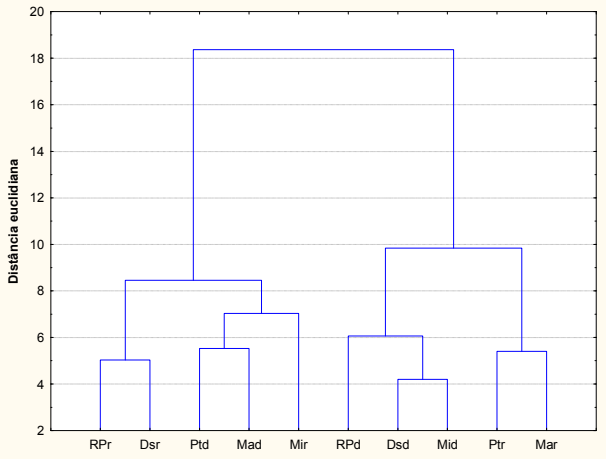

(b)

Fig. 3 Dendrogram of hierarchy analysis cluster showing two groups, in the depth of 0.00-0.10 m (a) e 0.10-0.20 m (b).

When analyzing the Euclidean distances, it is verified that attributes of the G1, in the layer of 0.00-0.10 m, being the smaller distances were verified when different attributes were compared in the same environment. The MI attribute presented the greatest distances in relation to the PR, while the smaller ones were verified in relation to the SD. This was also observed for the PR and SD attributes in the same preparation system. It is possible to verify that attributes from the G2, in the layer of 0.00-0.10 m, for PR and SD attributeS, the Euclidean distances was larger when compared between the preparations systems. This shows a differentiated effect of the soil preparation on the attributes in the superficial layer. Such differences between the treatments studied on the soil physical attributes in the superficial soil layer can be attributed to the action of the preparation tools; as well as to the reorganization of soil particles under soil preparation systems, causing a higher densification in the superficial layers in the reduced preparation [8]. Additionally, in post-soil machine traffic, there is an increase in compaction with changes in soil structural quality [9, 10]. However, this can occur even in the absence of soil disturbance, where compaction processes associated with the natural accommodation of the particles can be diagnosed. According to Collares et al. (2006) [9], the structural alteration can imply the increase of the density and the soil penetration resistance, with a reduction of the macroporosity.

In addition, smaller distances between MA and PT were observed for both preparations systems. Similarly to the G1 of the layer of 0.00-0.10 m, the G1 attributes of the layer of 0.10-0.20 m presented the smaller Euclidean distances for the attributes SDr and PRr, and MAd and PTd; while greater distance between PRr and MIr was observed. When analyzing the attributes that constituted Group 2 in the 0.10-0.20 m layer, similar relationships was observed in group 1, with the lowest distances between SDd and PRd; SDd and MId; MId and TPr; and TPr and MAr. It is emphasized that PR is more influencied by the mass-volume relations expressed by SD and the water content in the soil at the moment of its determination. Thus, the relationships between soil porosity attributes suggests that, at these depths, there is a significant effect of the clayey texture and consequently, the high microporosity on the structure and total volume of pores is on detriment to the type of soil preparation. Bergamin et al. (2010) report that in dystroferric Red Latosol, the mineralogical composition of the clay fraction conditions, the behaviour of microporosity is a detriment of soil management, contrary to macroporosity. On the other hand, is observed a direct relationship between SD and PR in both soil preparations systems, as expected, as well as the greater sensitivity of these attributes to reflect the

effects of management practices on the structure of soils cultivated with sugarcane [11]. In the present study, in this sense, Cabral et al. (2015) [12] observed a high correlation between SD and PR when studying the different systems of soil preparation in sugarcane reforestation area. Dalchiavon et al. (2013) [13] verified that, among the properties of the soil cultivated with sugarcane, SD was the one that most correlated with the yield of stalks, but with low correlation to PR. This due to PR is significantly influenced by soil moisture variability. Thus, the preparation of the soil should be carried out only once during the sugarcane cycle, its effect must be investigated in the most different edaphoclimatic environments, in order to maintain the adequate structural quality of the soil and its functions aiming to increase the longevity of sugarcane with high yield levels.

4. Conclusion

The soil physical attributes are more similar in the same environment, suggesting differentiated effect of the soil preparation on the attributes in the layers 0.00-0.10 and 0.10-0.20 m. In general, the relationships between soil porosity attributes in both treatments are influenced by the clayey soil texture and consequently by its high microporosity.

Acknowledgement

The authors thank the Foundation for the Support to the Development of Education, Science and Technology of the State of Mato Grosso do Sul (FUNDECT) and the Brazilian Federal Agency for the Support and Evaluation of Graduate Studies (CAPES) for the financial support to conduct and disseminate this research. The authors also thank CNPq and CAPES for the research and Post-Doctor grants awarded, respectively.

References

[1] S. N. S. Arcoverde, Atributos físicos e desempenho de cultivares de cana-de-açúcar submetidas a dois preparos do solo, Tese, Doutorado em Agronomia: Produção vegetal, Universidade Federal da Grande Dourados, Dourados, 2018, p. 136.

[2] L. Freitas, J. C. Casagrande, I. A. Oliveira, P. R. S. Júnior and M. C. C. Campo, Análises multivariadas de atributos químicos do solo para caracterização de ambientes, *Revista Agro@mbiente On-line* 8 (2014) (2) 155-164.

[3] I. A. Oliveira, M. C. C. Campos, L. Freitas and M. D. R. Soares, Caracterização de solos sob diferentes usos na região sul do Amazonas, *Acta Amazonica* 45 (2015) (1) 1-12.

[4] S. N. S. Arcoverde, A. M. Salviano, N. Olszevki, S. B. Melo, T. J. F. Cunha, V. Giongo and J. S. Pereira, Qualidade física de solos em uso agrícola na Região Semiárida do Estado da Bahia, *Revista Brasileira de Ciência do Solo*, *Viçosa* 39 (2015) (5) 1473-1482.

[5] A. M. Salviano, N. Olszevski, S. N. S. Arcoverde, S. B. de. Melo, V. Giongo, T. J. F. Cunha and J. S. Pereira, Soil chemical quality in agricultural land uses in the semiarid of Bahia, *Revista Agrarian* 11 (2018) (42) 328-336.

[6] G. K. Donagema, D. V. B. de Campos, S. B. Calderano, W. G. Teixeira and J. H. M. Viana (Org.), *Manual de métodos de análise de solos* (2nd ed.), Rio de Janeiro: Embrapa Solos, 2011, p. 230 (Embrapa Solos. Documentos, 132).

[7] ASABE (American Society of Agricultural and Biological Engineers), *Soil Cone Penetrometer*, Saint Joseph, 2006b. pp. 902-904 (ASABE standard: ASAE S313.3 FEB04).

[8] T. M. Moraes, F. B. Luz, H. Debiasi, J. C. Franchini and V. R. Silva, Soil load support capacity increases with time without soil mobilization as a result of age-hardening phenomenon, *Soil & Tillage Research* 186 (2019) 128-134.

[9] G. L. Collares, D. J. Reinert, J. M. Reichert and D. R. Kaiser, Qualidade física do solo na produtividade da cultura do feijoeiro num Argissolo, *Pesquisa Agropecuária Brasileira* 41 (2006) (11) 1663-1674.

[10] F. C. A. Valadão, O. L. Weber, D. D. Valadão Júnior, A. Scarpinelli, F. R. Deina, and A. Bianchini, Adubação fosfatada e compactação do solo: sistema radicular da soja e do milho e atributos físicos do solo, *Revista Brasileira de Ciência do Solo* 39 (2015) (1) 243-255.

[11] F. Camilotti, I. Andrioli, F. L. F. Dias, A. A. Casagrande, A. R. Silva, M. Mutton, and J. F. Centurion, Efeito prolongado de sistemas de preparo do solo com e sem cultivo de soqueira de cana crua em algumas propriedades físicas do solo, *Engenharia Agrícola* 25 (2005) (1) 189-98.

[12] M. C. M. Cabral, L. A. Carvalho, E. Novak and C. D. S. Schiarelli, Sistema de preparo de solo em área de reforma de canavial e as alterações físicas do solo, *Revista Agrarian* 8 (2015) (30) 376-386.

[13] F. C. Dalchiavon, M. P. Carvalho, R. Montanari, M. Andreotti and E. A. Dal Bem, Sugarcane trash management assessed by the interaction of yield with soil properties, *Revista Brasileira de Ciência do solo* 37 (2013) (6) 1709-1719.

Modern Environmental Science and Engineering (ISSN 2333-2581)
September 2019, Volume 5, No. 9, pp. 860-866
Doi: 10.15341/mese(2333-2581)/09.05.2019/010
Academic Star Publishing Company, 2019
www.academicstar.us

Ecological Interactions in Epiphytic Orchids in the Archaeological Zone "El Tajín", Papantla, Veracruz

Guadalupe Deniss Ortiz de Angel[1], José Luis Alanís Méndez[2], José G. García Franco[3], and Juan Manuel Pech Canché[2]

1. Faculty of Biological and Agricultural Sciences, Universidad Veracruzana, Mexico

2. Faculty of Biological and Agricultural Sciences, Universidad Veracruzana, Mexico

3. Ecología Funcional Lab, Institute of Ecology, A. C., Xalapa, Veracruz, Mexico

Abstract: Protected natural areas, as well as archeological zones are reservoirs of a region's biodiversity, and the latter represent a legacy of local culture. In this sense, knowledge of the species present is essential to highlight their importance and ensure their conservation. We studied the diversity and ecological interactions of orchids (Orchidaceae) epiphytes in the archaeological zone "El Tajín", municipality of Papantla, Veracruz, Mexico. From January 2015 to February 2016, the orchids species present their floral visitors, their phorophytes (hosts) as well as their vertical location in the trees were recorded. There were 202 colonies of *Lophiaris cosymbephorum*, 25 of *Oncidium sphacelatum* and eight of *Catasetum integerrimum*, distributed in 11 species of phorophytes. *L. cosymbephorum* was distributed in the five vertical strata, although with greater abundance in the outer part of the crown, on the contrary, *Catasetum integerrium* was more frequent in the basal part of the trunk. Floral visitors were: crickets (Gryllidae), beetles (Curculionidae: Baridinae) and ants (Formicidae: Lasius niger), the latter with the highest number of visits. No pollinators were recorded, possibly due to anthropogenic disturbances around the archaeological zone.

Key words: floral visitors, phorophytes, lophiaris cosymbephorum, vertical stratification

1. Introduction

Epiphytes are plants that grow on trees (phorophytes) attached to trunks and branches. Among the most representative epiphytic families are Orchidaceae, Araceae, Piperaceae and Bromeliaceae [1]. The family Orchidaceae comprises about 30,000 species, in Mexico 1300 species are reported [2]. The seeds of the orchids are very small and light-weight which allows them to disperse long distances from their parent plants through the wind [3]. The orchids have aerial roots which have a special fabric (velamen) that captures rainwater, and during droughts this root is filled with air which acts as an insulator against heat and drying [4].

Corresponding author: Guadalupe Deniss Ortiz del Angel, M.C.; research areas/interests: environmental sciences. E-mail: denortiz@uv.mx.

Orchids develop in a network of biological relationships which can be beneficial, antagonistic, or neutral to the individuals they interact with, thus they are related through ecological interactions [5]. Plant-insect interactions can be affected by anthropogenic disturbances which cause habitat loss, affecting the richness and abundance of various pollinators [6]. Under conditions of anthropic disturbance, protected natural areas serve as refuges because they are home to different species of flora and fauna. These areas are subject to special regimes of protection, conservation, restoration and development. Since archaeological zones are under protection, they are also considered fundamental for the conservation of different species of flora and fauna.

The Archaeological Zone of "El Tajín" served as a ceremonial center where the Totonaca culture

developed. It stands out for being the largest ancient settlement on the northern coast of the Gulf of Mexico, which was discovered in 1785 [7]. Among the most important buildings in this area is the pyramid of the Niches which has 365 of them, so it has been associated with the solar calendar [8]. However, before being declared World Heritage in 1992 by the United Nations Educational, Scientific and Cultural Organization (UNESCO), the archaeological zone of El Tajín and its surroundings (relics of Semievergreen forest) were disturbed by the inhabitants who settled there for housing purposes, using land for agriculture and livestock, in addition to extracting flora and fauna, and cutting down trees. After it was declared Cultural Patrimony of Humanity, a reforestation program was carried out in the gardens of the archaeological zone, these trees have been colonized by epiphytic plants.

Currently, the archaeological constructions of El Tajín are under the protection of the National Institute of Anthropology and History (INAH), while protecting the natural resources that are housed there. However, human settlements in its surroundings generate disturbances, impacting the scarce relics of Semievergreen forest and acahuales (secondary growth forest). Among the most affected flora are orchids, which are a fundamental element in the composition, structure and functionality of ecosystems. For example, the population of *Oncidium sphacelatum* has been affected since it is extracted for use in a traditional religious celebration. For this reason, the contribution made by the Archaeological Zone of El Tajín to the conservation of biodiversity is of great importance. This paper studied the diversity and ecological interactions in epiphytic orchids (Orchidaceae) in the "El Tajín" archaeological zone.

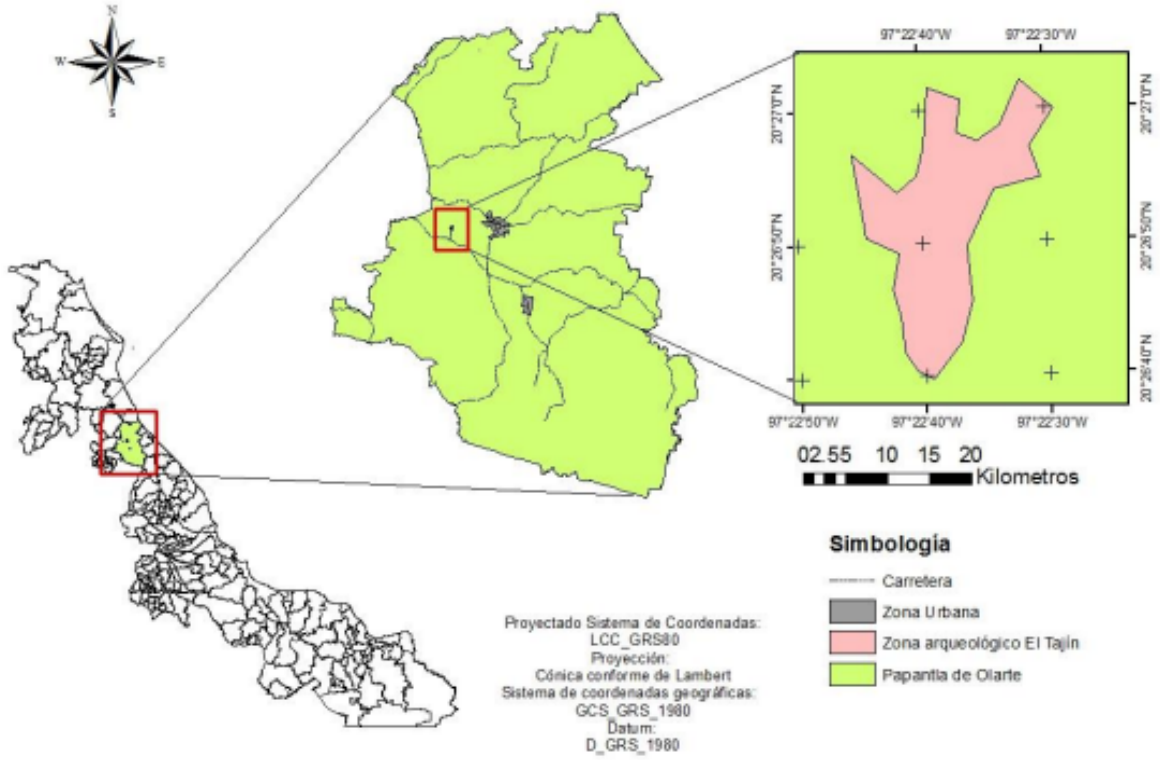

Fig. 1 "El Tajín" Archaeological Zone, Papantla, Veracruz, Mexico.

2. Materials and Methods

In the city of Papantla, Veracruz (Mexico) is located the ceremonial center El Tajín, area in which the Totonaca culture was developed, and is considered one of the most important archaeological settlements in Mesoamerica. This zone has 168 buildings, distributed

in architectural complexes and constructions classified as ceremonial temples, ball games, and houses.

The first routes to identify orchid phorophytes were made in April 2015, the trees were located using a global positioning system (GPS). Phorophyte species were identified based on Niembro et al. [9]. Orchid specimens were later collected and deposited in the herbarium of the Mexican Association of Orchidology (AMO).

In order to analyze the distribution of the orchids over the phorophytes, each phorophyte with orchid presence was subdivided into the five vertical zones proposed by Johansson [10], and the number of colonies present for each orchid species was counted.

Observations of floral visitors were made on the species *Lophiaris cosymbephorum*, which was the most frequent species, with the highest number of reproductive individuals. We selected six orchids located in *Crescentia cujete*, the most abundant phorophyte and with most of the orchids in bloom. The observations were made in periods of 20 minutes each hour from 08:00 to 17:00, from November 2015 to February 2016. The following data were recorded in a field record: floral visitors, number of visits to the flower, duration of the visit and visitor behavior. Floral visitors were photographed and videotaped during their activity. Finally, two individuals were collected that were herborized and deposited in the AMO herbarium as a reference.

Revision of the species of orchids epiphytes between the archaeological zone and the surrounding vegetation.

A bibliographic investigation was carried out on the available information on the vegetation surrounding the Natural Protected Area El Tajín [11], in order to identify if the orchid species found in the study area are the same as those described in the management programs. Subsequently, to corroborate this information, 10 transects (10 × 5 m) were made in the surrounding vegetation (east acahual and west acahual) to record the orchid species present and compared the species composition between the study area and the two secondary growth forests (acahuales).

3. Results and Discussion

3.1 Phorophytes Associated with the Species of Orchids Epiphytes in the Area

In the present study we found 37 phorophytes with the presence of orchids (Table 1). The phorophyte with the highest orchid abundance was *Parmentiera edulis* with 63 colonies of *L. cosymbephorum*, unlike *Manilkara zapota* and *Bauhinia divaricata* with one individual each. A previous study "The environment of El Tajín" [11], reported the tree species *Parmentiera edulis*, *Swietenia macrophylla*, *Manilkara zapota*, *Guazuma ulmifolia*, *Spondias purpurea*, *Crescentia cujete* to mention a few. And for the acahuales (surrounding area) *Guazuma ulmifolia*, *Pimienta dioica*, *Bauhinia divarcata* and *Sabal mexicana*. However, that study did not report the existence of associated orchids on these trees.

3.2 Orchids Epiphytes Established in the Archaeological Zone of El Tajín

Three species of orchids were found in the study area: *Lophiaris cosymbephorum* with 202 colonies, *Oncidium sphacelatum* with 25 colonies and *Catasetum integerrimum* with eight colonies. The genus *Oncidium* has a wide distribution in tropical ecosystems, and has also been recorded in the archeological zones of Calakmul and Chicanná in Campeche, México [13].

3.3 Vertical Distribution of Orchids on the Phorophytes

According to Johansson's vertical stratification [10], although *L. cosymbephorum* was distributed in the five strata, it was more abundant on the outside of the crown (Fig. 2). *O. sphacelatum* was distributed in four strata, of which it was more frequent in the trunk, while *C. integerrimum* was distributed in three strata. In this sense, Morales [13] reported *C. integerrimum*, at the

base of the crown (in cocoa agroecosystems), according to his study, this species is of rare and indefinite distribution so it can be established from the runk to the crown.

Table 1 Distribution of orchids by host tree species.

Phorophyte species (local common name)	Number of phorophytes	Orchid Species	Number of orchids
Bauhinia divaricata (pata de cabra)	1	*L. cosymbephorum*	2
Bernardia interrupta	5	*L. cosymbephorum*	*9*
Crescentia cujete (jícaro)	2	*L. cosymbephorum*	52
		O. sphacelatum	1
Guazuma ulmifolia (guácima)	9	*L. cosymbephorum*	56
		C. integerrimum	1
Mangifera indica (mango)	1	*O. sphacelatum*	3
Manilkara zapota (chicozapote)	1	*O. sphacelatum*	1
Parmentiera edulis (chote)	7	*L. cosymbephorum*	62
		O. sphacelatum	3
Sabal mexicana (palmito mexicano)	5	*C. integerrimum*	7
Spondias purpurea (ciruela)	2	*O. sphacelatum*	2
Swietenia macrophylla (caoba)	5	*O. sphacelatum*	13
Tamarindus indica (tamarindo)	1	*L. cosymbephorum*	5
		O. sphacelatum	2

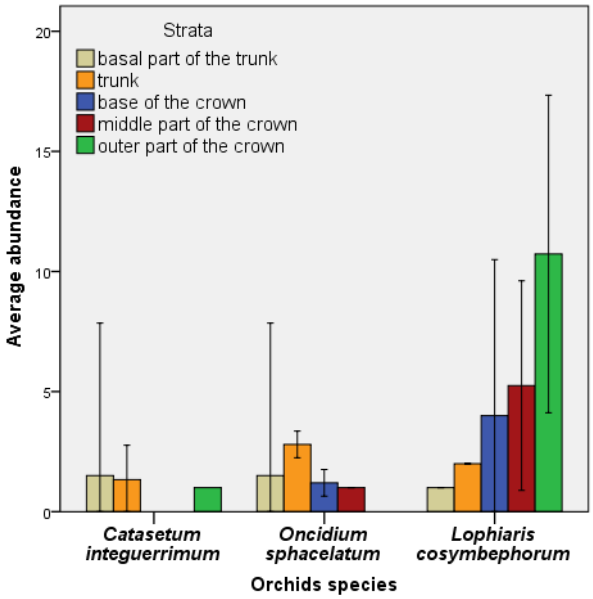

Fig. 2 Average abundance (+C.I.) of vertical stratum orchids in the phorophytes present in the El Tajín archaeological zone in Papantla, Veracruz. The classification of the strata (or sections in trees) follows Johansson's classification (1974).

3.4 Floral Visitors of the Orchids Species in the Archaeological Zone

The six individuals of the *Lophiaris cosymbephorum* orchid selected presented a total of 49 flowers (Table 2). The flowering time of the six individuals was between 10 and 35 days, and the longest flowering was 35 days.

The registered floral visitors were: Gryllidae (crickets), Curculionidae: Baridinae (beetles) and Formicidae: *Lasius niger* (ants) (Table 3), the latter with the highest number of visits. No pollinators were recorded, so there was no formation of *L. cosymbephorum* capsules. This may be due to various factors such as the absence of pollinating insects as the archaeological zone is surrounded by communities and lands used for citrus, maize, vanilla and livestock introduction.

Table 2 Number of flowers and time of flowering of individuals of *Lophiaris cosymbephorum*.

Individual	Total Open Flowers	Total days in Flowering
1	10	35
2	4	21
3	2	15
4	15	16
5	12	24
6	6	11

Table 3 Floral visitors of *Lophiaris cosymbephorum*.

Organism	Number of visits to *L. cosymbephorum*
Lasius niger (Formicidae)	350
Barinidae (Coleoptera)	27
Gryllidae (Orthoptera)	10

In these activities, owners close to the area use herbicides, pesticides and insecticides that could generally affect insects and possible pollinators of orchids. However, although there is no formation of capsules (fruits), orchid colonies continue to grow vegetatively. But by having sexual reproduction and not producing seeds, a future risk is generated for the population of this species as its genetic variability is reduced. The archeological zone, being a guarded area, allows the conservation of the present species, since they thrive there and the looting of orchids is not allowed.

3.5 Comparison of Epiphytic Orchid Species Present in the Archaeological Zone with Species of Surrounding Vegetation (Acahuales)

The acahuales are found on the sides of the archeological zone. The acahual of the east side with woody species of *Bernardia interrupta* and *Bahuinia divaricata* to mention a few, and the presence of 26 individuals of the orchid *Lophiaris cosymbephorum*. In the acahual on the west side, the predominant species was *Sabal mexicana*, where seven individuals of *Catasetum integerrimum* were recorded (Fig. 3). According to the secretary of the Environment in the management program, around El Tajín, the following species were reported within the archaeological zone: *Parmentiera edulis*, *Swietenia macrophylla*, *Manilkara zapota*, *Guazuma ulmifolia*, *Spondias purpurea*, *Crescentia cujete* among others, and for the acahuales (surrounding area) species such as *Guazuma ulmifolia*, *Pimienta dioica*, *Bauhinia divarcata* and *Sabal mexicana*; which agree with those recorded in this study. As for orchids, SEDEMA [11] reported *Epidendrum cochleatum*, *Vanilla fragans* and *Vanilla planifolia*. These species were not found in the present study. This may be due to the fact that the SEDAM study focused more on the description of tree species, leaving other life forms and diverse epiphytes in the background.

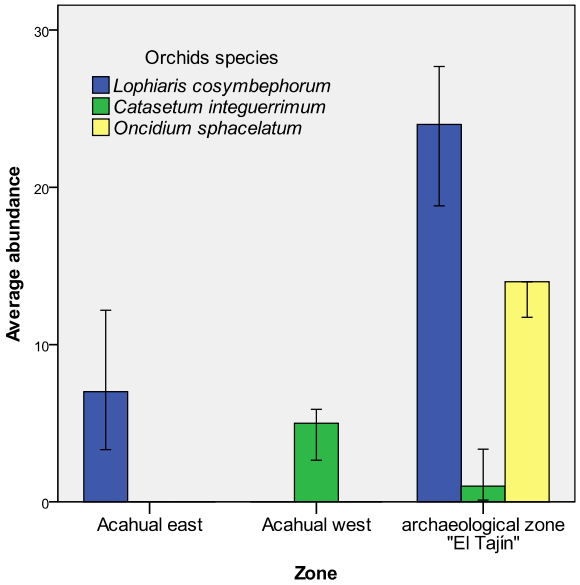

Fig. 3 Average Abundance (±C.I.) of three species of orchids per zone: Archaeological zone, acahual East and Acahual West. Forms of life and the various epiphytes.

4. Conclusion

Three species of orchids were recorded, and *Lophiaris cosymbephorum* was more abundant, followed by *Oncidium sphacelatum* and *Catasetum integerrimum*. The orchids were distributed in 37 phorophytes, of which *P. edulis* and *C. cujete* presented greater abundance and richness of orchids.

The average abundance of orchids per stratum according to Johansson's classification, *L. cosymbephorum* was distributed in the five vertical strata of the trees, being the external part of the crown where it was more abundant, unlike *C. integerrimum* that presented more in the basal part of the trunk.

Lophiaris cosymbephorum flourished in November 2015, ending in February 2016, and although ants of the species *Lasius niger*, an organism of the family Gryllidae and beetles of the subfamily Baridinae were recorded as floral visitors, no pollinator visits were recorded.

In the vicinity of the study zone, no orchid species were recorded from the archaeological zone, thus highlighting the importance of archaeological zones as sites for biodiversity conservation.

Acknowledgements

We thank Francisco Limón for the reading of a preliminary version of this paper and their suggestions to improve the manuscript.

References

[1] D. Granados-Sánchez, G. F. López-Ríos, M. Á. Hernández-García and A. Sánchez-González, Ecología de las plantas epífitas, *Rev. Chapingo* 9 (2004) (2) 101-111.

[2] M. A. Soto Arenas, R. Solano and E. Hágsater, Risk of extinction and patterns of diversity loss in Mexican orchids, *Lankesteriana* 7 (2007) (1-2) 114-121.

[3] O. L. Velasco and B. P. Beltrán, *Orquídeas del Parque Natural Sierra de Grazalema*, *Consejería de Medio Ambiente*, Junta de Andalucía, España, 2008, p. 272.

[4] G. R. A. Menchaca and M. D. Moreno, Manual para la propagación de orquídeas, CONAFOR, México, 2011, p. 56.

[5] E. Del Val and R. Dirzo, Mirmecofilia: las plantas con ejército propio, *Rev. Interciencia* 29 (2004) (12) 673-679.

[6] V. Parra-Tabla, F. Vargas, P. Feinsinger, J. Malo, and J. Leirana, Fragmentación de hábitats en la ecología de poblaciones de dos especies de orquídeas del estado de Yucatán, *Biol. Cons.* 94 (2000) 334-340.

[7] E. L. Rodríguez, A. Gómez-Pompa, A. J. López, R. N. Velázquez, D. N. Aguilar, T. M. Vázquez, G. C. Gallo, J. Duarte and G. Halffter, Atlas de los espacios naturales protegidos de Veracruz, México, Gobierno del Estado de Veracruz, Secretaría de Educación del Estado de Veracruz, México, 2011, p. 352.

[8] L. P. Jiménez, Cuaderno de Trabajo: Arquitectura y poder en El Tajín, Instituto de Investigaciones Histórico Sociales Universidad Veracruzana. México, 2003, p. 53.

[9] R. A. Niembro, V. M. Torres and S. O. Sánchez, *Árboles de Veracruz 100 especies para la reforestación estratégica*, Ed. Nelly Palafox, México, 2010, p. 257.

[10] D. Johansson, Ecology of vascular epiphytes in West African rain forests, *Acta Phytogeografica Suecica* 59 (1974) 1-129.

[11] Subsecretaria del Medio Ambiente, *Programa de manejo entorno de El Tajín*, Ed. Gobierno del estado de Veracruz-Llave, México, 2001, p. 115.

[12] S. Ludmer-Gliebe and G. L. Ibarra, Orchids amid the ruins, Yucatan Interlude, *Orchids* 80 (2011) (3) 174.

[13] L. J. Morales, Diversidad y conservación de orquídeas en plantaciones de cacao del sureste de México, Tesis de Maestría, Instituto de Ecología, A.C.. Xalapa, Ver., México, 2012.

Supplementary 1 ***Lophiaris cosymbephorum*** **with its floral visitors:** ***Lasius niger*** **and Curculionidae.**

Supplementary 2 *Lophiaris cosymbephorum*.

Modern Environmental Science and Engineering (ISSN 2333-2581)
September 2019, Volume 5, No. 9, pp. 867-871
Doi: 10.15341/mese(2333-2581)/09.05.2019/011
Academic Star Publishing Company, 2019
www.academicstar.us

Using the BIM 5D Tool for Public Works in Brazil

Leandro Dias Viana, and Eduardo Marques Arantes
Federal University of Minas Gerais, Brazil

Abstract: This article was developed with the purpose of analyzing the applicability of the BIM 5D tool for the elaboration of budgets of public works in Brazil. In order to do so, the government's initiatives in this regard were presented, as well as the functionalities of this tool that imply the facilities and gains for the public service in the elaboration of the budget of its works.

Key words: budgets, public constructions, BIM 5D

1. Introduction

Countries such as Finland, Denmark, Singapore, Norway, South Korea and the United Kingdom have made mandatory use of BIM in public works. The adoption of such a policy is motivated by the following benefits of BIM technology: improved coordination, reduction of errors and omissions as well as communication of projects, increase of productivity and efficiency of the construction industry, reduction of costs and deadlines [1].

In Brazil there are no government standards for the use of BIM, however, his employment in construction companies is growing at higher rates than in the others major global economies [1]. The use of this technology in public works, however, is still incipient, although they lack the benefits of BIM and are commonly objects of irregularities, as demonstrated by audits carried out by the Court of Auditors (TCU) in 2014 [2]. Therefore, improvements in the management of public works are needed to combat such irregularities.

With regard to use in the federal public administration, we have examples of the Brazilian Army and d Petrobras who have used BIM on some of its projects. Besides this, the Bank of Brazil has, throughout 2013 and 2014, several project bids in BIM within the Regional Aviation Program.

In relation to standards and guidelines for BIM, the government of the State of Santa Catarina published guidelines on "BIM Project Presentation Pad". "In it are defined the standardization and formatting that should guide the development of BIM projects in contracting with the State Government" [3].

2. Goals

The main objective of this study is to make a bibliographic analysis and from Brazilian government agencies initiatives in relation to the adoption of BIM and its benefits. It also aims to make an analysis of the applicability of the use of BIM, with special emphasis on the 5D tool, for budgeting public works in Brazil and to verify as it can contribute to greater assertiveness of budgets.

The benefits of using BIM technology in the area of project design and execution are widely disseminated in both academic and professional settings, which has led to the publication of various standards and manuals in the area by several countries and even its adoption as mandatory in Some of them. However, in relation to the use of this tool for budgeting works public, there is a gap as the studies demonstrate the benefits of BIM. The objective of this article is to fill this gap,

Corresponding author: Leandro Dias Viana, Post Graduate; research area/interest: construction management. E-mail: leandrodv@ufmg.br.

demonstrating how the use of BIM 5D can improve the assertiveness of budgets of Brazilian public works.

3. Justification

The justification of the theme for this work is that the study of BIM 5D is relevant in view of the large number of irregularities identified in public works.

The s Budget Guidelines Law (LDO) incumbent since 1998 the Court of Audit (TCU) to inspect the major works displayed them in order to identify the occurrence of serious irregularities. The TCU sends to the National Congress, annually, a list of enterprises in which indications of serious irregularities have been identified, especially those that lead to a recommendation to stop. Based on these reports, the National Congress decides on the blocking or release of the resources necessary for the execution of these enterprises. The analysis of those reports allows to evaluate the irregularities that occur in most public works.

Analysing Table 1, it is verified that the occurrences of overprice/overbilling in the works correspond to 15.8% of the irregularities detected in public works and occur in approximately 38% of the audits for the period under study, demonstrating their impact on the works.

Table 1 Summary of TCU audit findings in the period.

	Audit Finding	Number of findings			Audits	
		Quant.	%	% accu.	Quant.	%
1	Over-price/Supercharge	415	15.8	15.8	253	38
2	Poor/outdated basic/executive design	341	13	28.9	255	38
3	Poor supervision or lack of supervision	291	11.1	40	77	12
4	Existence of unjustifiable delays in works and services	195	7.4	47.4	48	7
5	Execution of low quality's services	131	5	52.4	42	6
6	Restrictions on competitive bidding	115	4.4	56.8	95	14
7	Failure to comply with legal and technical accessibility requirements for persons with disabilities or reduced mobility	88	3,4	60.2	17	3
8	Bidding Budget/Contract/Incomplete or Inadequate Additive	69	2.6	62.8	63	9
9	Other findings with percentage less than 2%	974	37.2	100		
	Total	**2619**			**668**	

Source: MATOS, CR DE and MIRANDA, C. DE O. Use of BIM in the fight against irregularities in public works.

According to TCU, overpricing is characterized "when the price of the work/service/input is unjustifiably higher than the price paradigm" and overbilling "when bill services of a work with overpricing or when bill services that have not been executed (whose quantitative measures are higher than those actually executed)" [2].

The OURT T Federal Audit points out the following factors as the cause of overpricing among others:

• By the measurement of quantities greater than those actually performed/supplied;

• By it breaches the initial economic-financial balance of the contract in disadvantage of the Administration by altering the quantity (spreadsheet game) and/or prices (changes in financial clauses) during the execution of the work;

So, the main causes of overbilling are quantitative problems. In this aspect, the use of the BIM model allows the extraction of the quantities of the various materials in the model, due to the physical information inherent to the modelling elements [4].

Obtaining the direct quantification of the BIM model results in agility and accuracy of the values compared to the conventional method, which is subject to human

errors inherent to the process, which propagate throughout the cost analysis [5].

In addition, in the case of project change, the surveys from BIM technology are updated instantaneously, a fact that does not occur in the conventional method [5].

By connecting these elements to an external database containing the cost information, you can perform analyses. The estimate of the cost of construction will be the product of the quantities obtained in the model with the cost of a database, that connection between the model and the database will vary depending on the software, allowing the value of the work to be predicted and controlled [4].

The study of the use of the BIM 5D model is then justified in order to create mechanisms to improve the budgets of public works and to reduce the prices of the same ones. The use of BIM to extract the quantities of the design services allows agility and precision in the process, since most quantitative can be extracted automatically avoiding errors inherent to the manual process.

4. BIM for Public Works in Brazil

In Brazil, the Federal Government's initiative in this area is through the Brasil Maior plan, in which the following objective was established: intensify the use of information technology applied to the construction and implementation of the construction information classification system — norm as BIM [2].

As a result of a cooperation agreement between the Ministry of Development, Industry and Foreign Trade (MDIC), Federation of São Paulo State Industries (FIESP), the Brazilian Agency for Industrial Development (ABDI) and Euclides da Cunha Foundation to Support University Federal Fluminense (FEC), in partnership with architectural offices, a library of most common components and materials, directed the program Minha Casa, Minha Vida (MCMV) was prepared [6].

The library for the MCMV program was developed in the REVIT software and made available as a template by the MDIC. This library is not endowed with innovative components but seeks to meet the main demographics of housing projects [7].

It is worth mentioning, however, that this library is very useful for modelling projects of other categories than just housing (commercial, educational, etc. ...), since many of the services executed are similar (Foundation, Structure, Masonry, coverage, etc. ...).

An interesting aspect to be remembered is that in the families developed for this template a field is available for insertion of the SINAPI code of said service.

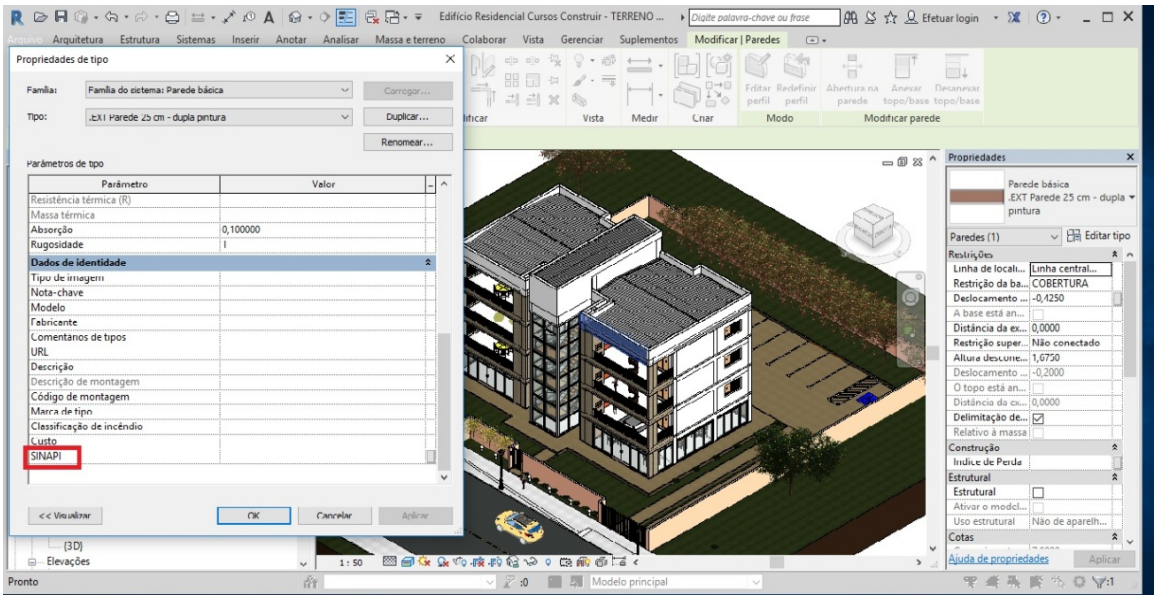

Fig. 1 Family example with SINAPI field template M CMV.

The public works budget with federal funds based on the SINAPI compositions has become a rule since Decree 7983/13 [8], as described:

"Art. 3. The overall reference cost of engineering works and services, except transport infrastructure services and works, shall be obtained from the composition of the unit costs provided for in the project that includes the bidding document, less than or equal to the median of its corresponding in the reference unit costs of the National System of Survey of Costs and Indices of the Civil Construction — Sinapi , excepting the items characterized as industrial assembly or that cannot be considered as civil construction."

And therefore, in order to comply with this guideline of the public budget, the use of this template not only fulfills perfectly what can be recommended.

In addition to this template was also recently instituted a commission to implement BIM by the current president of the republic:

"Article 1 The Strategic Implementation Committee of the Building Information Modeling — CE-BIM, with a temporary character and with the purpose of proposing, within the Federal Government, the National Strategy of Dissemination of the Building Information Modeling — BIM" [9].

The use of BIM for the preparation of projects can make a lot more correct lifting of quantitative project services, since the lifting of quantitative by traditional 2D method is susceptible to many human errors and through the BIM 5D are made to many services automatically and with complete accuracy. So, the use of this technology can be very useful in reducing the discrepancies identified in the annual reports of TCU.

Amiri [10] researched the use of BIM for quantitative survey in a case study in the city of Vancouver. It is emphasized that BIM software presents surveys more efficiently and more precisely, as long as the models are created for such. That is, the greatest effort must be made in the creation of the besides presenting a considerable accuracy, compared to the conventional method. Thus, based on the literature presented, it is possible to discern the great potential of the BIM technology in the survey of quantitative works.

5. Conclusion

Given the above facts, we can conclude that the use of the BIM model, in special the BIM 5D, can make public works budgets more assertive and, therefore, can strongly contribute to reducing the discrepancies that are annually noted of irregularities in public works by TCU.

Despite the benefits that the use of this technology can bring to the public service, in Brazil its use is still very timid making this subject of great relevance for scientific studies.

References

[1] Mcgraw Hill Construction, The business value of BIM for owners, available online at: http://i2sl.org/elibrary/documents/Business_Value_of_BIM_for_Owners_SMR_(2014).pdf.

[2] C. R. de Matos, A. C. de O. Miranda, Uso do BIM no combate às irregularidades em obras públicas, in: *Encontro Técnico Nacional De Auditoria De Obras Públicas*, Campo Grande. ENAOP, 2015 available online at: https://www.researchgate.net/publication/284283576_USO_DO_BIM_NO_COMBATE_AS_IRREGULARIDADES_EM_OBRAS_PUBLICAS.

[3] Santa Catarina (Estado), Secretaria de Estado do Planejamento, Diretoria de Planejamento, Comitê de Obras Públicas, Caderno de Apresentação de projetos em BIM, Florianópolis, 2014, available on line at: http://www.spg.sc.gov.br/index.php/visualizar-biblioteca/acoes/comite-de-obras-publicas/389-caderno-de-apresentacao-de-projetos-bim/file.

[4] W. Kymmell, *Building Information Modeling: Planning and Managing Construction Projects with 4D CAD and Simulations*, New York. The McGraw-Hill Companies. 2008.

[5] A. De P. Santos, C. E. Antunes and G. B. Balbinot, Levantamento de quantitativos de obras: comparação entre o método tradicional e experimentos em tecnologia BIM, *Iberoamerican Journal of Industrial Engineering* 6 (2014) (12)134-155.

[6] ASBEA (Associação Brasileira dos Escritórios de Arquitetura), Bibliotecas BIM e Cadernos de Práticas Recomendadas em coordenação modular, 2018, available

online at: http://www.asbea.org.br/escritorios-arquitetura/noticias/bibliotecas-bim-e-cadernos-de-praticas-recomendadas-em-coordenacao-modular-206880-1.asp.

[7] O. R. Tsan Hu et al., Análise e discussão da biblioteca de componentes REVIT, desenvolvida para o Ministério do Desenvolvimento, Indústria e Comércio Exterior, para o uso no Programa "Minha casa, minha vida", *Revista Mackenzie de Engenharia e Computação* 16 (2016) (1) 112-135.

[8] BRASIL, Decreto presidencial 7983/13 - Estabelece regras e critérios para elaboração do orçamento de referência de obras e serviços de engenharia, contratados e executados com recursos dos orçamentos da União, e dá outras providências, Presidência da República, 2013.

[9] BRASIL, Decreto de 5 de Junho de 2017 - Institui o Comitê Estratégico de Implementação do Building Information Modelling, Presidência da República, 2017.

[10] H. Amiri, Building Information Modeling for construction applications: Formwork installation and quantity takeoff, master's thesis in civil engineering, Faculty of Graduate Studies, University of British Columbia, 2012, p. 192.

Modern Environmental Science and Engineering (ISSN 2333-2581)
September 2019, Volume 5, No. 9, pp. 872-879
Doi: 10.15341/mese(2333-2581)/09.05.2019/012
Academic Star Publishing Company, 2019
www.academicstar.us

Modeling the Water Balance in the Micro Basin of the Region of Tabuleiro Costeiro, Brazil

Marcos Vinícius de Souza Chaves, Mariana Dias Meneses, Bruno Javier Carozo Arze, and André Quintão de Almeida

Federal University of Sergipe, Brazil

Abstract: The research was developed in the Rural Campus of the Sergipe Federal University in São Cristóvão, city of Sergipe state, in a place characterized by its predominant coverage of the Atlantic Forest and soil constituted by a Red and Yellow Argisoil with extension of 32 ha. The research collected climate data on purpose to model the main components for a water balance of the micro-basin, which were evaluated precipitation, runoff, evapotranspiration and soil water storage. During the period that lasted from September 1, 2017 to May 31, 2018, 1003.22 mm of rainfall and only 11.01 mm of runoff were recorded, showing the importance of evaluating evapotranspiration and the effects caused by the vegetation's type cover. The modeling was done daily and soil water storage was estimated through the water balance. At the end of the study, the participation of evapotranspiration was intense, due to the climatological characteristics of the region, representing 82.4% of the amount of precipitated water, which is evidenced by the low recorded value of runoff.

Key words: forest hydrology, coastal board, watershed's management

1. Introduction

Used for human consumption and for socioeconomic activities, it is withdrawn from rivers, lakes, dams, and aquifers, having a direct influence on health, quality of life and development of populations, water is one of the primary need for life, resource indispensable for the human being and the whole life of the planet. The availability of this resource is directly linked to species survival and socioeconomic development of countries.

The scarcity of this resource is becoming an increasingly common phenomenon. This is a result of increasing urban and industrial demand and increased waste production due to the incorrect use of water. The quality and quantity of water in a river basin can be hampered by several factors, including: management, climate and vegetation cover.

Corresponding author: Marcos Vinícius de Souza Chaves, Graduating Student; research areas/interests: agricultural engineering. E-mail: xavesmarcosvinicius96@gmail.com.

The hydrological cycle involves the physical processes of evaporation, transpiration, precipitation, infiltration, percolation, subsurface runoff, and surface runoff, which represent the different paths through which water circulates in the three phases of the Earth system: hydrosphere, lithosphere and atmosphere [12]. The water movement form of a river basin is linked to characteristics such as its shape, topography, area, geology, drainage network, soil and the type of vegetation cover. The area bounded by a contour within which all precipitated water when it is not evaporated, infiltrated or retained, flows to that point [6] is defined as a river basin. The hydrographic basin is the best representative for the integrated planning of natural resource management in the ecosystem, it involves and can be defined as the physiographic area drained by a system of connected watercourses converging to a bed or surface water [6].

The natural supply of water for a given region is dependent on the hydrological cycle. Thus, the

importance of understanding how and in what quantity the water travels through all the stages of its cycle, considering water as essential material for the maintenance of life. Due to this importance of climatological water balance and climatic classification for all the areas of study involved, it is necessary to record and analyse the data of the main components of the water balance of the Tabuleiro Costeiro region of Brazilian's Northeast, so the proposal presents a fundamental return, the evapotranspiration of the native culture of this watershed taking into account the climatic conditions of the coastal region.

2. Literature Review

The complexity of the study of water behaviour becomes high due to the factors involved such as soil characteristics and vegetation. These factors are changeable over time and have irregular behaviour, therefore, however precise the mathematical model, it is necessary to confront the data with reality due to the mutability of several factors [6]. During the water cycle, their infiltration, redistribution, evaporation and water absorption by plants are interdependent processes and, most of the time, occur simultaneously. To study the water cycle, it is necessary to consider the water balance. According to Pereira et al. [2], water balance is the way to account for and monitor the amount of water stored in the soil and is the result of applying the principle of mass conservation to water in a volume of vegetated soil. This is nothing more than the sum of the amounts of water entering and leaving an element of soil volume and, in a given period of time, the result is the net quantity of water that remains available to the plants [7].

The elements of precipitation and evaporation are considered to be the most important for the hydrologic cycle. In the municipality of Balsas, in the state of Maranhão, a high evapotranspiration potential was observed, where the average annual rate is 1720 mm and for annual rainfall of 1175 mm, being classified as a hot and humid tropical climate region by Passo et al. [9].

In a similar study, carried out in the region of Minas Gerais and with vegetation cover characteristic of Atlantic forest, using the same mathematical model (Penman-Monteith), the result founds were: "In terms of water balance, evapotranspiration corresponded to 89% of the total precipitate, deep drainage at 13.6% and storage variation was slightly negative during the analysis period" by Pereira [2].

The balance must be complexity defined by the size of the basin to be studied and the type of study must also be taking into consideration (the end that will take the result of water balance), some values that could not be accounted for in large basins in a large variation of time, with the decrease of the study area, the other factors become more relevant for their study, so, on a small scale, it would be interesting to analyse the interception, infiltration, percolation and surface runoff, which are significant for small areas and are very relevant for understanding of hydrological processes. In the meantime, that is, between the occurrence of precipitation and the output flow of the basin, all the other processes, composing the hydrological cycle, it happens. Silva et al. [12] also show the great difference in the type of model to be adopted and that the alteration of the balance model for its region brought an increase in annual evapotranspiration from 803 to 1298 mm in the Rio Doce region.

In the Ribeirão Marcela Hydrographic Basin, in a study whose objective was to analyse the water recharge, the most influential component in the water balance is evapotranspiration, with its participation of 56.7% of precipitation in the general average by Pontes et al. [8], then even without characterizing all the factors, classifying the main elements of the water balance brings good approximations for the study of water balance in watersheds. The different uses of water by the resident population in the basin, such as water abstraction for domestic supply, leisure use,

bathing, sewage disposal, and industrial effluents can still occur [1].

The acquisition of the results of the variables of the balance sheet has a variation with climate change, topography, and soil type. Brandão et al. [4] discuss the interference of vegetation cover for the climatic classification in the Northwest of Rio de Janeiro "it is necessary besides the analysis of the elements of the climate, to evaluate the history of the soil uses in a certain area or place", he goes on to explain "Past and present transformations in the physical environment can lead to sensitive changes in water balance, precipitation, and temperature" and concludes "transformed the exuberant Atlantic forest through a scenario similar to the semi-arid Northeast" [4].

Papers as by Martin et al. [11] show the importance of water balance and climatic classification for all areas of study involved and what the need to record and analyse the data of the main components of the water balance. The author, through the data of recorded climate, brings the simulation of soybean plantations in 33 regions of the state of São Paulo and some municipalities of nearby states, determining the best locations for soybean cultivation in the states of São Paulo.

In a study carried out to determine the precipitation reduction and moisture transport of the Amazon basin. Having a greener judgment according to Silveira et al. [8]: "If human activities do not allow that there is environmental regeneration, climate-vegetation balance will be affected, leading to a warmer condition and dry, which in turn, will have serious consequences for the ecosystems of the Amazon". In the case of the Tabuleiros Costeiros region of North-eastern Brazil, the proposal presents a fundamental return, the evapotranspiration of the native culture of this watershed considering the climatic conditions of the coastal region and the climatic classification.

3. Methodology

To accomplish the objective of model the water balance of the micro-basin was necessary before to instrument her and evaluate the parameters. So was delimitated the contour of de area, as well installed the necessary tools.

3.1 Area of Study

The study was conducted in the watershed of the Federal University of Sergipe (UFS), located in the Rural Campus of the institution, in São Cristóvão - SE, between the coordinates 10°55'38"and 10°56'00" South and 37°12'21"and 37°12'00" West (Fig. 1). The basin has an approximate area of 32 ha with a mild topography, with an average annual air temperature of 28°C and an average annual rainfall of around 1200 $mm.y^{-1}$ and an average altitude of 150 m. Its coverage is predominantly Atlantic Forest (~80%). With characteristic soils Red and Yellow Argisoil.

3.2 Surface Runoff

In order to calibrate the spillway's linigraph was made field measurements (Fig. 2). The method adopted on the field was to determine how much volume was flowing in a fixed time in several repetitions and then obtain a good approximation of mean for the readings of the equipment. Thus, through Eq. (1) it was possible to determine the flow rate consulted in the apparatus at the moment the measurements were collected.

$$Q = V.t^{-1} \quad (1)$$

where, Q is the flow, in m^3 s-1; V, is the volume, in m^3, and t, the time, in s.

Knowing that the spillway has a triangular shape with a 90º angle, knows the required height water for

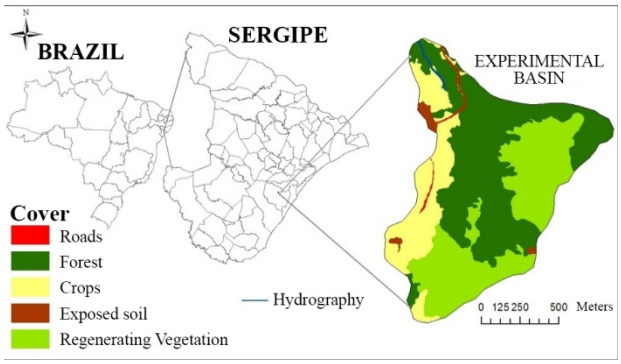

Fig. 1 Location of the study area.

Fig. 2 Calibrating the linigraph in the field for flow measurement.

the surface runoff measured in the field in that schedule, so the equipment was calibrated.

The conversion of factors is only a matter of physically analysing their meaning, so knowing that the humidity is given in a percentage of water quantity, multiply by the depth that the value represents in millimeters.

The runoff through the flow rate only brings the simple assumption that: all water that did not infiltrate in the area above the spillway descends through the spillway dam, and can then be read by the linigraph and transformed into millimeters by manipulating Equation (1) as follows:

$$Q = V.t^{-1}, \text{but } V=A.h*1000$$

where, Q is the flow, in m³ s-1; V, is the volume, in m³, and t, the time, in s, A is the basin area in m², the surface water in mm and 1000 is the conversion factor from meters to millimeters.

The area that will be used is the area above the spillway within the micro-basin of was delimited in 32 ha. For coherence the time for transformation of the flow in this formula must be equal to the humidity measurement intervals and thus, through Eq. (2), determine the evapotranspiration of the crop.

3.3 Water Storage in Soil

The other equipment to be calibrated is Diviner 2000®, Sentek Pty Ltda., Australia, which makes an indirect measurement for soil humidity. The equipment works as a capacitive probe, does not come into contact with the ground and measures the humidity at various depths. As a capacitive probe, the Diviner does not measure the humidity level, but rather the capacitance resulting from the medium of water, air, and soil, and must be calibrated for each type of soil, since the composition of each soil changes its conductivity. Thus, to calibrate it, only the actual soil moisture and its measurement are necessary to relate them and determine how much each measurement made on the apparatus is worth. For more precision, soil sampling (Fig. 3) was used to measure moisture when it was approximately saturated when the soil was filled with water, and another was made near the wilting point, dry soil.

Although not calibrated, humidity measurements are still made in capacitance, since the data is stored in the device itself and can be downloaded at any time, so the conversion can be done when the actual data is available. Periodic data are collected from 7 points ranging from 50 to 80 cm in depth, which were chosen over the spillway so that they could be reconciled to the soil humidity and runoff data with the area above the spillway and at different altitudes, near and far from the water stream so that data could be generalized for the whole region.

Fig. 3 Collecting soil humidity data.

3.4 Precipitation

The climatological station used in the study was the E5000 Meteorological Station, Irriplus, which measured the precipitation of the region from the beginning of September 2017 until May 2018 and was also responsible for monitoring the other weather data used in this paper. Based on these factors will be developed Eq. (2) of basin water balance.

3.5 Evapotranspiration

Evapotranspiration potential (Et0) is calculated by daily means of climatic data (precipitation, wind speed, radiation), this is the evaporation due to the transpiration of a completely covered surface of a reference culture (normally grass in full growth without water restriction, with reduced climatic stresses), being then a meteorological variable that is expressed from the climatic conditions. The method used to estimate Et0 will be Penman-Monteith, using the software ET0 Calculator from FAO.

Given that the weather conditions are not always ideal for the growth of vegetation, the value found in Et0 is multiplied by a correction factor, called Kc, which varies from culture to culture. The multiplication of Et0 with Kc determines the actual evapotranspiration (Etr). Therefore, since the Kc value for the native forest of the watershed region is unknown, it will be the variable analysed in Eq. (2) of the water balance.

3.6 Water Balance

From the data collected in the field during this period you can generate a precipitation \ surface runoff balance, so, with all the variables already measured is possible to estimate the Kc culture and an estimation of results by comparing the results obtained in other jobs or situations where the Kc would be from cultures simulating, for example, the transformation of the area into a rural property.

$$P = ET + ES + \Delta R. \quad (2)$$

where, P is the precipitation, in mm, ETR is the actual evapotranspiration, in mm, ES is the surface runoff, in mm, and ΔR is the soil humidity difference in a time period in mm.

4. Analyses and Result

The data presented by the micro-basin during the period from September 2017 to May 2018 were: total precipitation of 1003.22 mm, with a mean of 0.15 mm daily in that period, with a maximum of 20.33 mm on October 18th, 2018, with periods of low rainfall in November and December 2017 and January 2018. Potential Evapotranspiration (Et0) recorded was 826,60 mm, and surface runoff was 11.01 mm. The distribution of these factors throughout this period are presented in Figs. 4, 5 and 6.

The Et0 score average was 91.4mm during the study period, with a maximum of 5.2 mm on January 1th 2018, with high monthly values where radiation has greater intensity, combined with low humidity values.

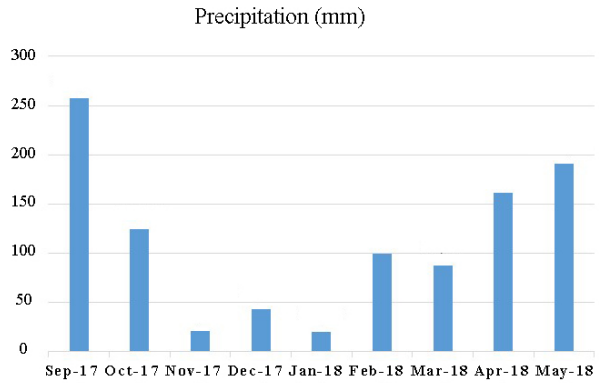

Fig. 4 Precipitation distribution graph.

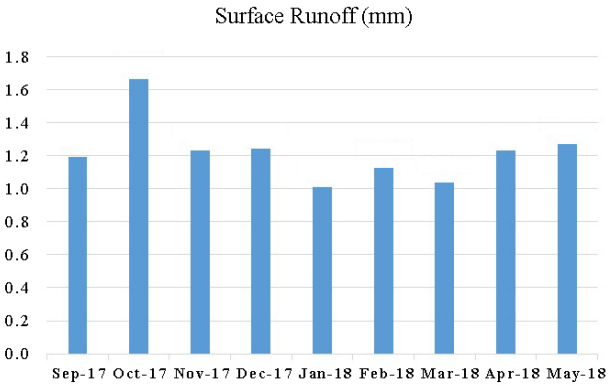

Fig. 5 Runoff distribution graph.

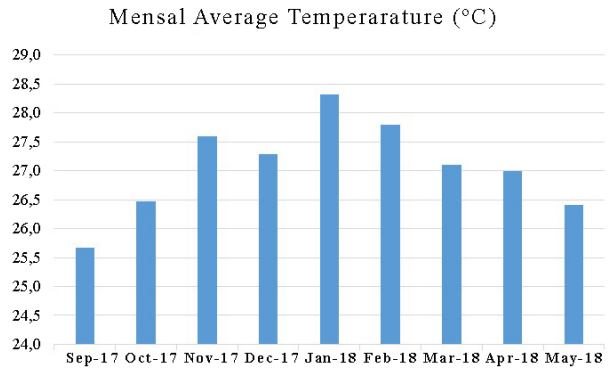

Fig. 6 Mensal average Temperature graph.

The relationship of climate data is in Table 1 and the illustration of the Et0 distribution in the graph of Fig. 7.

With a total volume of 11.01 mm in the period, the spillway did not present dry periods, having a maximum and minimum of 0.14 mm on October 18th, 2017, and 0.01 mm on January 10th, 2018, respectively. It is possible to observe how the basin responds almost immediately in the relation of runoff and precipitation in the graph of Fig. 9.

The micro basin also had a mean temperature of 27.4°C, with a maximum value of 42.8°C and on March 28th, 2018 and a minimum of 20.1°C on September 30th, 2017. Fig. 8 shows how the temperature varies in this period by relating it to the mean temperature, as well as the intrinsic relationship of the Et0 with the micro-basin temperature in the graph of Fig. 10.

Table 1 Climate date and monthly Et0.

	Sep. 17	Oct. 17	Nov. 17	Dec. 17	Jan. 18	Feb. 18	Mar. 18	Apr. 18	May. 18
Wind speed (km/month)	12.96	15.03	21.61	21.44	14.59	18.51	17.18	8.32	7.26
Temp. (ºC)	25.7	26.5	27.6	27.3	28.3	27.8	30.5	30.3	30.4
Humidity (%)	85.92	86.43	83.94	83.65	76.90	83.69	74.08	60.40	84.16
Rad. (MJ/m².day)	385.70	443.85	488.99	463.59	335.49	395.44	449.88	385.55	359.31
ETP (mm)	80.50	93.00	106.60	100.30	102.90	86.80	99.70	78.60	78.20

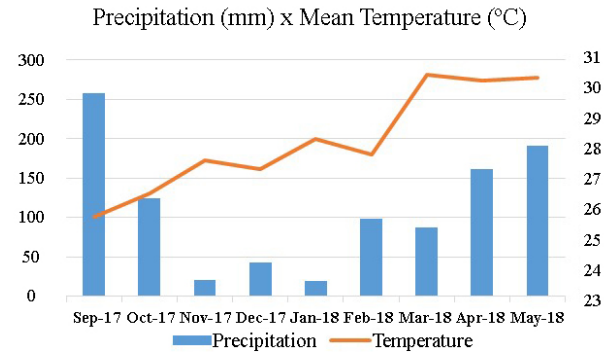

Fig. 8 Relation between precipitation temperature.

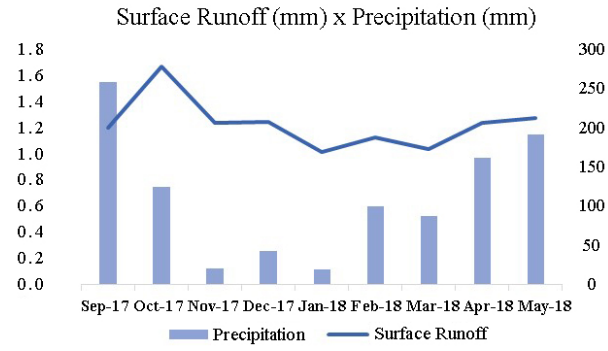

Fig. 9 surface runoff altering according to precipitation.

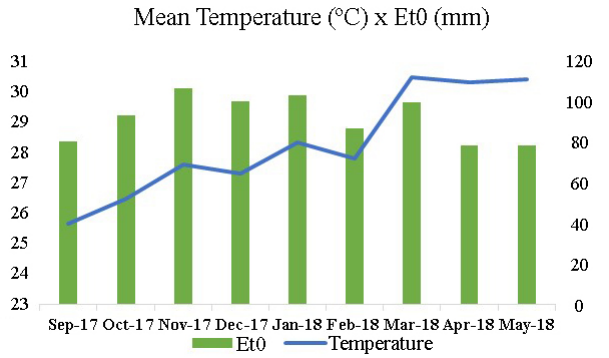

Fig. 10 Variation of ETP with an average score of temperature.

The Et0 has 82.4% of the precipitation value and the flow of 1.1% of the same. To determine the Kc in a micro basin with the dimensions of this studied, we would have that the best possibility, would be to relate also the participation of the humidity in the soil. However, in order to simplify the model of the basin at the present moment, we can consider Et0 in Eq. (2), since soil humidity variation does not yet present

concrete data due to the unavailability of the relationship between soil capacitance and its moisture due to its characteristics. However, through Equation (2) of the model followed, the soil water storage can be estimated in a simply by considering the Et0 equals Etp, taking as reference previous papers, where this value of the parameter represents great amount of the water balance, as Pereira [2]. The soil water storage is represented in the graph of Fig. 11.

In the Fig. 12 have a representation of the variation of soil storage water and the surface runoff in a daily interval, showing clearly how the micro-basin responses at rain effects.

5. Conclusion

Thus, Et0 results in 82.4% of the precipitation value, and the surface runoff of 1.1% of the precipitation, which was 1003.22 mm recorded in this period of 273 days, is in agreement with the expected results for this coverage, in view of similar work. In this way, the timber micro-basin of the Timbó river is characterized by small surface runoffs due to the intense use of water in the soil by the forest, which preventing large floods from occurring. This soil can retain in itself large amounts of water, caused by him type, having a significant amount of humidity for forest use for a large period. And this demonstrates the importance of the type of vegetation cover and the importance of the native forest preservation from this response in a providential way to the maintenance of the water cycle and the preservation of the climate.

This work will be extended for another 2 years, storing the results in a database that at the end of the period will be used to determine the climatic classification of the watershed.

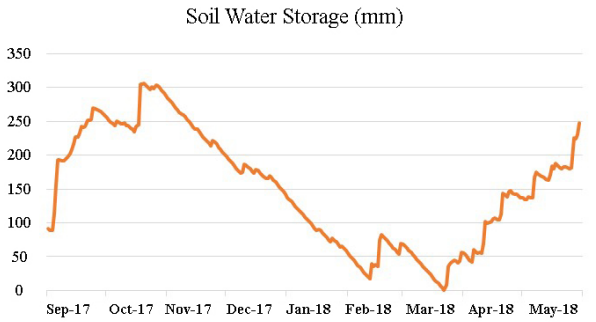

Fig. 11 Soil water availability graph.

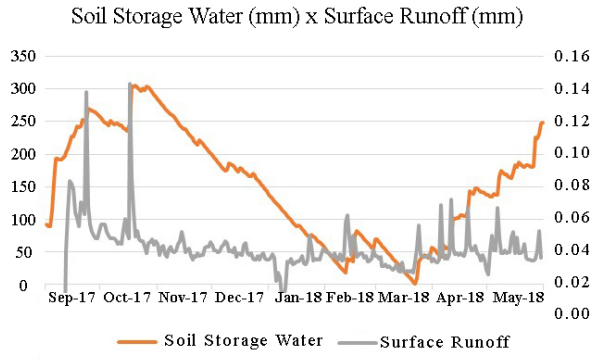

Fig. 12 Relation flow and storage.

References

[1] A. R. Paz, *Hidrologia Aplicada*; Universidade Estadual do Rio Grande do Sul, Caxias do Sul, 2004, pp. 4-35.

[2] A. R. Pereira, L. R. Angelocci and P. C. Sentelhas, *Agrometeorologia: fundamentos e aplicações práticas*, 2002.

[3] J. C. Bertoni and C. E. M. Tucci, *Hidrologia Ciência e Aplicação*, 2001, pp. 33-34.

[4] C. B. Brandão, A. S. Silva, R. A. C. Miranda and A. J. T. Guerra, *A Determinação do Perfil Climatológico do Município de Santo Antônio de Pádua-RJ e Sua Aplicabilidade na Recuperação de Áreas Degradadas*, Anuário do Instituto de Geociências – UFRJ, Rio de Janeiro, 2015, pp. 5-12.

[5] F. M. Costa, *Análise por Métodos Hidrológicos e Hidroquímicos de Fatores Condicionantes do Potencial Hídrico de Bacias Hidrográficas – Estudo de Casos no Quadrilátero Ferrífero (Mg)*, Dissertação de Mestrado, Departamento de Geologia Universidade Federal de Ouro Preto, 2005.

[6] I. Santos, H. D. Fill, M. R. V. B. Sugai, H. Buba, R. T. Kishi, E. Marone, L. F. Lautert; *Hidrometria Aplicada,* Instituto de Tecnologia para o desenvolvimento, Curitiba, 2001.

[7] K. Reichardt, *Processos de Transferência no Sistema Solo-planta-atmosfera*, 1985.

[8] L. G. Silvera, F. W. S. Correia, S. C. Chou, A. Lyra, W. B. Gomes, L. Vergasta, P. R. T. Silva, Reciclagem de Precipitação e Desflorestamento na Amazônia: Um Estudo de Modelagem Numérica, *Revista Brasileira de Meteorologia* 32 (2017) (3) 417-432.

[9] L. M. Pontes, G. Coelho, C. R. Mello, A. M. Silva, G. C. Oliveira and M. R. Viola, *Avaliação de modelo de balanço*

hídrico com base na estimativa da recarga potencial, *Rev. Ambient* 11 (2016) (4) 914-928.

[10] M. L. V. Passo, G. C. Zambrzycki and R. S. Pereira, *Balanço hídrico climatológico e classificação climática para o município de Balsas – MA*; Revista Scientia Agraria, Curitiba, 2017, pp. 83-89.

[11] T. N. Martin, D. D. Neto, P. A. Vieira, A. R. Pereira, P. A. Manfron and P. J. Christoffoleti, Modelo modificado de estimação da produtividade deplecionada e potencial da soja, Acta Scientiarum, Maringá, 2012, pp. 369- 378.

[12] W. C. Silva, A. Ribeiro, J. C. L. Neves, N. F. Barros, F. P. Leite, *Modelo de balanço de água e simulação do crescimento do eucalipto na bacia do Rio Doce, Brasil*, *Acta Scientarum* (34) (2013) (4) 403-412.

[13] W. P. Lima, *Princípios de manejo de bacias hidrográficas*, Piracicaba: ESALQ/USP, 1976.